Title	MOF
Author(s)	Singh, Ankit
Citation	
Issue Date	2018-06
Type	Thesis or Dissertation
Text version	ETD
URL	http://hdl.handle.net/10119/15432
Rights	
Description	Supervisor:　　　　　,　　　　　　　,

Japan Advanced Institute of Science and Technology

Utilization of MOF Materials for Enhanced Performance in Electrochemical Energy Devices

Ankit Singh

Japan Advanced Institute of Science and Technology

Doctoral Dissertation

Utilization of MOF Materials for Enhanced Performance in Electrochemical Energy Devices

Ankit Singh

Supervisor: Professor Noriyoshi Matsumi

School of Materials Science
Japan Advanced Institute of Science and Technology

June 2018

Utilization of MOF Materials for Enhanced Performance in Electrochemical Energy Devices

Abstract

Keywords: Metal Organic Frameworks (MOFs), Ionic Liquids (ILs), Li-ion Batteries Electrolytes, Zinc-air batteries, Electrochemical Synthesis, Oxygen Reduction Reaction (ORR)

The demand of energy has gradually increased and it has become a threat for the future generation. The depletion of fossil fuel based economy has raised the interest in the field of electrochemical energy storage and conversion devices. Batteries and fuel-cells are some of the most important energy storage devices for the social development. It has been observed over the period of time that storage and conversion of energy are of high importance and effective functional materials are required to enhance the performance of this innovative technologies. In this regard porous materials which can facilitate the energy transportation have marked their significance in the past few years. Metal Organic Frameworks are currently a hot research topic because of their highly advantageous features to be used for energy storage such as high surface area, tunable pore size and multifunctionalities. These can be synthesized according to the desires and therefore allows its utilization in various next-generation devices.

Despite of having many electrochemical energy storage devices, its commercialization has been hindered due to several factors associated with its performance. Therefore there is an urge to overcome these performance and cost related limitations to fulfil the future energy demand. Unceasing research on the exploration of MOF utilization in energy applications has inspired us to work in this fascinating field. Considering the vitality of these energy devices, the present research work will be addressing various hurdle stones in each of this technologies and a possible solution to overcome these problems. The chapters of the thesis include the utilization of MOF materials in various energy related applications. In chapter 1, the introduction of MOFs and its applications in various electrochemical devices was reviewed.

Chapter 2 is mainly focused on exploiting the electrochemical advantages of MOF as a safe and efficient electrolyte in Li-ion batteries. The strategy involved in this research was to synthesize modified MOF in ionic liquid system to possess enhanced inherent properties such as high ionic conductivity, low activation energy and improved charge discharge characteristics.

During the development of modified MOF in ionic liquid system by electrochemical method, we observed the growth of MOF on the working electrode. This observance inspired us to work on the modification of electrode surface by MOF and conducting polymers. In chapter 3, the decoration of electrode surface first by MOF and then by conducting polymer was demonstrated. In this research an attempt was made to investigate the application of modified MOFs in zinc-air batteries. The zinc-air batteries fabricated using modified anodes solved the problems like self-corrosion and showed improved discharge performance. Zinc-air batteries fabricated using MOF-5 modified Zn anode showed 4 times better performance than the pure Zn anodes. These results show the promising nature of this material in improving Zn-air battery performance.

To further improve the performance of metal-air batteries and fuel-cells, an efficient ORR electrocatalyst is needed. In this regard, chapter 4 deals with the preparation of MOF nanoparticles on functionalized acetylene black surface using simple synthetic procedure. The decoration of ZIF-8, an example of MOF, significantly improved the surface area of the carbon matrix for better electrocatalytic activity. The hybrid nanocomposite material showed high activity towards oxygen reduction reaction with excellent methanol tolerance. This research proposes the significance of this material in replacing the high cost platinum based electrocatalysts for ORR.

Preface

The present dissertation is submitted for the Degree of Doctor of Philosophy at Japan Advanced Institute of Science and Technology, Japan. The dissertation is consolidation of results of the works on the topic "Utilization of MOFs Materials for Enhanced Performance in Electrochemical Energy Devices" under the direction of Prof. Noriyoshi Matsumi at the School of Materials Science, Japan Advanced Institute of Science and Technology during July 2015-June 2018.

Metal Organic Frameworks (MOFs) are currently one of the most promising materials for the energy storage devices and are widely used in Li-ion batteries, fuel cells and other energy storage materials. These materials possess various attractive features like high surface area, tunable pore size and simple synthetic procedures due to which its utilization in various applications is increasing. The author's main focus is to utilize the interesting features of MOFs in addressing the problems and challenges of current energy storage materials. Successful completion of this research would yield electrochemical energy devices of high performance and prolonged cyclability.

The work presented in this thesis covers the synthesis and characterization of MOFs based materials alongwith their performance parameters as observed in various applications. Also their real time application in Li-ion batteries and Zinc-air batteries have been studied extensively. Finally the conclusions and future prospects of the studies are summarized in the final chapter. To the best of my knowledge, the work is original and no part of the thesis has been plagiarized.

School of Materials Science   Ankit Singh

Japan Advanced Institute of Science and Technology

June 2018

Acknowledgement

Firstly, the author expresses his sincere gratitude to the supervisor Prof. Noriyoshi Matsumi, School of Materials Science, Japan Advanced Institute of Science and Technology, for his kind guidance, valuable suggestions and heartfelt encouragements throughout this work. I am thankful to him for his patience, motivation and immense knowledge.

I would also like to thank the members of my Review committee *Assoc. Prof. Kazuaki Matsumura* (JAIST), *Assoc. Prof. Toshiaki Taniike* (JAIST), *Assoc. Prof. Yoshifumi Oshima* (JAIST) and *Assoc. Prof. Masamichi Nishihara* (Kyushu University), who have spent their valuable time to read my thesis and gave valuable comments and remarks to enhance the quality of my thesis from various perspectives.

The author is thankful to *Prof. Safir Ahmad Hashmi*, Department of Physics and Astrophysics, University of Delhi, India for giving him an opportunity to join their team as intern and carry out experiments in the field of supercapacitors during minor research. Furthermore, the author wishes to express her special thanks to *Prof. Safir Ahmad Hashmi* and their lam members for their warm support and valuable suggestions during the author's stay in India.

The author also takes an opportunity to thank Ass. Prof. Raman Vedarajan (now working as Scientist in ARCI, Centre for fuel cell technology, India) for his guidance and encouragement at a professional and personal level. I am also grateful to other lab members, for their valuable inputs, cooperation and stimulating discussions throughout my time at JAIST.

The author expresses his heartfelt gratitude to his family and friends especially Surabhi, who is both for their rentless encouragement and support at difficult times. Finally, the author expresses his humble gratitude to the Almighty for all the good things.

School of Materials Science   Ankit Singh

Japan Advanced Institute of Science and Technology

June 2018

Table of Contents

List of Abbreviations

Abbreviation	Definition
AB	Acetylene Black
AC	Alternating current
Ag/AgCl	Silver/ Silver chloride
AMImCl	1-allyl-3-methylimidazolium chloride
AMImTFSI	1-allyl-3-methylimidazolium bis[(trifluoromethane)sulfonyl]imide
BDC	1,4-benzenedicarboxylate
BET	Brunauer–Emmett–Teller
BMImCl	1-butyl-3-methylimidazolium chloride
CV	Cyclic voltammetry
DC	Direct current
DEC	Diethylene carbonate
DMF	Dimethylformamide
DMSO	Dimethylsulfoxide
EC	Ethylene carbonate
EDS	Energy-dispersive X-ray spectroscopy
FAB	Functionalized Acetylene Black
FESEM	Field Emission Scanning Electron Microscopy
FT-IR	Fourier-transformed Infra-red spectrosocpy
GC	Glassy carbon
GO	Graphene oxide
Hg/HgO	Mercury/Mercuryoxide
ILs	Ionic Liquids
LBO	Lithium boron oxide
LiB	Lithium-ion battery
LiTFSI	Lithium bis[(trifluoromethane)sulfonyl]amide
LSV	Linear Sweep Voltammetry
MOF	Metal Organic Framework
OCV	Open circuit potential
ORR	Oxygen reduction reaction
PC	polycarbonates
PEO	Polyethylene oxide
PTFE	Polytetrafluoroethylene
PTh	Polythiophene
RDE	Rotating Disk Electrode
SEI	Solid electrolyte interface
SEM	Scanning electron microscopy
TEM	Transmission electron microscopy
THF	Tetrahydrofuran
VFT	Vogel-Fulcher-Tammann
XPS	X-ray photoelectron spectroscopy
XRD	X-ray Diffraction
ZIF	Zeolitic imidazolate framework

Chapter 1
Introduction

As we all know that with the growing population the need of energy resources has been increasing and renewable energy sources like solar power and wind power, are unable to fulfil the demand of the society. Looking at the current energy demand there is an urge to harvest and search for the sustainable energy sources like batteries, supercapacitors and fuel cells to meet the practical need of clean energy. These electrochemical energy storage devices can efficiently store the energy from different sources and can be utilized later as per the need. Despite of having different working mechanism in these electrochemical energy devices, they work on some key components like electrodes which are responsible for most of the reactions occurring alongwith an efficient electrolyte for charge and ion transportation. Generally the electrochemical properties like catalytic activity and physical properties such as conductivity of the materials used in these devices decide the performance. Therefore, during the development of efficient energy storage devices, functional materials which are able to accelerate the transportation of energy carriers are studied widely to select the most suitable materials for this innovative technologies [1].

1.1 Metal Organic Frameworks (MOFs)

Over the past it has been discovered that porous materials are the most fascinating functional materials to be used in these electrochemical devices. Among the class of porous materials Metal Organic Frameworks (MOFs) have attracted tremendous attention of all the researchers working in various fields. The name MOFs was first introduced by Prof. Omar Yaghi in 1995. Though the field of MOF is relatively young, it has been widely explored in the past few decades. More than 20,000 structures of MOFs have been discovered in this short period and this count is growing with every year [5].

Metal Organic Frameworks, or MOFs, are crystalline materials with high porosity (~ 90% free volume) and huge surface areas (beyond 6000 m^2/g) [3]. MOFs have emerged as excellent materials for wide range of applications ranging from gas storage, catalysis, separations and energy storage applications [2,4–6]. MOFs are formed by the combination of organic and inorganic chemistry where transition metals acts as a metal clusters and organic units as linkers. The variation in metal ions and organic linkers leads to the synthesis of target structures with desired properties. MOFs have gained huge attention of researchers all over the world due to its extraordinary properties but one of the distinctive feature of these crystalline materials is their diverse topology and tunable structures. **Fig. 1** shows the examples of some already reported MOFs.
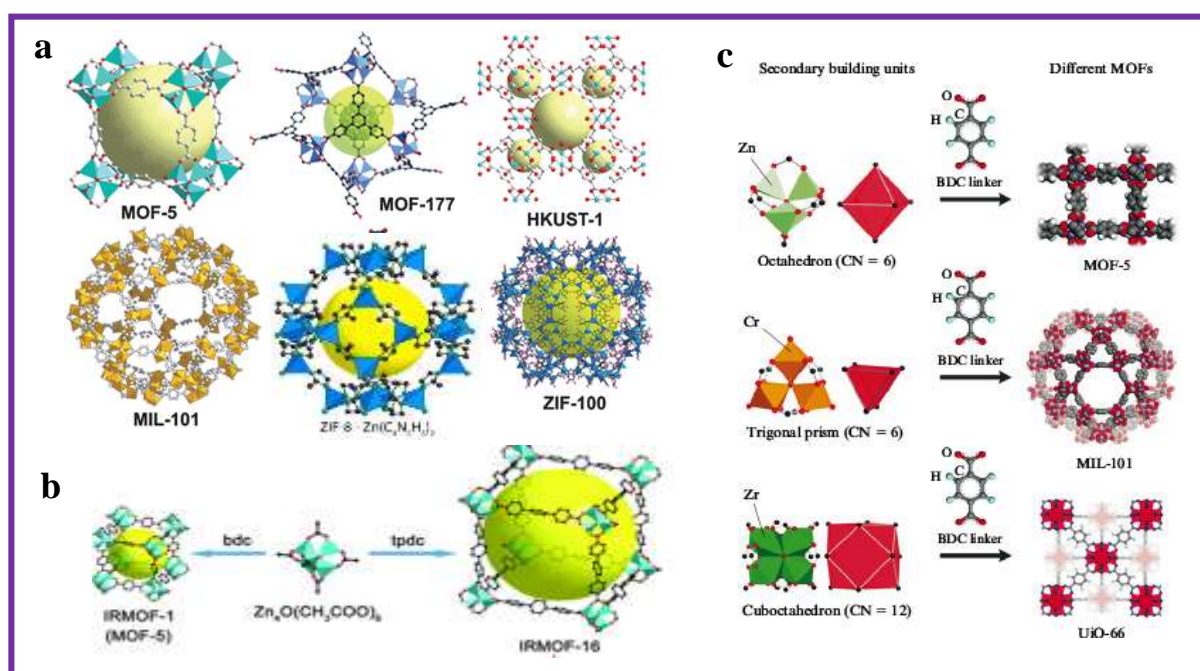

Fig. 1 Illustration of already reported examples of MOFs structure [1][2][3].

The same metal cluster can be linked to organic linkers to give various different types of MOFs structure and vice versa as shown in **Fig. 1b-c**.The most interesting feature of MOFs is porosity as it allows the guest molecules to diffuse into the bulk structure. Moreover the pore

size can be tuned according to the size and shape of the guests. This ultrahigh porosity of MOFs is because of the long organic linkers that grants longer storage space inside the structure.

The structure of MOF contains both inorganic and organic units. The most commonly used organic linkers also known as bridging ligands are carboxylates, or anions like phosphonate, sulfonate and also heterocyclic compounds. The secondary building units of MOF structure are metal ions or clusters (eg. Zn, Co, Fe, Ni, Mg) and mixture of metals are also used for the synthesis.

1.1.1 Growth mechanism of MOFs

The synthesis of MOFs is often regarded by the term "design", which means construction according to desires. The understanding of functionality of organic linkers and metal coordination environment can direct the synthesis. The synthetic conditions to establish MOF structure without the decomposition of bridging ligands (organic linkers) is the key factor in MOF synthesis. The complex relationship between the synthetic conditions and knowledge of building units have slowed down the discovery of MOFs. Different synthetic methodologies and strategies by various groups have been employed all over the world. Zeolite chemistry and coordination chemistry have accounted for introducing wide variety of synthetic method ranging from solvothermal, hydrothermal, electrochemical, microwave-assisted approaches [7]. The reason behind the different synthetic methods adopted in the field of MOFs is that they can lead to variety of different MOFs from the same reaction precursors. The hydrothermal and solvothermal synthetic methods are the most superior conventional methods for the synthesis of MOFs. These methods require several hours to days for reaction completion. To reduce the reaction time and synthesize MOF with controlled morphology other synthetic methods discussed above were employed.

Fig. 2 summarizes the various synthetic methods and strategies that were adapted for the synthesis of MOFs in the history. In principle the nucleation or growth of MOF is governed by the reaction of organic linker or a bridging ligand with a metal ion having more than one labile or vacant site. The topology of the MOF structure is governed by both organic linkers and secondary building units i.e. metal ions or clusters.
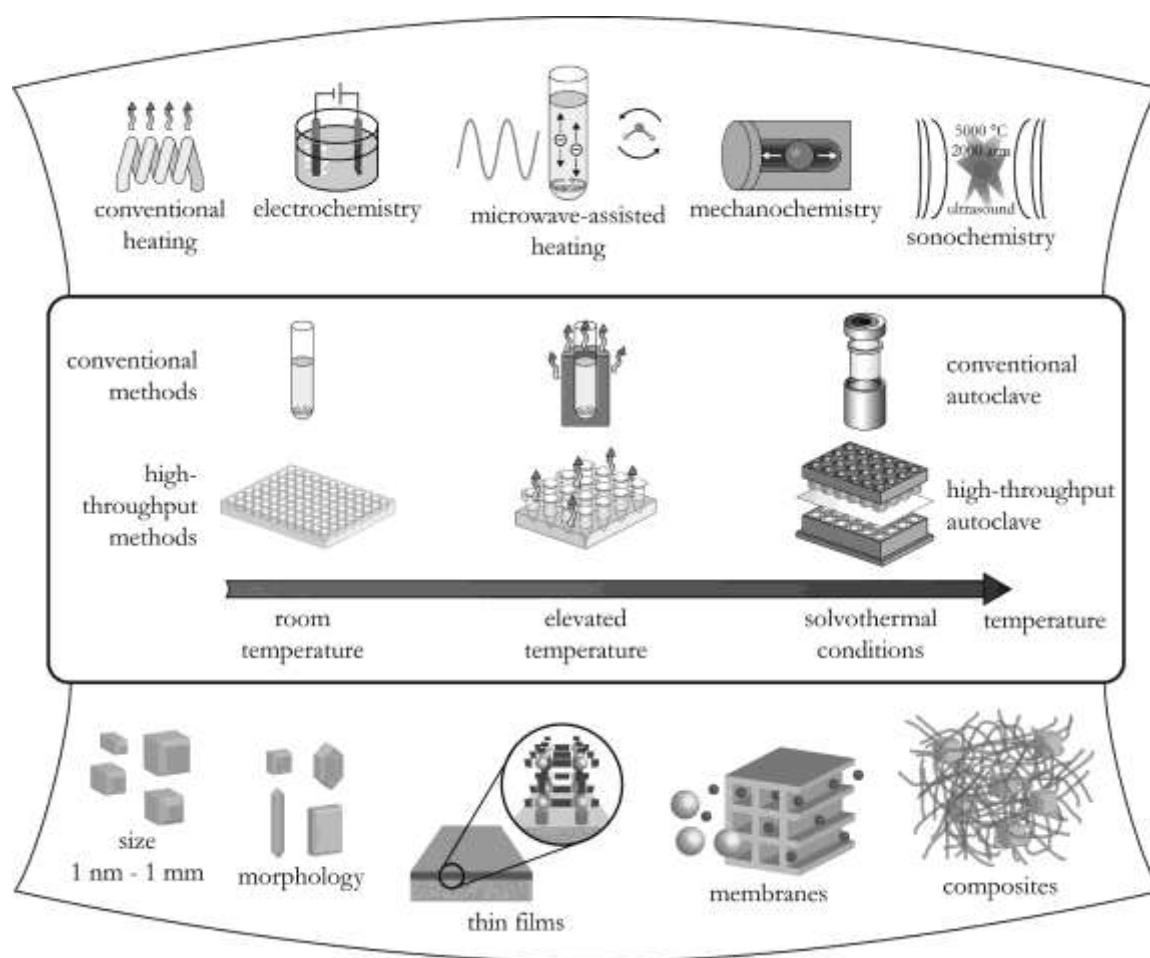

Fig. 2 Schematic representation of various synthesis methods, reaction temperatures and resulting MOFs [6].

The above described properties and astonishing functionalities of MOFs and its derivatives have made them potential candidate for the development of energy storage devices. In these past 20 years of investigation, their application in the field of energy have become an area of interest for many researchers. Their organic-inorganic hybrid composition with high surface area and multifunctionalities can be exploited in various energy applications. The exceptionally high porosity and surface area are well suited for the gas storage, catalysis and separation applications. This property of MOFs makes them an excellent adsorbents to be used in automobile gas tanks and fuel cells. Also, the involvement of metal clusters used for the formation of MOFs triggered the research interests to investigate its performance in electrochemical energy storage devices. The presence of these metal clusters which mainly includes the transition metal acts as active metal centers for catalytic performance and activity responsible for the performance. MOFs involve wide range of organic ligands that are electro- and photoactive which also contributes to its exploration in the field of energy. Compared to other porous materials MOFs inherit some additional advantage like tunable pore structure and open metal sites coordinated with organic ligands. Replacing or changing the organic ligands/metal centers in MOFs can tune the materials in fabricating different electrodes, electrolyte and electrocatalysts material for clean energy technology. Development of nanotechnology and present-day characterization techniques have helped to modify these attractive materials by efficient strategies in developing the energy devices. These improvements in the evolution of MOFs and its related materials have spread the research interest on various aspects of MOFs for its utilization in wide range of applications. This exciting research field inspires many to study the significance of MOFs and MOFs derived materials in the field of energy storage and conversion like batteries, fuel cells and many other.

1.2 MOFs for lithium ion battery (LIB) applications

1.2.1 Introduction of LIBs

LIBs come under the category of secondary batteries and are the most progressive battery technology in this modern society. LIBs are considered as the powerhouse in the digital market and the advancement of LIBs was not achieved overnight, it's a result of intensive hard work of many researchers. LIBs are widely accepted as the next generation power source to meet the requirements of electronic market. Intensified research is going on to improve the performance of the LIB for future electric and hybrid vehicles. The reason behind LIB's great success in the recent past is because of its high specific energy, cell voltage and great capacity retention [8,9].

LIBs in comparison to other commercialized rechargeable batteries are highly advanced in terms of high energy density. The superiority of LIBs over other battery technology in terms of its gravimetric and volumetric energy density is clearly shown in **Fig. 3 [10]**. Although the theoretical energy density of Li-metal battery is higher than that of LIBs, the poor rechargeability and susceptibility towards fire makes it unsafe for commercialization.
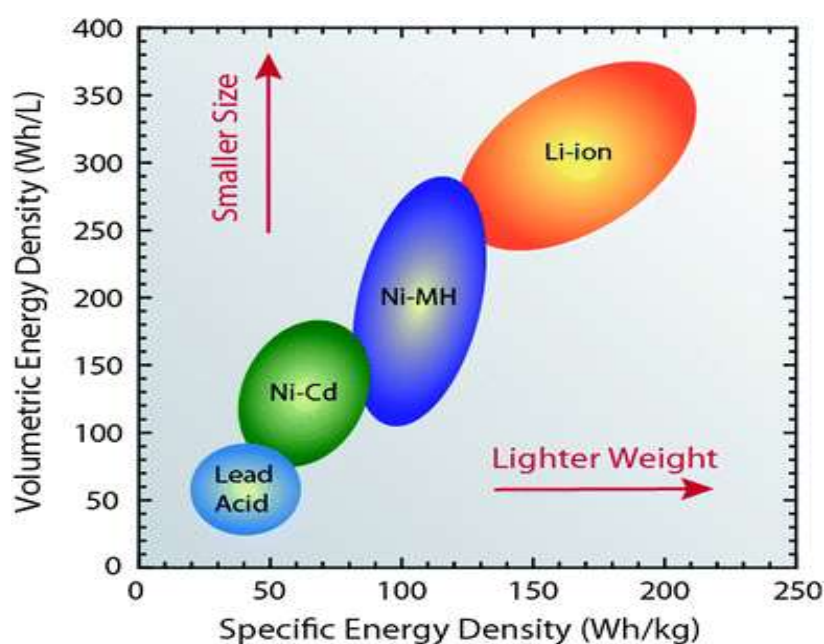

Fig. 3 Comparison of energy densities of different kind of batteries [9].

A LIB is made up of unit called electrochemical cell in which the chemical energy is converted to electric energy by a specific electrochemical reaction.

Typically, a LIB consists of three primary components [11]:

1) Cathode (Positive electrode)- the electrode at which reduction occurs,

2) Anode (Negative electrode)- the electrode at which oxidation occurs and

3) Electrolyte- ion conducting media between the cathode and anode which often acts as a separator also to avoid the internal short-circuit.

During the process of discharge, the anode or negative electrode gets oxidized and releases an electron. The electron then moves to the cathode or positive electrode which accepts electron through the outer circuit. The operation of typical LIB is illustrated in the **Fig. 4** using carbon as anode and $LiCoO_2$ as cathode.
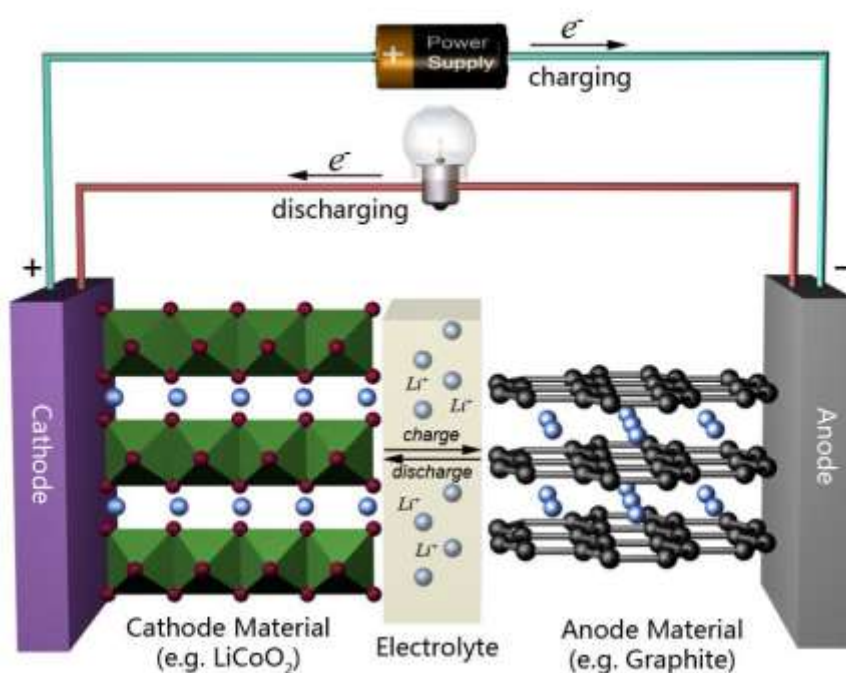

Fig. 4 Schematic representation of charge-discharge process in LIB using graphite as anode and $LiCoO_2$ as cathode adapted from Department of chemistry, University of Illinois, Urbana.

1.2.1.1 Cathode

Cathode materials are one of the major component of LIBs in determining the energy density of the cell [12–14]. The chemistry of LIBs is based on intercalation and de-intercalation compounds [15,16], cathode materials provide the lithium ions which gets intercalated to the anode material during charging process and are extracted during discharge process. Various factors like cell voltage, capacity, cycle life and inertness towards the other components of the cell should be taken into consideration before the choice of the cathode materials. The cathode materials for LIBs are classified into three groups (**Fig.5**) [17]:

    a) Layered

    b) Spinel

    c) Polyanion-type

a) $LiCoO_2$ was the first commercialized cathode material for LIBs having **layered structure** (**Fig. 5a**). It offers a cell voltage of 3.9 V with high theoretical capacity of 274 mA h g^{-1}. The cathode materials with layered structure having general formula as $LiMO_2$ (M= Mn, Cr, Co, Ni, etc.) are one of the most suitable materials owing to their low cost and high specific capacity [18–21].

b) **Spinel**-structured cathodes have a distinct 3-dimensional robust structure which offers low cost and environmental friendly materials for high performance LIBs applications [22,23]. Among various spinel-structured materials, the best example is $LiMn_2O_4$ (**Fig. 5b**) with high cell voltage, superior cycling and excellent rate capability.

c) **Polyanion-type** cathode materials are known to show high thermal stability than other type of materials and are considered as most promising cathode materials for LIBs [24–26]. These materials are often referred as olivine-type with general formula $LiMPO_4$. Examples of such olivine-type material is $LiFePO_4$ (**Fig. 5c**) that has slightly distorted hexagonal

closed packed geometry and has some great advantages like flat discharge potential ~ 3.4
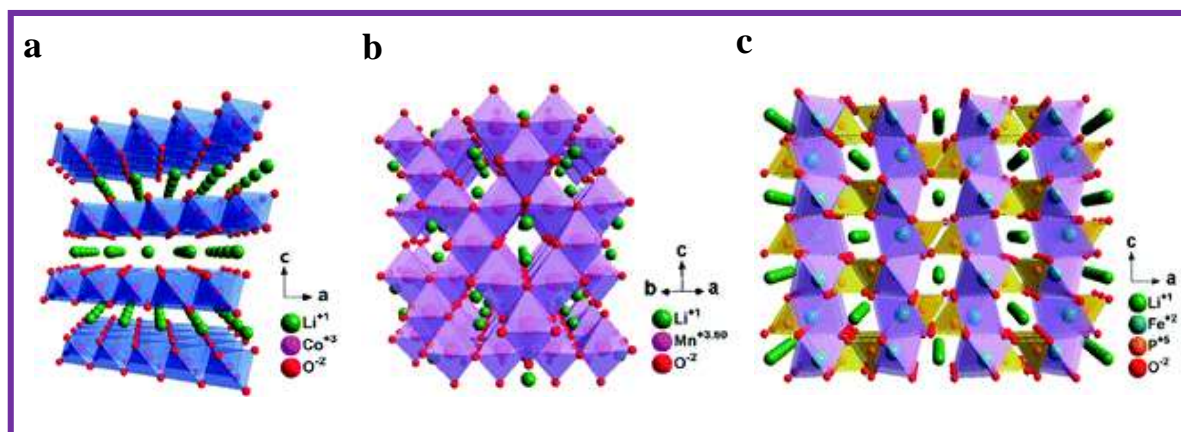
V with high thermal and chemical stability.

Fig. 5 Crystal structures of (a) layered- $LiCoO_2$, (b) spinel- $LiMn_2O_4$ and (c) olivine- $LiFePO_4$ [16].

1.2.1.2 Anode

Anode materials are paired with cathode materials for the fabrication of LIBs. The

anode materials acts as a host for Li-ion ion and it should allow the reversible intercalation and

de-intercalation without much structural changes. For anode materials, certain properties have

to be considered like excellent porosity, low cost, good conductivity, excellent durability, light

weight and ability to form stable solid electrolyte interface (SEI).

Anode materials for LIBs can be classified into three main categories for simplicity:

a) Carbon based materials

b) Alloy materials

c) Silicon materials

a) **Carbon-based materials** are currently used in the commercial LIBs due to its excellent conductivity, hierarchical structure for Li-ion intercalation, high availability and low cost. Extensive research is going on to improve the performance of carbon based anodes like graphite. The formation of dendrites with continuous deposition of Li-ions in the charge-discharge process and low working potential are some of the biggest challenges in large scale applications. The theoretical capacity of these graphite based anodes is 372 mAh g^{-1}.

b) **Alloy materials** (like Sn, Al, Mg, Ag and their alloys) can compensate the disadvantages of graphite based anodes like poor capacity as well as safety issues [27–29]. They possess high theoretical capacity nearly 2-10 times more than that of carbon based anodes. In Sn alloy (**Fig. 6**) [30] anodes the problem of lithium deposition can be resolved by increasing the onset potential over Li/Li$^+$. These anode materials also suffer from problems like large change in volume on intercalation and de-intercalation leading to capacity loss.
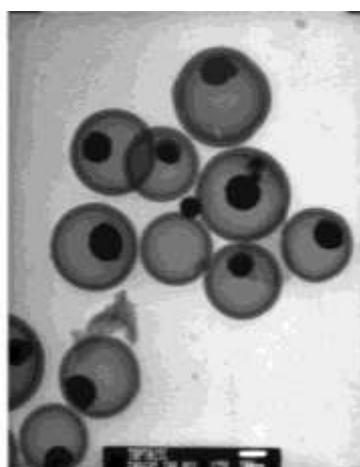
Fig. 6 Tin-encapsulated hollow carbon spheres an example of alloy anode materials [29].

c) Recently, **silicon** has emerged as a very efficient and promising anode material for LIB applications due to its high gravimetric capacity and volumetric capacity amongst all the other known elements[31–34]. A conversion reaction takes place during the process of intercalation and de-intercalation in Si-based anodes. Their form changes to amorphous

from a crystalline state resulting in large capacity loss on subsequent charge-discharge cycles. **Table 1.1** lists the advantages and disadvantages of various anode materials.

Table 1.1 Advantages and disadvantages of various types of anode materials.

Material	Advantages	Disadvantages
Carbon	(1) High electronic conductivity (2) Nice hierarchical structure (3) Abundant and low-cost resources	(1) Low specific capacity (2) Low rate capacity (3) Safety issues
Alloys	(1) High specific capacity (400–2300 mA h g^{-1}) (2) Good security	(1) Low electronic conductivity (2) Large volume change (100%)
Transition metal oxides	(1) High specific capacity (600–1000 mA h g^{-1}) (2) Nice stability	(1) Low coulombic efficiency (2) Large potential hysteresis
Silicon	(1) Highest specific capacity (3579 mA h g^{-1}) (2) Rich, low-cost, clean resources	(1) Large volume change (300%)

1.2.1.3 Electrolyte

Electrolyte is a substance that contains free ions for conduction between anode and cathode. Electrolytes play a decisive role in the performance of battery, therefore in order to employ it in LIBs it should meet certain important requirements:

a) High solubility in various organic solvents.

b) High ionic conductivity which is an important characteristic of the electrolyte.

c) High thermal and chemical stability with wide electrochemical stability window.

d) The materials should be able to form stable, solid and conductive solid electrolyte interface (SEI) for better performance.

e) Low cost and less toxic.

Electrolytes can be classified into four types depending on the cell design and its application:

a) Conventional liquid electrolytes

b) Polymer electrolytes

c) Gel electrolytes

d) Solid state electrolytes

a) Previously, **liquid electrolytes** such as ethylene carbonate (EC), diethylene carbonate (DEC) and propylene carbonate (PC) were used extensively in commercial LIBs [35,36]. These liquid electrolytes possess high conductivity, less viscosity and can form very stable solid electrolyte interface (SEI) which makes them an excellent and suitable candidates to be used in LIBs. These liquid electrolytes show extraordinary electrochemical behaviour due to its above mentioned properties. But at the same time these electrolytes suffered from the problems like leakage, ignition at high temperatures and reactivity with undesired cell components.

To overcome the problems of conventional liquid electrolytes, researchers employed room temperature ionic liquids (ILs) as a safer and greener electrolytes [34,37,38]. ILs have gained enormous attention in various applications and do not crave for any introduction in today's world. These are molten salts comprising of cations and anions and are generally characterized by weak interactions. They exhibit properties like high ionic conductivity, non-volatility, great electrochemical stability and are soluble in various inorganic and organic compounds [39–41] (**Fig. 7**). The use of ILs in commercialized LIBs is hindered because of its high viscosity that results in reduced mobility of free ions.
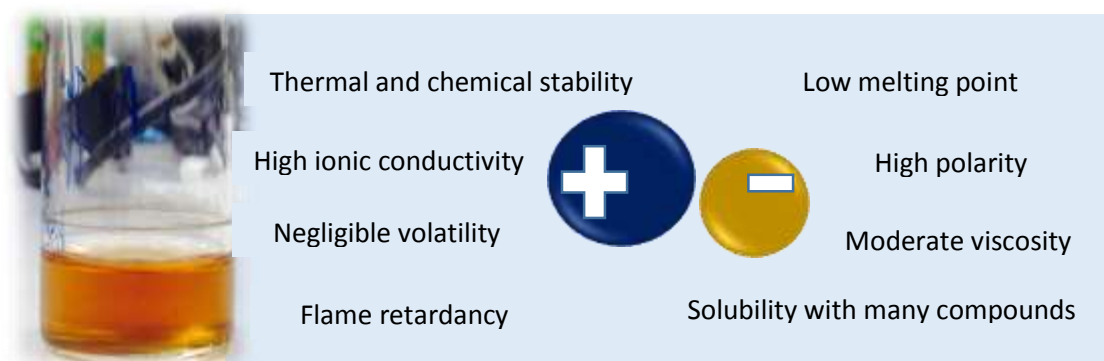

Fig. 7 Properties of ionic liquids.

b) **Polymer Electrolytes** are salt solutions which are dissociated in the high molecular weight polymer host to form an ionically conducting phase. It have many advantages like high ionic conductivity, low volatility, easy processability, wide electrochemical window and solvent free condition. Polyethylene oxide (PEO) (also termed as polyethylene glycol (PEG)) are commonly used in combination with Li salts. They were designed to overcome the issues of liquid electrolytes such as leakage and safety risks. But the conductivity of polymer electrolytes was relatively lower than that of the liquid electrolytes at room temperature. The mobility of ions in the polymer electrolytes predominantly occurs through the polymer segmental motion as shown in **Fig. 8 [42]**.

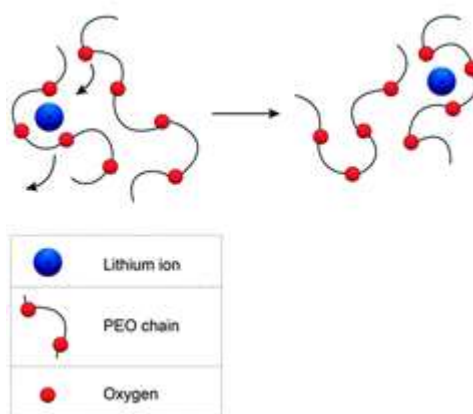|	
🔵	Lithium ion
〰️	PEO chain
🔴	Oxygen

Fig. 8 Illustration of Li-ion conduction in PEO-based electrolytes via polymer segmental motion [41].

c) **Gel polymer electrolytes** represents the state of the electrolyte which is neither completely solid nor liquid. In these gel electrolytes the polymer membrane is swollen with a solvent and lithium salts are dissolved in it. Since the solvent is trapped inside the polymer matrix it avoids the problem of leakage and at the same time it possess the properties of both solid and liquid electrolytes. It shows better ionic conductivity compared to polymer electrolytes because of the diffusive properties of liquids to facilitate the ion mobility but mechanical stability is generally lower.

d) **Solid state electrolytes** overcome the limitations of liquid electrolytes as well as gel polymer electrolytes. It was introduced in LIBs because it can act both as separator and electrolyte. This unique concept of solid state electrolytes is interesting because it provides high durability, high energy density, light weight and also offers the cell design. For this purpose, various solid state electrolytes were synthesized using polyethylene oxide (PEO) and its derivatives. But the crystalline nature of solid state electrolytes does not allow high conductivity as it was required.

1.2.2 MOFs as electrolyte materials for LIBs

In 2011, B.M. Wiers et al. studied the conduction of Li-ion inside the metal organic framework structure [43]. Lithium isopropoxide was added to the $Mg_2(dobdc)$ framework by grafting method after soaking for 2 weeks (**Fig. 9a**). The suggested mechanism of lithium ion conduction inside the pores of the framework is through ion hopping from site to site. The resulting system showed highly improved ionic conductivity in the range of 10^{-4} S cm^{-1}. The ease of lithium transport inside the metal organic framework accounted for activation energy of just 0.15 eV.

In another research, C.Yuan et al. synthesized a composite polymer electrolyte by the incorporation of nano-sized metal organic framework in the polyethylene oxide matrix [44]. The system showed high conductivity of 3.16 x 10^{-5} S cm^{-1} at room temperature with enhanced electrode interfacial stability. The synthesized solid PEO-LiTFSI/MOF-5 electrolyte exhibited high electrochemical stability window of ~ 4.57 V. The results suggested that the incorporation of Lewis acidic surface properties by nano-sized particles can greatly enhance the conductivity and interfacial properties (**Fig. 9b**). The addition of these porous metal organic frameworks as fillers also improved the cycling performance of the synthesized electrolyte material.
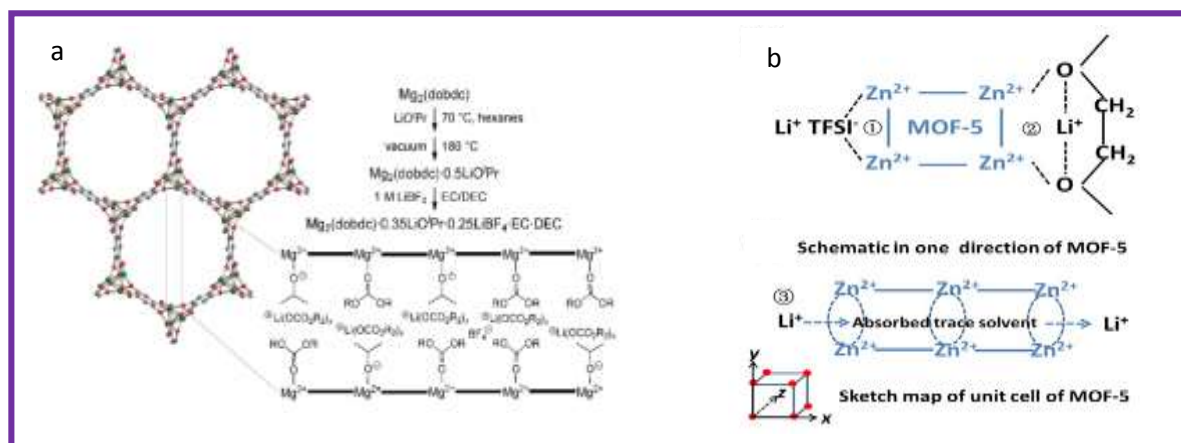
Fig. 9 (a) Schematic of grafting Li-salt in Mg$_2$(dobdc) framework. (b) Illustration of improved Li-ion conduction by MOF-5 [42][43].

In similar study by C. Gerbaldi et al., aluminium based metal organic framework was used as filler in poly (ethylene oxide)-based nanocomposite polymer electrolyte (NCPE) membranes [45]. Besides significant enhancement in ionic conductivity by two orders they showed interesting thermal and interfacial characteristics. A solid state lithium polymer cell was fabricated by using this electrolyte material to achieve outstanding cycling profile stable till 50 °C (**Fig. 10**). The addition of specific amount of Al-BTC (aluminium benzenetricarboxylate) MOF in the polymer matrix of PEO based system advances the electrolyte to form thinner and safer LIBs.
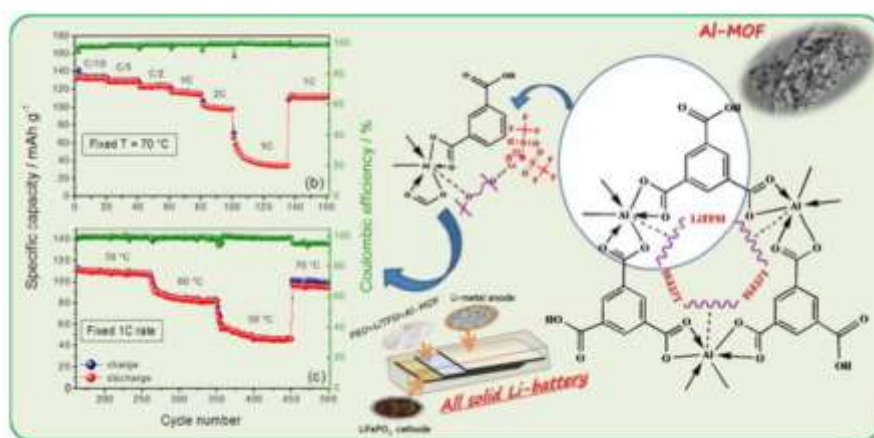

Fig. 10 Illustration of cycling behaviour with aluminium based metal organic framework as filler in PEO based electrolytes [44].

More recently, K. Fujie et al. showed the first study of Li ion conduction in ionic liquid incorporated MOF as host materials [46]. LiTFSA mixed with EMI-TFSI ionic liquid was incorporated in ZIF-8 framework to enhance the ionic conductivity and its phase behaviour was studied. The system showed better ionic conductivity inside the pores than the bulk suggesting the role of conductive paths for the ions provided by MOFs.

1.3 MOFs for zinc-air battery applications

1.3.1 Zinc-air battery- Introduction

The transition from a fossil fuel to clean energy economy is inevitable process in our society. This gradual transition has led to active research in the field of energy storage and conversion. Batteries are known from a very long time to store electrical energy and they find use in various applications ranging from a mobile phone to electric vehicles. Among many battery technologies in the market, Li-ion batteries have proven to be dominant in the modern society to meet the requirements of next generation electronic and electrical devices. Even after tremendous research over Li-ion batteries, the commercialization is still hindered because of its high cost and limited energy density. The limited energy densities of Li-ion batteries is because of its intercalation chemistry.

In recent past metal air batteries, that features very high theoretical energy density have gained much attention as an alternative to high cost Li-ion batteries. Zinc-air battery which involves the electrochemical coupling of anode and breathable air electrode or cathode is one of the promising battery technology among other metal-air batteries [47,48]. It has almost five

times higher theoretical energy density compared to Li-ion batteries as shown in **Fig. 11 [49]**.

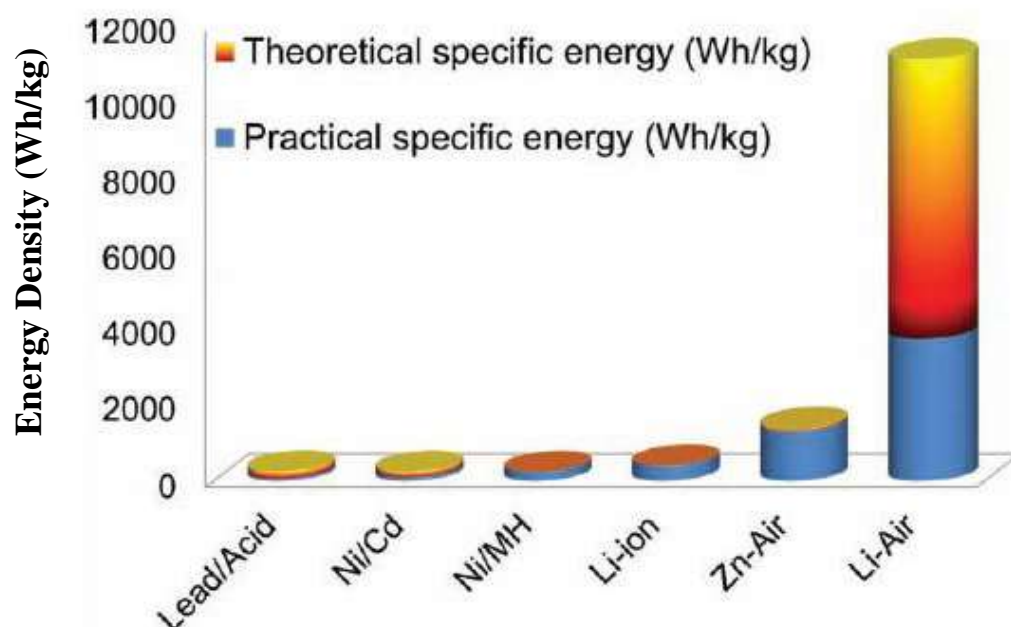It also allows to reduce the cost of the battery and improve safety for future applications.

Fig. 11 Comparison of energy densities (theoretical and practical) of different batteries [48].

1.3.2 Zinc-air battery- Configuration and operation

Zinc-air battery has three main components- a negative zinc electrode (anode), a positive air electrode (cathode) with a catalytic layer that allows the diffusion of oxygen from air and converts it to OH^- and aqueous alkaline electrolyte (**Fig. 12**) [50]. Apart from the three main electrochemical components, there is a membrane separator that avoids the contact of positive and negative electrodes with each other.
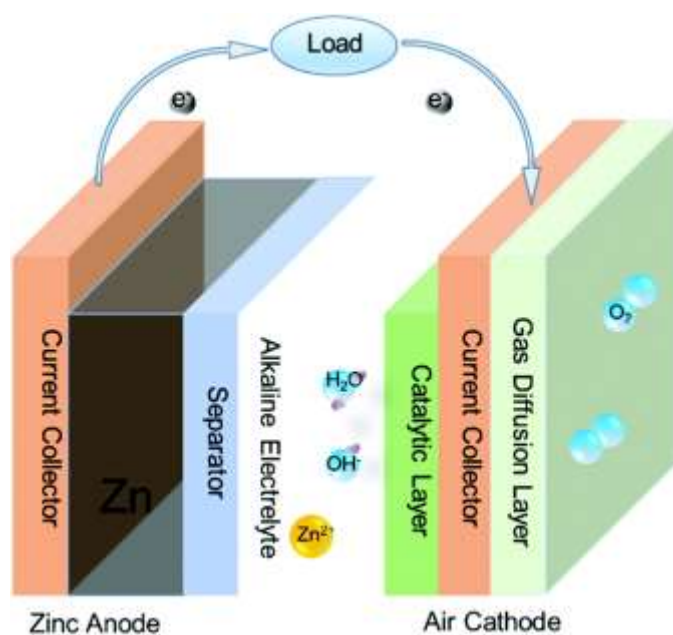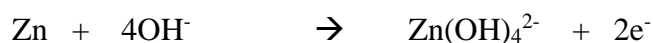
Fig. 12 Schematic showing Zinc-air battery configuration [49].

During the discharge of zinc-air battery following reactions takes place at the electrode:

At positive electrode oxygen is reduced to OH^- ions by the electrocatalyst [51–53]:

$$O_2 + 4e^- + 2H_2O \rightarrow 4OH^-$$

At negative electrode zinc oxidation takes place and soluble zincate ions are formed:

$$Zn + 4OH^- \rightarrow Zn(OH)_4^{2-} + 2e^-$$

Once the alkaline electrolytes reaches the supersaturated state, insoluble zinc oxide is formed by the decomposition of zincate ions:

$$Zn(OH)_4^{2-} \rightarrow ZnO + H_2O + 2OH^-$$

Overall reaction:

$$2Zn + O_2 \rightarrow 2ZnO$$
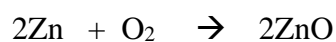
1.3.2.1 Cathode materials

In zinc-air batteries cathode is often referred as air electrode because oxygen diffuses through cathode and the reduction of oxygen to OH^- takes place. For a material to act as cathode for zinc-air batteries, it should have properties like high porosity and excellent electrocatalytic activity.

Zinc-air battery does not require precious metal catalyst like platinum and palladium for oxygen reduction reaction. It has been observed that the use of precious noble metals tends to decrease the performance of the battery once they diffuse to the zinc anode. These noble metal decrease the hydrogen overvoltage and thereby enhances the corrosion and gas production[54]. The electrocatalyst for zinc air batteries typically includes CNT mixed with CoO (**Fig. 13a**) [55], Mn_3O_4 nanoparticles loaded onto graphene (**Fig. 13b**) [56] and catalysts consisting of metal-nitrogen-carbon (M-N-C). These M-N-C type materials are synthesized by pyrolizing nitrogen precursors with metals like Fe- and Co- on carbon support [57,58]. The above mentioned electrolcatlayst shows better electrochemical performance in comparison to noble metal catalyst for primary zinc air batteries. The electrocatalyst is supported on to the porous carbon material to act as an air cathode for battery applications. In order to avoid the leakage of the alkaline electrolyte from the porous air electrode, it is often mixed with superhydrophobic materials like polytetrafluoroethylene (PTFE) for hydrophobization.
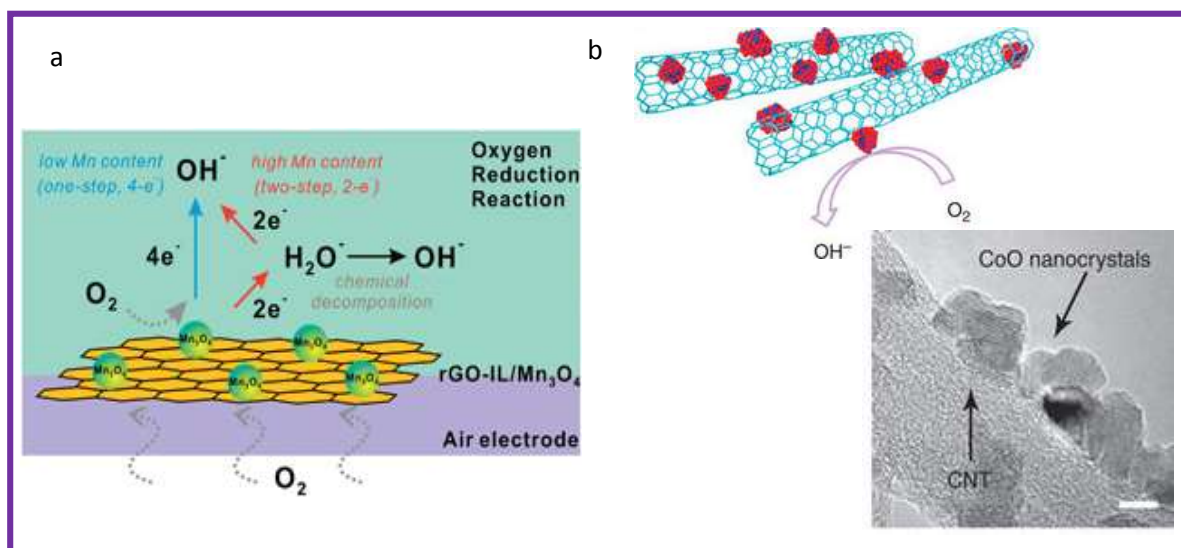
Fig. 13 (a) Schematic showing Mn_3O_4 nanoparticles supported over reduced graphene oxide for oxygen reduction reaction. (b) Illustration of CoO nanocrystals decorated CNT supported by TEM image [54][55].

1.3.2.2 Electrolytes

Zinc-air battery generally operates in alkaline medium like potassium hydroxide (KOH) or sodium hydroxide (NaOH) to achieve better performance [59]. KOH is considered most suitable electrolyte system because of its high conductivity, low cost, low viscosity and high oxygen diffusion coefficients [54]. Other electrolytes, like NaOH is considered as less active as the reaction products of NaOH with atmospheric CO_2 have lower solubility that leads to clogging of air electrode pores. The concentration of KOH is kept around 30 wt% for the electrolyte to minimize the zinc anode corrosion and evolution of hydrogen gas.

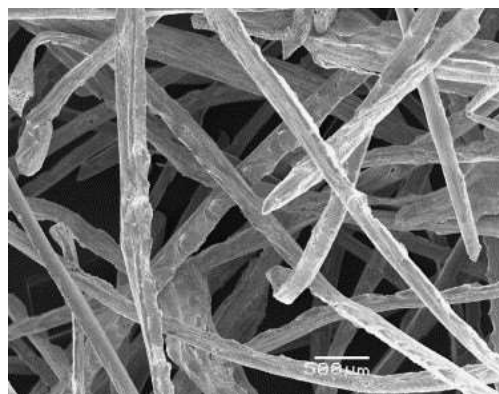### 1.3.2.3 Anode material

Zinc is employed as anode material for Zinc-air batteries as it features low equivalent weight, high specific energy density, abundance, low toxicity and above all it is the most electropositive metal stable in highly alkaline media. It was observed over the years that the zinc particles with high surface area are preferred for high performance in zinc-air batteries.
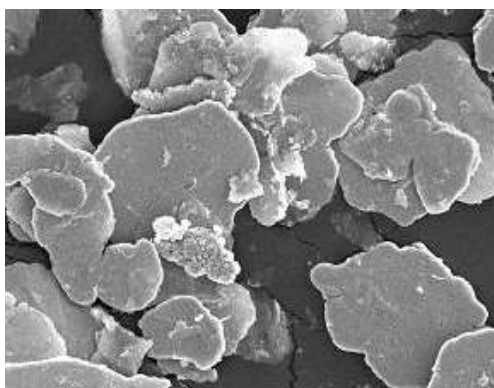
Zinc in various different states from sheet, fibres, flakes and ribbons have been developed for battery applications (**Fig. 14**) [50,60,61].
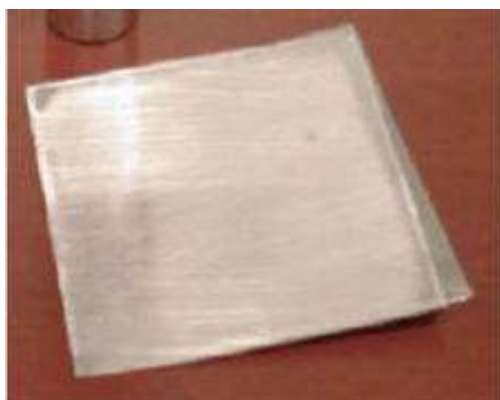
Zinc sheet

Zinc fibres

Zinc flakes
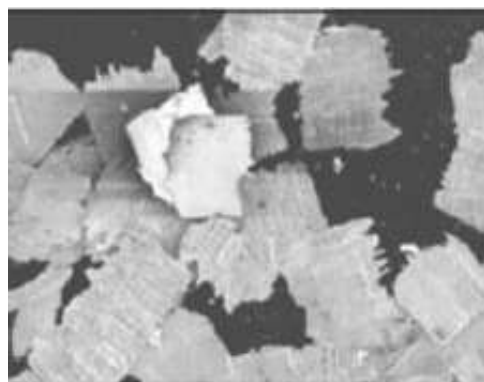
Zinc ribbons

Fig. 14 Various forms of zinc used in zinc-air batteries as anode materials [49][59][60].

But as the surface area of the zinc anode increases, the rate of corrosion also increases drastically and lowers the efficiency of the battery. Because of this, despite being relatively mature battery technology and early start, the zinc air battery applications were not extended because of the problem of self-corrosion. It applications are limited only in hearing aids or other medical and telecommunication fields due to its poor cycle life. Many attempts were made to slow down the dissolution of zinc in aqueous alkaline media or supress the self-corrosion. Previously, mercury was used along with zinc to reduce the self-corrosion but due

to high toxicity and environmental issues the use of mercury was stopped [62]. Different strategies were employed to replace the use of mercury and enhance the performance of zinc-air battery by lowering down the self-corrosion and H_2 evolution.

a) **Alloying**- To stabilize the zinc anode, it's alloying with different metals like cadmium, bismuth, tin, magnesium etc. was done. But this strategy could not bring up the change as most of the metals were non-toxic and dangerous for environment similar to mercury. One of the interesting and acceptable alloy of zinc and nickel gained attention, as it reduces the corrosion when compared with pure zinc. The impedance results and potentiodynamic experiments revealed that the corrosion rate was less after adding Ni and significant suppression in hydrogen gas evolution was seen by A.R El-Sayed et al [63].

b) **Additives**- Mixing of zinc with metal oxides like In_2O_3, Bi_2O_3, etc. was also evaluated as an effective approach to suppress H_2 evolution and improve battery performance [64].

c) **Surface coating-** Al_2O_3 was also mixed with zinc to evaluate the electrochemical performance of the battery [64]. And it was observed that among the three metal oxides, Al_2O_3 showed most favourable characteristics when mixed with zinc as anode. Therefore later it was surface coated over the zinc and the unit cell was fabricated for electrochemical measurements. It was observed that the surface modification was much more effective than just adding the metal oxide as additive. Discharge efficiency was greatly enhanced by coating Al_2O_3 on the surface of zinc and showed promising future (**Fig. 15b**).

In another study by Y. Cho et al., Lithium boron oxide (LBO) was coated over the zinc particles for surface modification [65]. The surface modified zinc particles with

LBO coating showed increased discharge capacity as shown in **Fig. 15a** and hydrogen evolution suppression. The enhanced performance of the cell fabricated by using LBO coated zinc as anode was attributed to the thin porous oxide layer that prevents the zinc electrode from corrosion in alkaline medium.
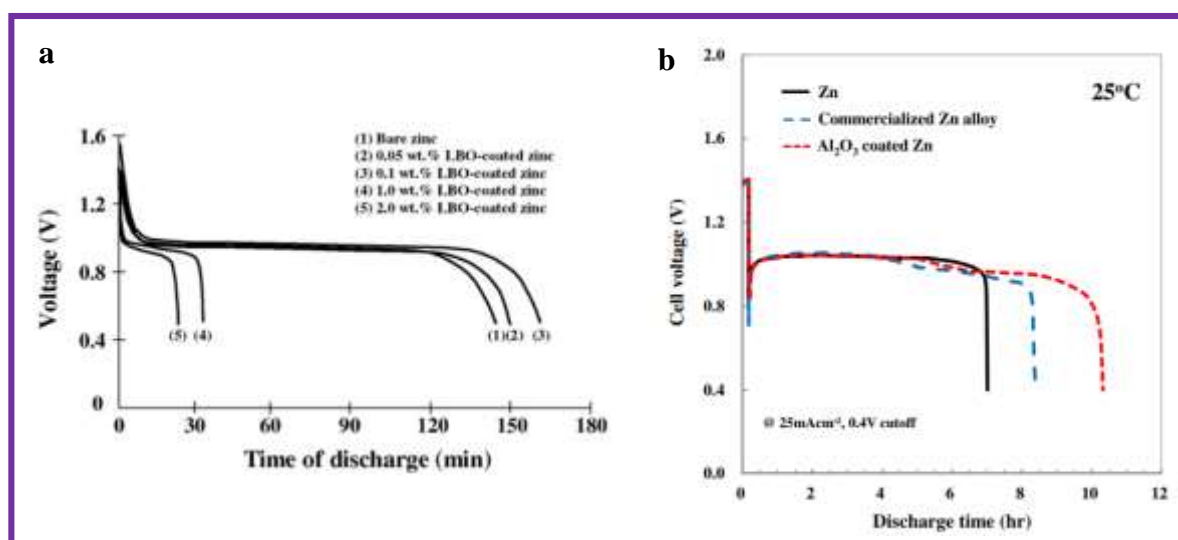
Fig. 15 (a) Comparison of discharge curves among bare zinc and LBO coated zinc, (b) Comparison of pure Zinc, commercialized zinc and Al_2O_3 coated zinc discharge profile in KOH electrolyte [63][64].

1.3.3 MOFs for surface modification of Zn anode for Zinc-air batteries

After taking inspiration from above literatures where surface modification of zinc showed outstanding results, for the first time we present the development of zinc–air batteries with an extended life by the use of modified MOFs leading to decreased self-corrosion, and improvement of discharge performance after anode modification.

1.4 MOFs for Oxygen Reduction Reaction (ORR) application

1.4.1 Oxygen Reduction Reaction- Introduction and challenges

Oxygen is the most abundant element in the earth's crust and very important for life processes. At the same time Oxygen Reduction Reaction (ORR) is also equally important not only for biological process but for electrochemical processes as well (including corrosion, sensors, metal-air batteries) especially in fuel cell applications [66–70]. The reduction of oxygen in aqueous electrolytic solutions occur mainly by two pathways – 1) the direct reduction from O_2 to H_2O by 4-electron process or 2) the 2-electron pathway where O_2 get reduced to H_2O_2 as shown in **Fig. 16**. Each pathway has its own importance and applications. The 2-electron pathway that leads to the formation of H_2O_2 is used in hydrogen peroxide production, while the 4-electron process is essential for metal-air batteries and fuel cell applications [71].
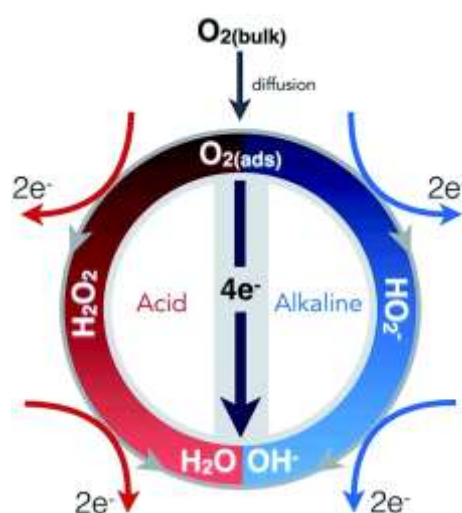

Fig. 16 Illustration of two different reduction pathways of oxygen in two different aqueous medium acidic and alkaline [70].

The mechanism of oxygen reduction reaction is quite complicated and includes formation of various intermediates, depending on the electrode material, electrolyte and catalyst. Table 1.3 mentions the ORR processes and respective thermodynamic electrode potentials are also listed [72].

Table 1.3 Thermodynamic electrode potentials of ORR processes [71].

Electrolyte	ORR reactions	Thermodynamic electrode potential at standard conditions, V
Acidic aqueous solution	$O_2 + 4H^+ + 4e^- \rightarrow H_2O$	1.229
	$O_2 + 2H^+ + 2e^- \rightarrow H_2O_2$	0.70
	$H_2O_2 + 2H^+ + 2e^- \rightarrow 2H_2O$	1.76
Alkaline aqueous solution	$O_2 + H_2O + 4e^- \rightarrow 4OH^-$	0.401
	$O_2 + H_2O + 2e^- \rightarrow HO_2^- + OH^-$	−0.065
	$HO_2^- + H_2O + 2e^- \rightarrow 3OH^-$	0.867
Non-aqueous aprotic solvents	$O_2 + e^- \rightarrow O_2^-$	Strongly dependent on solvent
	$O_2^- + e^- \rightarrow O_2^{2-}$	

The role of electrocatalysts in ORR is to facilitate the high current densities at potentials close to equilibrium potential. And the reduction of oxygen should be selectively by 4-electron process without the formation of hydrogen peroxide as it leads to corrosion. Sluggish kinetics of oxygen reduction reaction lowers down the overall performance of the cells, therefore the search for new and better electrocatalyst is a formidable challenge for the electrochemists. The solution of this problem can lead to massive transformation in the field of electrochemical energy storage and conversion.

Since the discovery of platinum took place for oxygen reduction reactions, platinum-based electrocatalysts is serving as one of the best for ORR undisputedly. But huge loading of

platinum is needed to overcome the sluggish kinetics of ORR that leads to very high cost [73]. The large scale commercialization of ORR based technologies is impeded by the problems like high cost, methanol poisoning etc. This has led to huge attention of researchers to substantially reduce the Pt loading or find inexpensive non-precious metal catalysts while maintaining its ORR activity.

1.4.2 MOFs derived electrocatalysts for ORR

It has been described previously that the high surface area and porosity of MOFs can be tailored by tuning the structure carefully [74,75]. Porous carbon derived from MOFs have gained tremendous attention in the search of developing high performance electocatlaysts for ORR [76–78]. They exhibit very high surface area, high porosity, corrosion resistant property and low cost which can be most attractive properties for ORR electrocatalysts. Though porous carbon can be synthesized by various other methods like pyrolysis and chemical activation of polymeric aerogels or organic precursors, the choice of precursor is crucial for making it highly active. Developing electrocatalysts from MOFs as novel precursor is greatly appreciated world-wide by the science communities. The synthesis of electrocatalysts from MOFs have completely overshadow the traditional synthesis because of several advantages such as: a) their structure can be tuned accordingly depending on targeted properties to achieve high pore volume and ultra-high surface area, b) the use of metal clusters as secondary building block in the synthesis of MOFs allows to implement transition metals with high electrocatalytic activity, c) and it also allows to easily impregnate several heteroatoms in the resulting porous carbon materials for high activity while selecting organic ligands which acts as a linker in MOF synthesis [75].

1.4.3 Metal free electrocatalysts derived from MOFs

Zhang et al. synthesized efficient metal free ORR catalyst by selecting chemically and thermally stable porous ZIF-8 as precursor and template (**Fig. 17a**) [79]. N-doped graphitic porous carbon polyhedras (NGPCs) featured high degree of graphitization, surface area and showed high electrocatalytic activities. The metal free electrocatalyst was synthesized using ZIF-8 precursor because of its high nitrogen content incorporated in the aromatic ring. It was observed with morphological characterization that the structure of parent NMOF was maintained after the pyrolysis in temperature range 700-1000 °C also (**Fig. 17b**). The cyclic voltammograms in 0.1 M KOH solution saturated with oxygen showed steep rise in reduction current and the shift in peak potentials was observed to higher voltages on increasing pyrolysis temperature. The catalyst obtained after 10h of pyrolysis at 1000 °C (NGPC-1000-10) revealed highest current density of 4.3 mA cm^{-2} comparable to Pt/C (4.5 mA cm-2) vs Ag/AgCl as shown in **Fig. 17c**. The same catalyst reduced oxygen by dominant 4-electron process with high cycling stability. The results showed promising nature of metal free electrocatalysts derived from MOF as an alternative to conventional Pt-based catalysts.
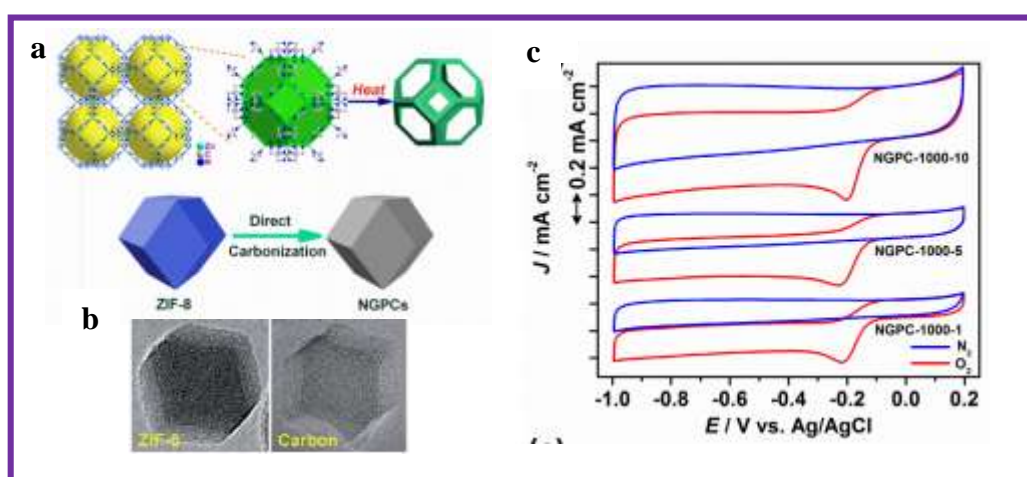

Fig. 17 (a) Illustration of ZIF-8 structure and synthesis of NGPCs after carbonization, (b) TEM images of ZIF-8 and NGPC showing retained structure of parent MOF, (c) CVs of NGPC-1000 showing effect of carbonization time on current density [78].

MOFs derived porous carbon materials to synthesize electrocatalyst has been explored by many reseachers. In a study by J. Li et al. MOFs was used as a template material to synthesize porous carbon material with ternary doping of nitrogen, phosphorus and sulphur for ORR [80]. These N, P and S heteroatom doping was done in porous carbon to increase its activity with the synergistic effect. The conventionally synthesized MOF-5 was completely dried and soaked in methanol solution of dicyandiamid (DCDA), triarylphosphine (TPP) and dimethyl sulfoxide (DMSO). The soaked MOF-5 in N, P and S precursors was then pyrolized at 900 $^{\circ}$C in presence of nitrogen and washed thoroughly with acid solution to remove trace metal before electrochemical measurements. The morphological characterizations showed that pore structure got changed after doping and the presence of new active sites are responsible for high catalytic activity. The synthesized NPS-C-MOF-5 also showed excellent methanol tolerance and stability compared to commercial Pt/C catalysts.

1.4.4 Non-precious metal electrocatalysts derived from MOFs

It is well known that non-precious metal catalysts are highly effective in enhancing the ORR activity due to its exposed active sites, electron transfer and low cost. In the vast library of synthesized MOFs, Zn and Co based MOFs are highly popular to generate non-precious metal catalysts for ORR. The active sites in the non-precious metal catalysts is the topic of debate till date. In recent studies it has been observed that the nitrogen-metal moieties on carbon support are highly active sites for the reduction of oxygen. Lou's group reported that N-doped carbon nanotube frameworks (NCNTFs) (**Fig. 18a**) designed by pyrolizing ZIF-67 in H_2/Ar atmosphere are highly active electrocatalyts for ORR and OER [77]. ZIF-67 served as a single precursor for the formation of crystalline NCNTFs and also acted as a source of carbon and nitrogen for the growth. The electrochemical performance of the crystalline NCNTFs as

bifunctional oxygen electrocatalyst completely overshadowed the performance of Pt/C catalyst as shown in **Fig. 18b**.

J. Wei et al. developed porous Co-N$_x$/C catalysts (ZIF/rGO-700-AL) by graphene-directed route as high performance ORR catalyst (**Fig. 18c**) [81]. The epoxy and hydroxyl functional groups present on graphene oxide directed the synthesis of ZIF nanocrystals by coordinating with metal ion (Co^{2+}) of ZIF. After the growth of ZIF crystals over GO sheets the composite material was carbonized at 700 °C for 3 h in argon atmosphere. The embedded Co particles on the carbon matrix of GO was observed by TEM. The hierarchically porous Co-N$_x$/C catalysts possess extremely high surface area, open active sites and enhanced electrical conductivity. Outstanding stability and high ORR catalytic activity was observed by electrochemical measurements in both alkaline and acidic medium (**Fig. 18d**).
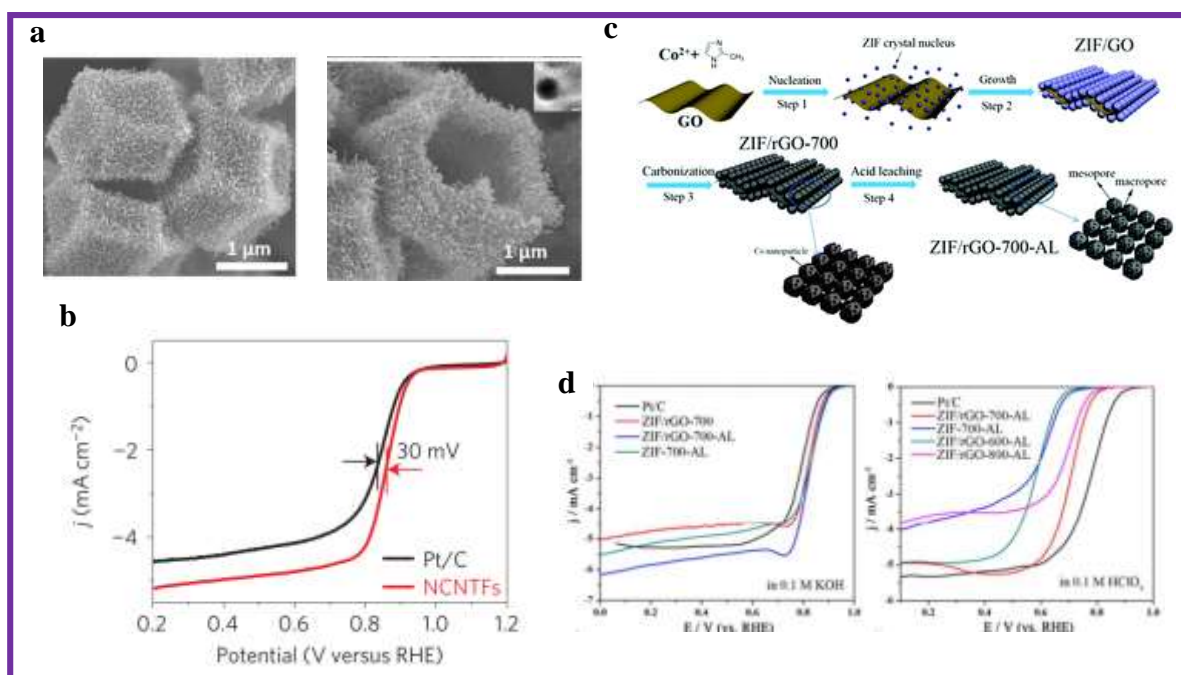

Fig. 18 (a) FESEM images of NCNTFs, (b) LSV curves of NCNTFs and Pt/C catalyst, (c) Schematic showing the preparation of nanoporous Co-N$_x$/C catalyst, (d) LSV curves of ZIF/rGO-700-AL catalyst in alkaline and acidic medium [76][80].

1.4.5 Non-carbonized metal electrocatalysts from MOFs

Jiang et al. reported the utilization of copper containing MOF with highly porous nanocage structure as non-precious metal catalysts for ORR [82]. A novel MOF (NPC-4) was synthesized by assembling methyl functionalized carboxylate connected with di-copper paddle-wheel to give nano porous cage like structure. The high O_2 uptake capacity was observed for novel MOF after complete activation of MOF pores by solvent exchange method. To enhance the activity of NPC-4, the detachment of catalyst was avoided by introducing reduced graphene oxide (RGO) immobilized glassy carbon electrode as an electron transfer mediator. The synthesized NPC-4/RGO electrocatalyst shifts the onset potential to more positive side at -0.13 V vs Ag/AgCl compared to already reported MOF derived catalysts. The usage of RGO and MOF with activated pores leads the reduction of oxygen by 2-4 electron pathway and opens up new direction in various fields.

In another report, pyridine modified graphene was used as building block for the growth of MOF by M. Jahan et al [83]. In this study, the RGO was functionalized with pyridine ligands which acts as struts to attach metalloporphyrin nodes for the formation of hybrid graphene-MOF structure (**Fig. 19**). Also, RGO attributed to the enhanced electrocatalytic activity by serving as electron mediator and effect of its weight % also influences the catalytic activity. The synergistic effect of RGO and pyridinium linker leads to the improved crystallization of iron porphyrin catalysts and helps in reduction of oxygen via 4 electron process. The composite also showed excellent methanol tolerance and higher selectivity for oxygen reduction compared to other reported catalysts.
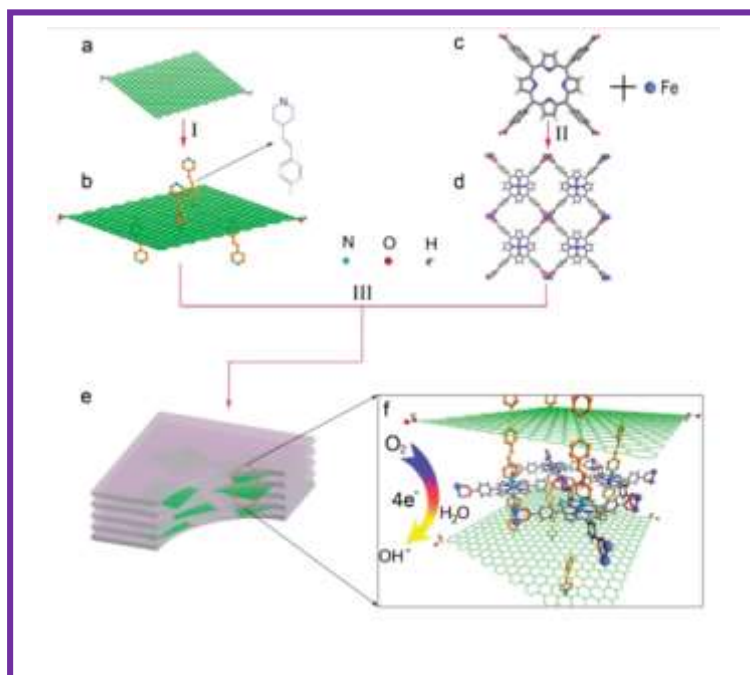
Fig. 19 Schematic showing the process for the formation of graphene-porphyrin MOF composite [82].

1.5 Research Outlook

All these above mentioned reports confirms the capability of MOF as an effective material in the field of energy storage and conversion because of its fascinating properties. Over the time many strategies were adapted as discussed above to employ MOFs and MOF derived materials to improve the performance of the energy storage devices. These interesting results have raised the interest of researchers to exploit the highly advantageous features of MOF in various fields of energy storage.

The above mentioned work in various literatures inspires us to utilize MOFs in energy storage materials and help in the development of the society. Hence, the present work aims to utilize MOF in three different fields discussed below:

1) Li-ion batteries- An attempt will be made with ionic liquid incorporated modified MOFs to serve as a better and safer electrolyte system for Li-ion batteries with increased thermal stability, high ionic conductivity and other electrochemical aspects.

2) Zinc-air batteries-Further, dimensionally and morphologically controlled MOFs will be decorated over anode carefully to reduce self -corrosion of the negative zinc electrode, reduce dendrite formation, and improve discharge performance.

3) ORR electrocatalysts- MOFs with active carbon material will be tested for its efficiency as electrocatalysts for ORR and its methanol tolerance will also be evaluated for application in fuel cells and metal-air batteries.

Successful completion of this research would yield electrochemical energy devices of high performance and prolonged cyclability.

1.6 References

[1]   H. B. Wu, X. W. Lou, Sci. Adv. 3 (2017) 9252.

[2]   J. L. C. Rowsell, O. M. Yaghi, Microporous Mesoporous Mater. 73 (2004) 3.

[3]   H. C. Zhou, J. R. Long, O. M. Yaghi, Chem. Rev. 112 (2012) 673.

[4]   B. Li, H. M. Wen, W. Zhou, B. Chen, J. Phys. Chem. Lett. 5 (2014) 3468.

[5]   H. Wang, Q.-L. Zhu, R. Zou, Q. Xu, Chem 2 (2017) 52.

[6]   Y. Zhao, Z. Song, X. Li, Q. Sun, N. Cheng, S. Lawes, X. Sun, Energy Storage Mater.
2 (2016) 35.

[7]   N. Stock, S. Biswas, Chem. Rev. 112 (2011) 933.

[8]   D. Deng, Energy Sci. & Eng. 3 (2015) 385.

[9]   C. K. Chan, X. F. Zhang, Y. Cui, Nano Lett. 8 (2008) 307.

[10]   S. Goriparti, E. Miele, F. De Angelis, E. Di Fabrizio, R. Proietti Zaccaria, C. Capiglia,
J. Power Sources 257 (2014) 421.

[11]   P. Roy, S. K. Srivastava, J. Mater. Chem. 3 (2015) 2454.

[12]   R. Dash, S. Pannala, Sci. Reports 6 (2016) 27449.

[13]   S. T. Myung, F. Maglia, K. J. Park, C. S. Yoon, P. Lamp, S. J. Kim, Y. K. Sun, ACS
Eergy Lett. 2 (2016) 196.

[14]   M. Mancini, P. Axmann, G. Gabrielli, M. Kinyanjui, U. Kaiser, M. Wohlfahrt-
Mehrens, ChemSusChem 9 (2016) 1843.

[15]   A. Van der Ven, J. Bhattacharya, A. A. Belak, Accounts Chem. Res. 46 (2012) 1216.

[16]   L. Tian, Q. Zhuang, J. Li, Y. Shi, J. Chen, F. Lu, S. Sun, Chin. Sci. Bull. 56 (2011)
3204.

[17]   R. Chen, T. Zhao, X. Zhang, L. Li, F. Wu, Nanoscale Horizons 1 (2016) 423.

[18]   Z. Lu, D. D. MacNeil, J. R. Dahn, Electrochem. Solid-State Lett. 4 (2001) A191.

[19]   K. Mizushima, P. C. Jones, P. J. Wiseman, J. B. Goodenough, Mater. Res. Bull. 15 (1980) 783.

[20]   K. M. Shaju, G. V. Subba Rao, B. V. R. Chowdari, Electrochim. Acta 48 (2002) 145.

[21]   B. Ammundsen, J. Paulsen, Adv. Mater. 13 (2001) 943.

[22]   H. W. Lee, P. Muralidharan, R. Ruffo, C. M. Mari, Y. Cui, D. K. Kim, Nano Lett. 10 (2010) 3852.

[23]   J. H. Kim, S. T. Myung, Y. K. Sun, Electrochimica Acta 49 (2004) 219.

[24]   Z. Gong, Y. Yang, Energy & Environ. Sci. 4 (2011) 3223.

[25]   L. Liu, B. Zhang, X. Huang, Prog. Nat. Sci. Mater. Int. 21 (2011) 211.

[26]   H. Chen, G. Hautier, A. Jain, C. Moore, B. Kang, R. Doe, L. Wu, Y. Zhu, Y. Tang, G. Ceder, Chem. Mater. 24 (2012) 2009.

[27]   B. Wang, B. Luo, X. Li, L. Zhi, Mater. Today 15 (2012) 544.

[28]   M. N. Obrovac, V. L. Chevrier, Chem. Rev. 114 (2014) 11444.

[29]   J. Yin, M. Wada, S. Yoshida, K. Ishihara, S. Tanase, T. Sakai, J. Electrochem. Soc. 150 (2003) A1129.

[30]   D. Deng, M. G. Kim, J. Y. Lee, J. Cho, Energy & Environ. Sci. 2 (2009) 818.

[31]   F. Ozanam, M. Rosso, Mater. Sci. Eng. 213 (2016) 2.

[32]   Y. Zhang, X. G. Zhang, H. L. Zhang, Z. G. Zhao, F. Li, C. Liu, H.M. Cheng, Electrochim. Acta 51 (2006) 4994.

[33]   S. Bourderau, T. Brousse, D. M. Schleich, J. Power Sources 81-82 (1999) 233.

[34]   V. Baranchugov, E. Markevich, E. Pollak, G. Salitra, D. Aurbach, Electrochem. Commun. 9 (2007) 796.

[35]   H. P. Chen, J. W. Fergus, B. Z. Jang, J. Electrochem. Soc. 147 (2000) 399.

[36]   T. Vogl, S. Menne, A. Balducci, Phys. Chem. Chem. Phys. 16 (2014) 25014.

[37]   A. Lewandowski, A. Świderska-Mocek, J. Power Sources 194 (2009) 601.

[38]   M. Ishikawa, T. Sugimoto, M. Kikuta, E. Ishiko, M. Kono, J. Power Sources 162 (2006) 658.

[39]   G. P. Pandey, S. A. Hashmi, J. Mater. Chem. 1 (2013) 3372.

[40]   D. Wei, A. Ivaska, Anal. Chim. Acta 607 (2008) 126.

[41]   V. V. Singh, A. K. Nigam, A. Batra, M. Boopathi, B. Singh, R. Vijayaraghavan, Int. J. Electrochem. 2012 (2012) 1.

[42]   D. Bresser, S. Passerini, B. Scrosati, Chem. Commun. 49 (2013) 10545.

[43]   B. M. Wiers, M. L. Foo, N. P. Balsara, J. R. Long, J. Am. Chem. Soc. 133 (2011) 14522.

[44]   C. Yuan, J. Li, P. Han, Y. Lai, Z. Zhang, J. Liu, J. Power Sources 240 (2013) 653.

[45]   C. Gerbaldi, J. R. Nair, M. A. Kulandainathan, R. S. Kumar, C. Ferrara, P. Mustarelli, A.M. Stephan, J. Mater. Chem. 2 (2014) 9948.

[46]   K. Fujie, R. Ikeda, K. Otsubo, T. Yamada, H. Kitagawa, Chem. Mater. 27 (2015) 7355.

[47]   K. N. Jung, S. M. Hwang, M. S. Park, K. J. Kim, J. G. Kim, S. X. Dou, J. H. Kim, J.-W. Lee, Sci. Reports 5 (2015) 7665.

[48]   Y. Li, H. Dai, Chem. Soc. Rev. 43 (2014) 5257.

[49]   J. S. Lee, S. Tai Kim, R. Cao, N. S. Choi, M. Liu, K. T. Lee, J. Cho, Adv. Energy Mater. 1 (2011) 34.

[50]   X. Cai, L. Lai, J. Lin, Z. Shen, Mater. Horizons 4 (2017) 945.

[51]   M. Prabu, P. Ramakrishnan, H. Nara, T. Momma, T. Osaka, S. Shanmugam, ACS Appl. Mater. & Interfaces 6 (2014) 16545.

[52]   X. Wang, P. J. Sebastian, M. A. Smit, H. Yang, S. A. Gamboa, J. Power Sources 124 (2003) 278.

[53]   A. A. Mohamad, J. Power Sources 159 (2006) 752.

[54]   V. Caramia, B. Bozzini, Mater. Renew. Sustain. Energy 3 (2014) 1.

[55]   Y. Li, M. Gong, Y. Liang, J. Feng, J. E. Kim, H. Wang, G. Hong, B. Zhang, H. Dai, Nat. Commun. 4 (2013) 1805.

[56]   J. S. Lee, T. Lee, H. K. Song, J. Cho, B. S. Kim, Energy & Environ. Sci. 4 (2011) 4148.

[57]   C. W. B. Bezerra, L. Zhang, K. Lee, H. Liu, A. L. B. Marques, E. P. Marques, H. Wang, J. Zhang, Electrochim. Acta 53 (2008) 4937.

[58]   M. Lefèvre, E. Proietti, F. Jaouen, J. P. Dodelet, Science 324 (2009) 71.

[59]   S. H. Lee, D. J. Park, W. G. Yang, K. S. Ryu, Ionics 23 (2017) 1801.

[60]   C. J. Lan, T. S. Chin, P. H. Lin, T. P. Perng, J. New Mater. Electrochem. Syst. 9 (2006) 27.

[61]   X. G. Zhang, J. Power Sources 163 (2006) 591.

[62]   H. Zhou, Q. Huang, M. Liang, D. Lv, M. Xu, H. Li, W. Li, Mater. Chem. Phys. 128 (2011) 214.

[63]   A. R. El-Sayed, H. S. Mohran, H. M. Abd El-Lateef, Metall. Mater. Trans. 43 (2011) 619.

[64]   S. M. Lee, Y. J. Kim, S. W. Eom, N. S. Choi, K. W. Kim, S. B. Cho, J. Power Sources 227 (2013) 177.

[65]   Y. D. Cho, G. T. K. Fey, J. Power Sources 184 (2008) 610.

[66]   H. Zhu, S. Zhang, Y.-X. Huang, L. Wu, S. Sun, Nano Lett. 13 (2013) 2947.

[67]   K. I. Ozoemena, RSC Adv. 6 (2016) 89523.

[68]   W. T. Yao, L. Yu, P. F. Yao, K. Wei, S. L. Han, P. Chen, J.-S. Xie, ACS Sustain. Chem. & Eng. 4 (2016) 3235.

[69]   C. Zhu, H. Li, S. Fu, D. Du, Y. Lin, Chem. Soc. Rev. 45 (2016) 517.

[70]   J. Kang, H. Kim, N. Saito, M.-H. Lee, Sci. Technol. Adv. Mater. 17 (2016) 37.

[71]   D. Shin, B. Jeong, M. Choun, J. D. Ocon, J. Lee, RSC Adv. 5 (2015) 1571.

[72]   C. Song, J. Zhang, Electrocatalytic Oxygen Reduction Reaction. In PEM Fuel Cell Electrocatalysts and Catalyst Layers; Springer (2008) 89.

[73]   Y. Nie, L. Li, Z. Wei, Chem. Soc. Rev. 44 (2015) 2168.

[74]   W. Lu, Z. Wei, Z.-Y. Gu, T.-F. Liu, J. Park, J. Park, J. Tian, M. Zhang, Q. Zhang, T. Gentle Iii, M. Bosch, H.-C. Zhou, Chem. Soc. Rev. 43 (2014) 5561.

[75]   M. H. Yap, K. L. Fow, G. Z. Chen, Green Energy & Environ. 2 (2017) 218.

[76]   S. Zhao, H. Yin, L. Du, L. He, K. Zhao, L. Chang, G. Yin, H. Zhao, S. Liu, Z. Tang, ACS Nano 8 (2014) 12660.

[77]   B. Y. Guan, L. Yu, X. W. Lou, Energy & Environ. Sci. 9 (2016) 3092.

[78]   W. Wang, X. Xu, W. Zhou, Z. Shao, Adv. Sci. 4 (2017) 1600371.

[79]   L. Zhang, Z. Su, F. Jiang, L. Yang, J. Qian, Y. Zhou, W. Li, M. Hong, Nanoscale 6 (2014) 6590.

[80]   J.-S. Li, S.-L. Li, Y.-J. Tang, K. Li, L. Zhou, N. Kong, Y.-Q. Lan, J.-C. Bao, Z.-H. Dai, Sci. Reports 4 (2014) 5130.

[81]   J. Wei, Y. Hu, Z. Wu, Y. Liang, S. Leong, B. Kong, X. Zhang, D. Zhao, G. P. Simon, H. Wang, J. Mater. Chem. 3 (2015) 16867.

[82]   M. Jiang, L. Li, D. Zhu, H. Zhang, X. Zhao, J. Mater. Chem. 2 (2014) 5323.

[83]   M. Jahan, Q. Bao, K. P. Loh, J. Am. Chem. Soc. 134 (2012) 6707.

Chapter 2

Modified Metal Organic Frameworks (MOFs)/Ionic Liquids Matrices for Efficient Charge Storage in Li-ion Batteries

Abstract

In this study, an ionic liquid incorporated modified MOF was synthesized to serve as an efficient electrolyte system for Li-ion batteries. Further, the MOF (IL) was doped with a lithium salt, lithium bis(triflouromethylsulfonyl) imide (LiTFSI) by a modified procedure. Samples with varying amount of MOF (IL) in ionic liquid were prepared, characterized and evaluated for their electrochemical behavior. A high conductivity in order of $10^{-2} - 10^{-3}$ Scm^{-1} at 51 ºC and a low activation energy of ion transport was observed in all samples. The systems showed high electrochemical stability to be employed as gel electrolyte in Li-ion secondary batteries. These systems showed highly reversible capacity of over 3000 mAhg^{-1} in the charge-discharge studies carried out after fabricating anodic half-cell composed of Si/electrolyte/Li. These results illustrate the feasibility of the prepared modified MOF (IL) as potential solid state electrolytes for Li-ion secondary batteries.

2.1 Introduction

Metal Organic Frameworks (MOFs) [1] or coordination polymers are of extreme interest due to several unique features and their applications in the fields of gas storage [2,3], separation [4], catalysis [5,6], sensors [7] and these have been studied extensively as ionic conductors [8–12]. Apart from these properties, an extraordinary feature of MOFs which makes them more interesting is that the supramolecular design of MOFs allows easy tunability depending upon the organic ligands and metal centres giving a versatile desirable properties in synthesized matrices. Recently many studies have been conducted for the application of MOFs in electrochemical energy storage devices especially, Li-ion batteries.

C. Yuan *et al*. [13] reported that the use of nano sized particles of MOF with Lewis acidic surface are of special interests to increase ionic conductivity. These porous fillers with large surface-to-volume ratio are more helpful to stabilize the electrolyte/Li interface. B. M. Wiers *et al*. [11], synthesized a solid lithium electrolyte by the addition of lithium isopropoxide (LiO^{i}Pr) to a Mg_2(dobdc) (dobdc^{4-} = 1,4-dioxido-2,5-benzenedicarboxylate) MOFs with open metal sites. The resulting electrolyte showed enhanced ionic conductivity of 3.1×10^{-4} Scm^{-1} at 300 K. C. Gerbaldi *et al*. [14] synthesized a poly(ethylene oxide)-based nanocomposite polymer electrolyte (NCPE), prepared by the incorporation of specific amounts of aluminium(III)-1,3,5-benzenetricarboxylate (Al-BTC) MOFs as filler for all-solid-state LiB to improve the ionic conductivity.

Simultaneously, ionic liquids have also gained significant attention in the fields of catalysis [15,16], extraction [17,18], electrochemistry [19] and chemical reactions as green solvents [20,21] owing to their exclusive properties such as high solubility, non-volatility, non-flammablility, wide electrochemical window and high thermal stability [22]. Ionic liquid due

to their inflammable property and designability allows many possibilities for new MOFs. Ionic liquid incorporated MOFs have been studied widely in the fields of catalysis [23,24] and gas adsorbents [25]. Very recently H. Kitagawa *et al*. [26] studied lithium ion diffusion in ionic liquid incorporated MOFs. In these studies, ionic conductivity and Li-ion diffusion was looked upon.

However, till date there are no reports on charge-discharge behaviour of lithium ion secondary batteries fabricated using such electrolytes. In the present work, dimensionally and morphologically controlled MOFs was carefully used to ease the ion transport in the electrolyte system. The obtained MOF based solid ion-gel electrolyte enabled efficient charge-discharge behaviour with maximum discharging capacity of over 3000 mAhg^{-1} with a Si anode.

Why MOF-5?

The initial choice of MOF was MOF-5 because there are numerous reports focussing on the electrochemical preparation. Also apart from having high surface area, MOF-5 also shows high porosity and thermal stability. The preparation of MOF-5 allows to keep metal salt concentration little higher that can generate more Zn_4O clusters [13]. These metal clusters enables the MOF to have more number of Lewis acidic sites which can be helpful in anion trapping for enhanced conductivity.
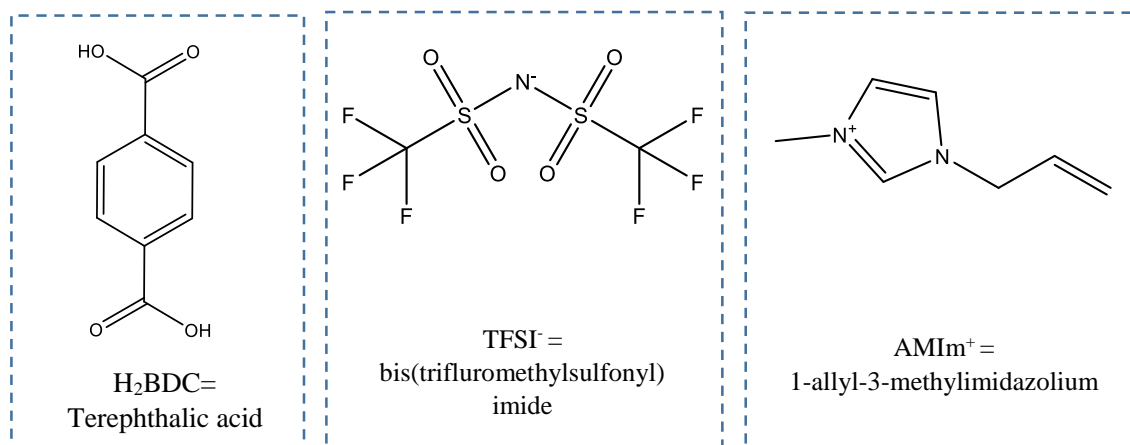
2.2 Experimental

1-Allyl-3-methylimidazolium bis(trifluoromethylsulfonyl) imide (AMImTFSI) was synthesized according to the literature [27]. MOF (IL) was synthesized with a modification in an already reported electrochemical method [28] and with an introduction of different ionic liquid. Dimethylformamide (DMF) and tetrahydrofuran (THF) was purchased from WAKO Co. Ltd. and used as received. Chloroform, for washing the product, was purchased from WAKO Co. Ltd. Scanning Electron Microscopy (SEM) analysis was done on a Hitachi S-4500 (Hitachi Ltd., Chiyoda-ku, Japan). X-ray diffraction data was collected using Rigaku SmartLab (Rigaku, Japan) operating at 40 kV, 30 mA at a rate of 1° min^{-1}, using Cu Kα radiation. Ionic conductivity was measured with a complex-impedance gain phase analyzer (Solartron model 1260; Schlumberger, Germany) under the frequency range from 0.1 Hz to 1 MHz. DC current measurements were carried out on ECstat-100 (EC-FRONTIER Co. Ltd., Japan). Linear sweep voltammetry measurements were carried out on Biologic VSP s/n 1190.

For charge-discharge studies, silicon based anodic half-cell was prepared using CR2025 type coin cells with silicon as the working electrode (ϕ15 mm, Kindly donated by NISSAN Co.), lithium metal as the counter electrode (ϕ15mm, Honjo metals, Japan) and a disc shaped polypropylene based membrane (Celgard$^{\circledR}$) as separator (16 mm). The prepared silicon based anodic half-cell was charged and discharged in a galvanostatic mode with a cut off potentials limit (2.1 V to 0.03V) at a current rate of 0.1C (0.0172 mA) using compact charge and discharge system of EC Frontier; ECAD-1000.

2.2.1 *Synthesis of MOF/ionic liquid matrix by electrochemical method* [28] : Synthesis of the MOF (AMImTFSI) was achieved by a constant dissolution of Zn^{2+} ion from Zn anode (**Scheme 1**). The dissolution was carried out by applying a constant direct current (DC) of 150 mA. A

titanium electrode was employed as cathode. The electrolyte used in this procedure was a solution containing terephthalic acid (H$_2$BDC) (0.5 g, 0.003 moles), zinc nitrate hexahydrate (0.65 g, 0.002 moles) and (1-allyl-3-methylimidazolium bis(trifluoromethylsulfonyl) imide) AMImTFSI (4.6 g, 0.011 moles) in DMF (50 mL). The electrochemical galvanostatic procedure was carried out for 4 hours at room temperature. A white powder formed during the procedure, was filtered and washed with DMF first and then with chloroform. The sample was then dried in oven at 80 ºC under vacuum to afford pure MOF (AMImTFSI) or MOF (IL) **1** (**Fig. 1**).

Scheme 1

0.5g H$_2$BDC   +   0.65g Zn(NO$_3$)$_2$.6H$_2$O   +   4.6g AMImTFSI $\xrightarrow[\text{4 h}]{\text{DMF (45 mL)}}$ MOF-5 (AMImTFSI) **1**

H$_2$BDC=
Terephthalic acid

TFSI⁻ =
bis(trifluromethylsulfonyl) imide

AMIm⁺ =
1-allyl-3-methylimidazolium
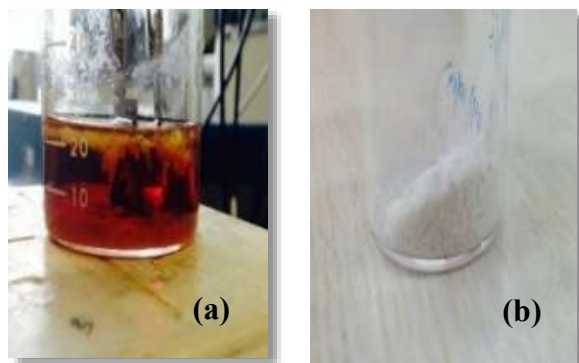
Fig. 1 (a) A white colour MOF (IL) floating during
electrochemical synthesis at room temperature, **(b)** MOF (IL)
crystals after drying at 80 °C under vacuum.

2.2.2 _Lithium salt doping in MOF/ionic liquid matrix by grafting method_ [12] *:* Synthesized

MOF (IL) **1** sample was activated at 120 °C under vacuum for 24 hours, and the activated MOF

(IL) **1** was then soaked in 1.0 M solution of Li-TFSI in THF for 3 days at 80 °C. After treating

Li-TFSI (THF) for three days, the sample was washed three times with 20 mL of fresh THF by

centrifugation. The sample was then kept for overnight activation under vacuum at 120 °C to

obtain lithium incorporated MOF (IL) **2**.

2.3 Characterization

The synthesized AMImCl prepared according to the literature [27] was characterized

using 400 MHz nuclear magnetic resonance (NMR) spectrometer (Bruker) by ^{1}H NMR in

DMSO as shown in **Fig. 2**. Anion exchange of AMImCl was carried out with LiTFSI leading

to the formation of AMImTFSI. Silver nitrate test was performed to determine the completion

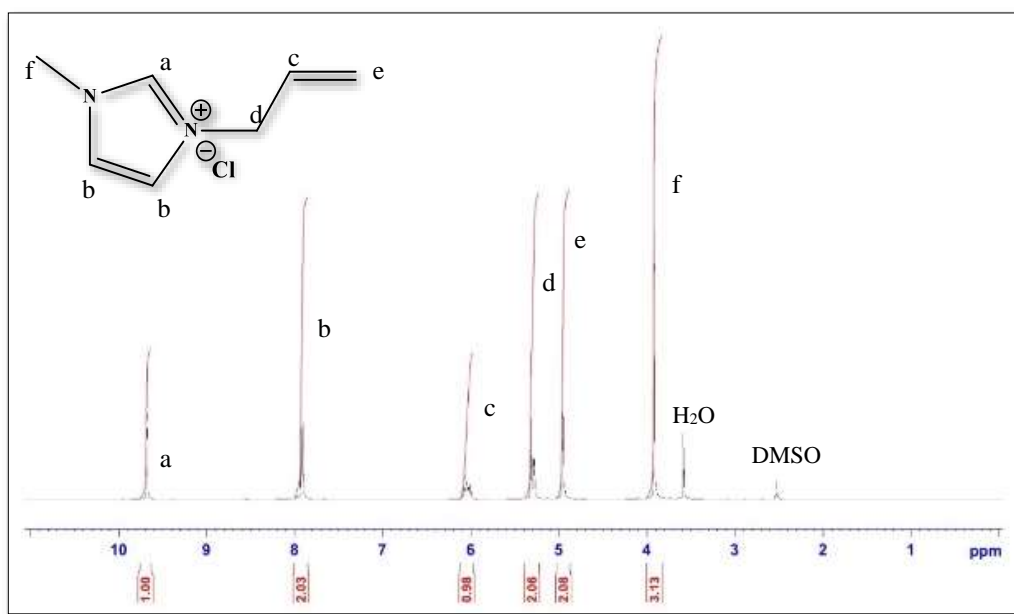of successful ion exchange (**Fig. 3 and 4**).
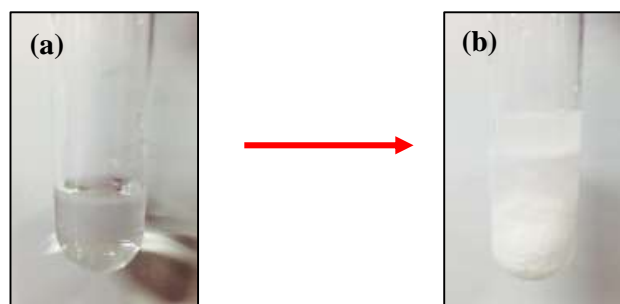
Fig. 2 ^{1}H NMR spectrum of AMImCl in DMSO.

Fig. 3 AMImCl **(a)** before and **(b)** after silver nitrate test.
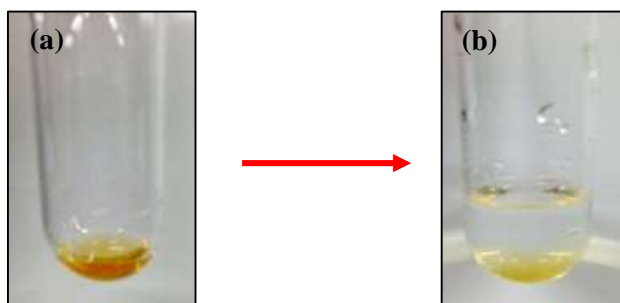

Fig. 4 AMImTFSI **(a)** before and **(b)** after silver nitrate test.

The MOF (IL) **1** matrix, obtained as white crystalline material was characterized by XRD, FTIR, and SEM and was then subjected to electrochemical measurements for further analysis. X-ray diffractograms were shown in **Fig. 5.** XRD pattern of the ionic liquid modified MOF-5 is different from the conventional MOF-5. The Metal Organic Frameworks are very flexible and can change their structure to great extent on solvent removal [29]. A number of reports identify this aspect in MOF-5 and have substantiated it beyond any doubt. Similarly, in the present studies too, the XRD pattern of as-synthesized (blue) MOF (IL) is in good agreement with peaks observed in case of pure MOF-5 (red). But when the sample is washed and dried, the peaks shifts towards larger angles. When the solvent is removed in case of MOF (IL), the side chains of ionic liquid interacts strongly, leading to the complete contraction of MOF (IL).
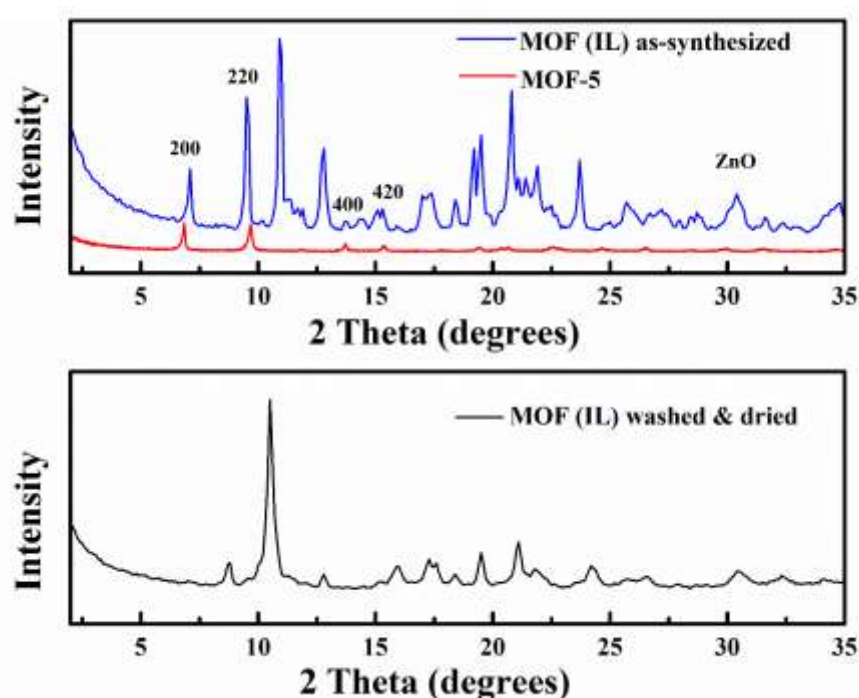

Fig. 5 X-ray diffractograms of conventional MOF-5, MOF (IL) as-synthesized (without washing) and MOF (IL) washed and dried **1**.

The FT-IR spectra in **Fig. 6** confirmed the formation of matrix, well resembling that of MOF-5. The peak present at 1665 cm^{-1} in the IR spectra indicates the shift in the peak position for the carboxylate group of BDC (1,4 benzenedicarboxylate) linker from 1610 cm^{-1}, due to interaction with the Zn$_4$O clusters, showing the presence of bonding between organic linker and metal species. The deprotonated carboxylic acid linker bonded to the MOF-5 metal centre is also indicated by the peak at 1436 cm^{-1} [30]. These two peaks suggest that there is a bonding indicative of MOF-5. The peaks at 1505 cm^{-1} and 1597 cm^{-1} were indicative of the asymmetric stretching vibrations and the peak at 1388 cm^{-1} due to the symmetrical stretching vibration of the carboxylic acid groups in BDC. Peaks in the range of 1284–730 cm^{-1} can be attributed to the in-plane vibration of the BDC group. The two peaks in the range of 740–830 cm^{-1} are due to CH=CH aromatic plane bends, which show that the phenyl ring was 1,4-substituted [28]. And the new peak in the spectrum of MOF (IL) **1** at around 1322 cm^{-1} can be attributed to C-N stretch confirming the presence of ionic liquid in MOF matrix.
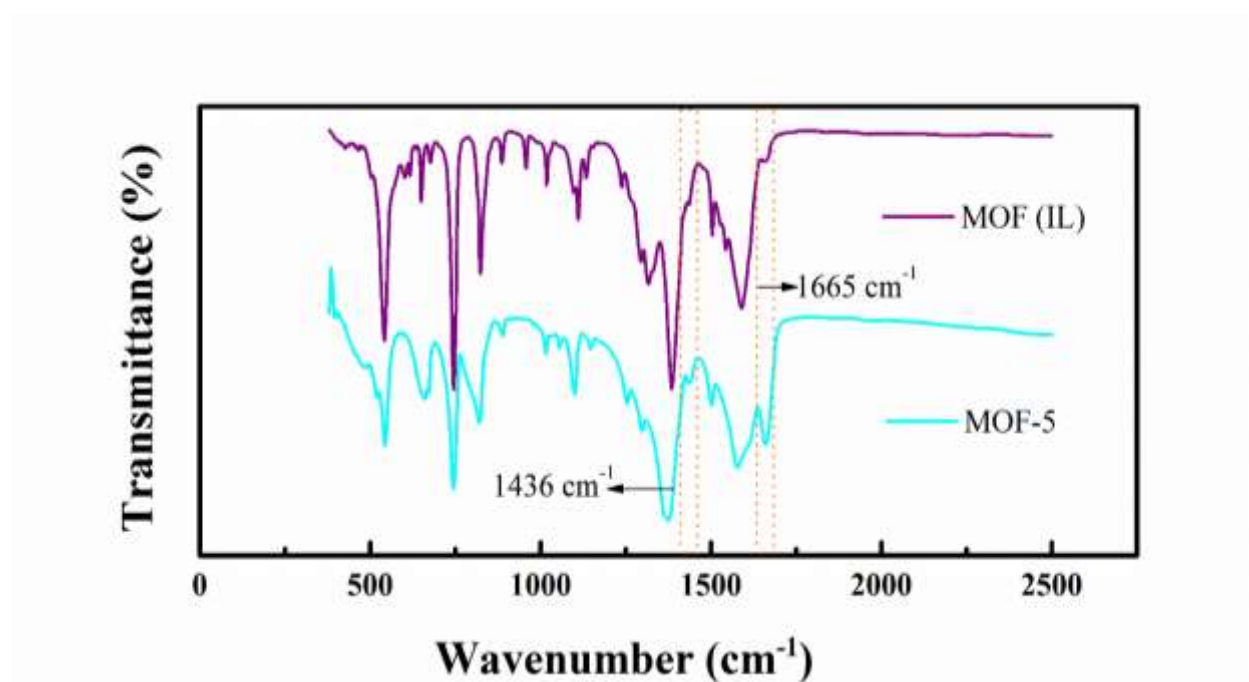

Fig. 6 Infrared spectra of conventional MOF-5 and MOF (IL) **1**.

Morphological characterization of synthesized MOF (IL) **1** was done by SEM. **Fig. 7** shows a SEM image of MOF (IL) **1** synthesized by electrochemical method showing a specific flower shaped geometry. This indicated that the morphology of MOFs depends both on the synthetic methods and ionic liquid system used as template.
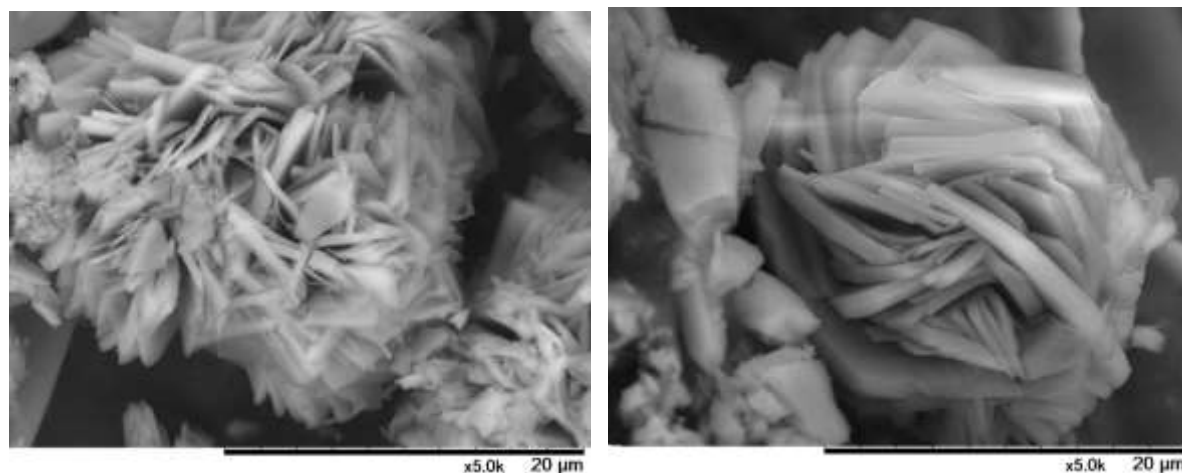

Fig. 7 SEM images of MOF (IL) **1** showing flower shaped morphology.

2.4. Results and Discussion

2.4.1 Ionic conductivity

Three samples with different weight % of **2** in AMImTFSI were prepared and ionic conductivity measurements were performed by AC impedance method. As mentioned in Experimental Section, it should be noted that lithium salt was incorporated into MOF (IL) **1**, and the resulting MOF (IL) **2** was used after washing with THF. Hence, the present system (**2**/AMImTFSI) does not require an external addition of Li salt. The temperature dependence of ionic conductivity for different electrolyte compositions of **2** in AMImTFSI are shown in **Fig. 8(a)**. Arrhenius plots showed linear profiles with rise in temperature, indicating no decomposition or phase change over the temperature range. As expected the ionic conductivity

decreased with increase in wt% of **2** in AMImTFSI because of the change in physical state from liquid to gel (soft solid). This small decrease in the ionic conductivity of the sample can be associated with the amount of ionic liquid as it acts as ion carrier. Also as the observed conductivity is due to all the constituting cations and anions present in the sample i.e. ions of ionic liquid alongwith Li salt (AMIm$^+$, TFSI$^-$, and Li$^+$) therefore the ionic conductivity decresases slightly with increase in wt% of **2** in AMImTFSI. The ionic conductivities of the samples were calculated and were in the order of $10^{-2} \sim 10^{-3}$ Scm^{-1}. The sample in liquid state with 10 wt% of **2** in AMImTFSI showed slightly higher ionic conductivity i.e. 1.0×10^{-2} Scm^{-1} at 51 $^{\circ}$C.

To obtain more information on conduction behavior of the prepared samples, Vogel-Fulcher-Tammann (VFT) fitting [31–33] shown in **Fig. 8(b)** was carried out. The temperature dependence of ionic conductivity was determined by VFT Equation**,**

$$\sigma = AT^{1/2}\, e^{\frac{B}{T-T0}}$$

where T_0= ideal glass transition temperature of electrolyte; T = temperature of measurement; A = pre-exponential factor and B = activation energy .

The VFT parameters are listed in **Table 1**. It was interesting to observe a decrease in activation energy with increasing wt% of **2** in AMImTFSI. The decrease in activation energy of ion transport can be associated with the change in ion conductive path owing to the ordered structure of MOF (IL).
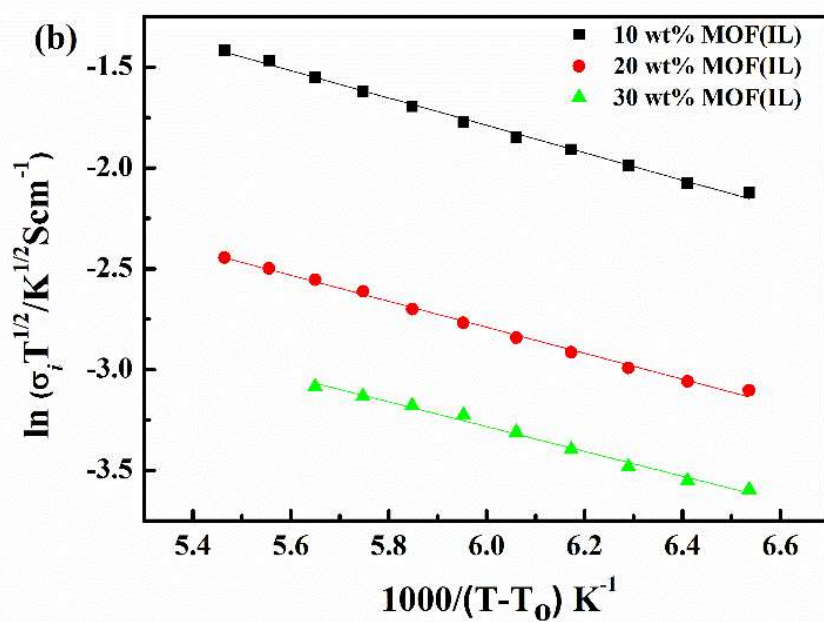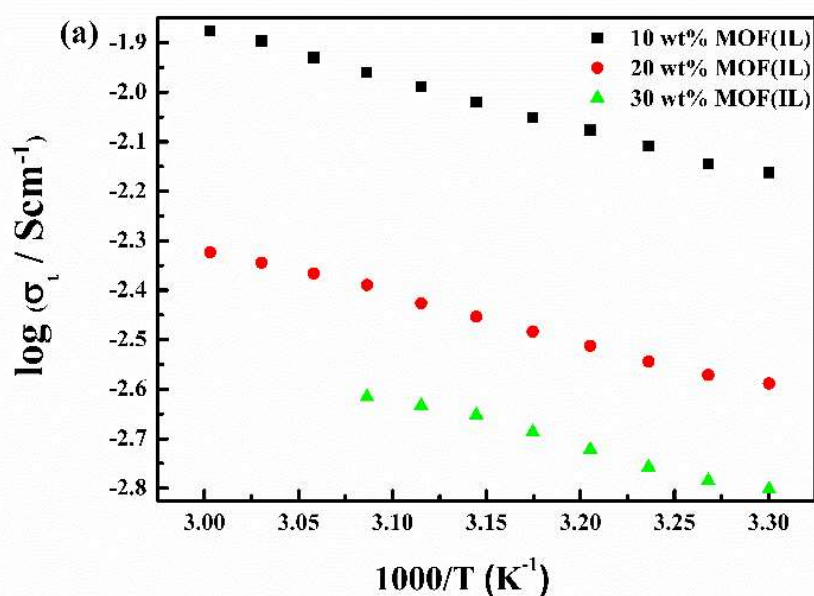
Fig. 8 (a) Arrhenius and **(b)** VFT plots for different compositions of MOF (IL) **2**

in AMImTFSI.

Table 1: VFT parameters for different compositions of **2** in AMImTFSI.

State	Sample in AMImTFSI	A $(Scm^{-1}K^{1/2})$	B (K)	R^2	σ at 324K (Scm^{-1})	eV
Liquid	10 wt% MOF (IL)	11.21	722.4	0.999	1.0×10^{-2}	0.062
Liquid	20 wt% MOF (IL)	3.99	662.2	0.998	5.0×10^{-3}	0.057
Gel	30 wt% MOF (IL)	1.88	636.5	0.998	2.3×10^{-3}	0.054

And the high ionic conductivity of the solidified ion-gel electrolyte is because of higher possibility of long distance migration under dimensionally controlled ion conductive path rather than in fully amorphous random-walk system. Though other coordination polymers also show ordered structure and regulation in ion conductive path, here ionic liquids itself will act as ion carrier. So the synergistic effect of ordered structure and the presence of ionic liquid as the solvent for ion conduction, led to the high ionic conductivity which is also evident from the low values of activation energy.

The solidified ion-gel electrolyte system showed comparable ionic conductivity in the range of ~10^{-2}-10^{-3} S cm^{-1} with other ionic liquid based gel electrolytes like Mg-BTC (MOF) incorporated CPE composed of PEO and LiTFSI (10^{-2}-10^{-5} S cm^{-1}) [34] and with PEO + LiTFSI + Al-BTC (MOF) (10^{-3}-10^{-7} S cm^{-1}) [14]. Also our system showed slightly higher ionic conductivity compared to ionic liquid/PEO-PMA gel electrolytes (10^{-3}-10^{-5} S cm^{-1}) [34].

VFT plots showed the activation energies in the range of 0.054–0.0.062 eV (5.3–6.0 kJ mol^{-1}). These activation energy values are much lower than that of the well-established ceramic electrolyte LIPON–Li$_3$PO$_4$ (0.55 eV, 53.0 kJ mol^{-1}) [35] and in LISICON–Li$_{14}$ZnGe$_4$O$_{16}$ (0.40 eV, 38.5 kJ mol^{-1}) [36]. In addition, our solidified ion-gel electrolytes showed almost 20 times

lower activation energy compared to the PEO/Li$^+$ polymer electrolyte (1.66 eV, 160.4 kJ mol^{-1}) [37] and 5 times lower than that of the porous CB[6]-based solid lithium electrolyte (0.32 eV, 31 kJ mol^{-1}) [38]. With a high conductivity in the order of ~10^{-2}-10^{-3} S cm^{-1} and activation energy less than 0.062 eV, these modified MOF based solidified gel electrolyte can be considered as prospective electrolyte for the battery system.

2.4.2 DC polarization measurements

Chronoamperometry experiments for all the three samples were done to study the steady state current and Li-ion diffusion in MOF (IL) matrices using cell setup shown in **Fig. 9**. A DC voltage of 0.03 V was applied across the Li/electrolyte/Li type cell for an indefinite period of time until the current reached a steady state. As shown in **Fig. 10** the steady state current flowing was contributed only by Li-ion conduction which shows that Li salt was successfully incorporated into the MOF (IL) **1** matrices. All these experiments were done in a glove box filled with argon gas with very low moisture content.
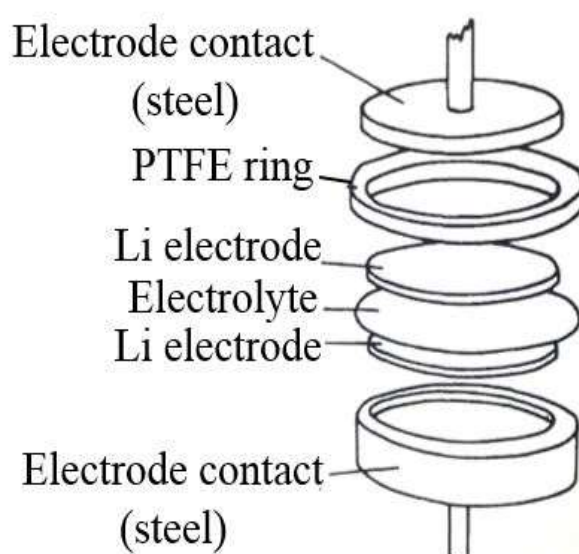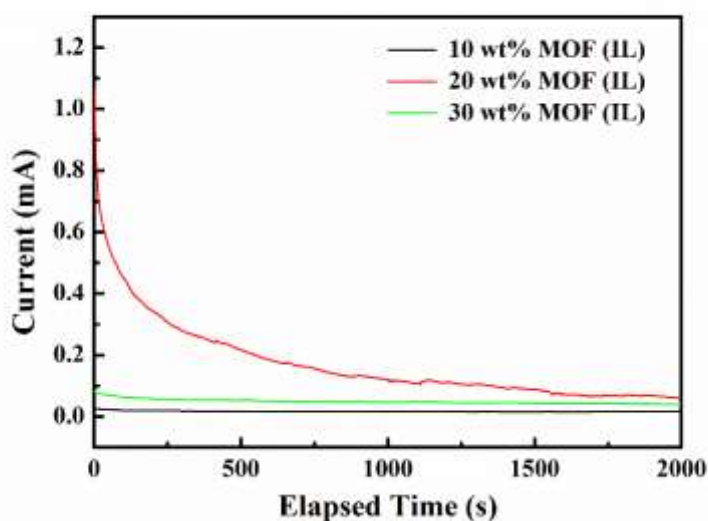

Fig. 9 Cell setup for DC polarization.

Fig. 10 DC Polarization profiles at room temperature for Li/electrolyte/Li
cell with different wt% of MOF (IL) **2** in AMImTFSI.

2.4.3 Linear sweep voltammetry scan (LSV)

Electrochemical window of the synthesized electrolytes with different compositions of **2** in AMImTFSI was determined by LSV in Li/electrolyte/Pt cell configuration at a scan rate of 10 mV s^{-1} within 0 to 6 V range of potential. LSV curves obtained for different compositions are shown in **Fig. 11(a)**.

For all the samples, a potential working window of 5.22 to 5.55 V was obtained. After 5.22 V / 5.55 V, sudden increase in the current exhibited the occurrence of an electrochemical reaction. To observe lithium plating and stripping processes, **Fig. 11(b)** shows cyclic voltammetry experiment performed for 20 wt% of **2** in AMImTFSI at a scan rate of 10 mV s^{-1} in Li/electrolyte/Li cell. Almost ideally reversible peaks for both lithium stripping and lithium plating processes were observed.

This indicated that the MOF (IL) matrices possess high electrochemical stability and are able to appease the requirement of high voltage lithium ion batteries.
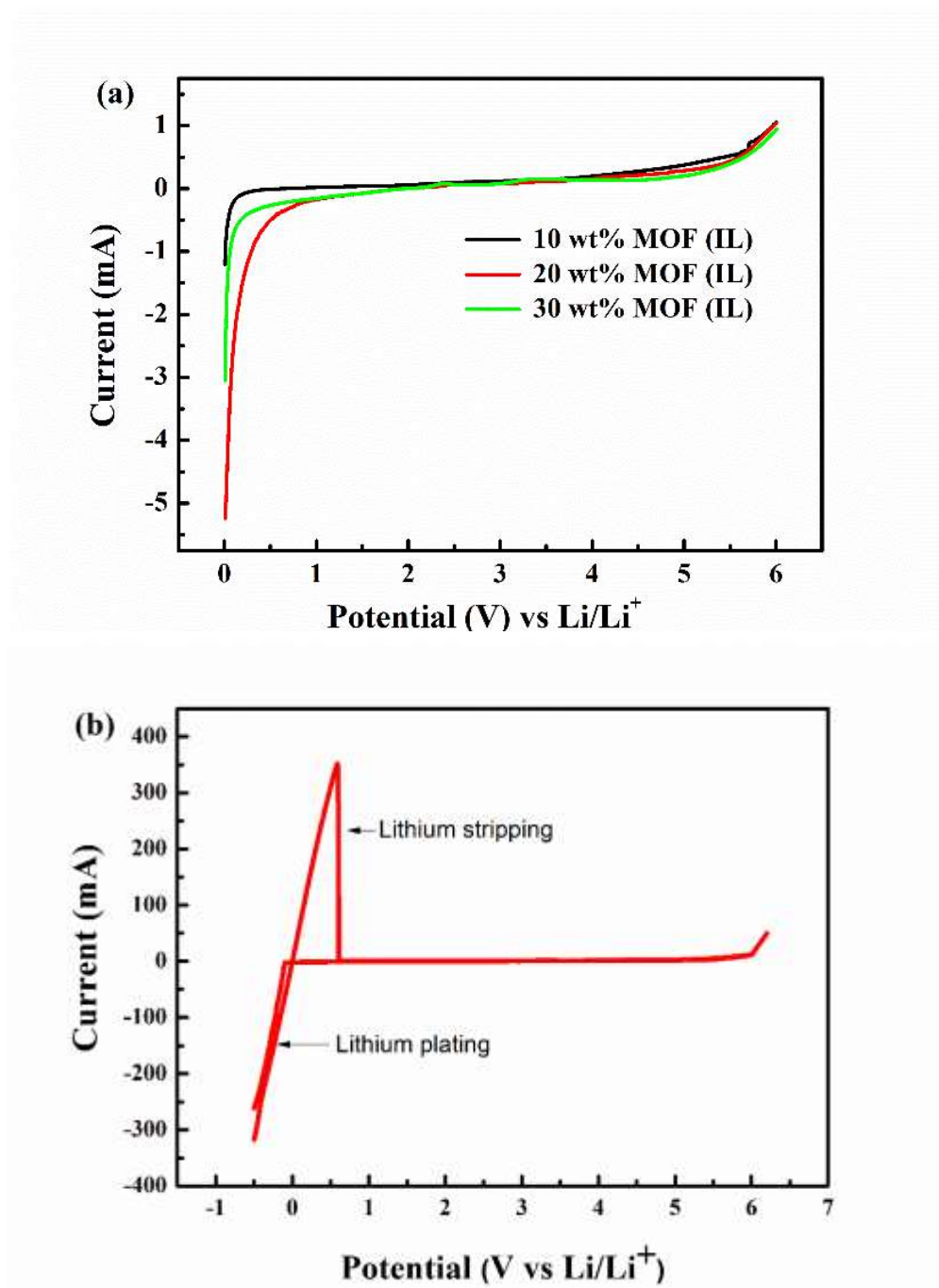

Fig. 11 (a) LSV curves of Li/electrolyte/Pt cells with different electrolyte compositions (Pt as working electrode and Li as counter and reference electrode). **(b)** Cyclic Voltammogram of Li/electrolyte/Li cells with 20 wt% of **2** in AMImTFSI electrolyte composition.

2.4.4 Charge-discharge characteristics

The charge-discharge characteristics were studied for the 30 wt% of **2** in AMImTFSI electrolyte composition in a coin anodic half-cell configuration shown in **Fig. 12** using Si anode (theoretical capacity; 4200 mAhg^{-1}) with 30 μL of EC : DC=1:1 at various current rate of 0.1C (0.0172 mA) to 2C (**Fig. 13**). The 30μL of EC:DEC was added to the electrolyte composition during the cell fabrication just to wet the electrode surface. The EC:DEC also allows quick formation of solid electrolyte interface. The 30 wt% of **2** in AMImTFSI is a gel state product compared to other two compositions (liquid), therefore the charge-discharge behavior of this particular electrolyte composition was studied extensively. Although the other electrolytes have better electrochemical parameters, the objective of the study to arrive at a gel state electrolyte was the motivation behind the choice of this electrolyte.

The result of 10 charge-discharge cycles of **30 wt%** of **2** in AMImTFSI at 0.1C, 0.5C, 1C and 2C is shown in **Fig. 13(a)**. The first cycle showed highly irreversible capacity because of SEI formation in the first cycle. But the capacity tends to stabilize after the first cycle which suggests the formation of stable conductive SEI layer after the first cycle. The stability of the SEI layer is also evident from the retention of the high reversible capacity at higher current rates.
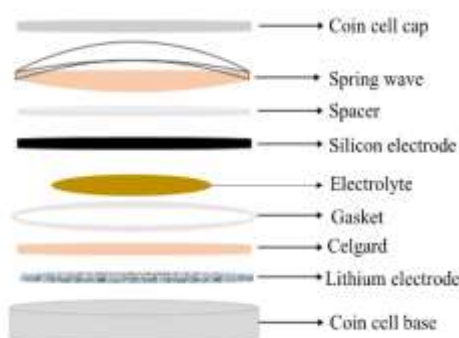

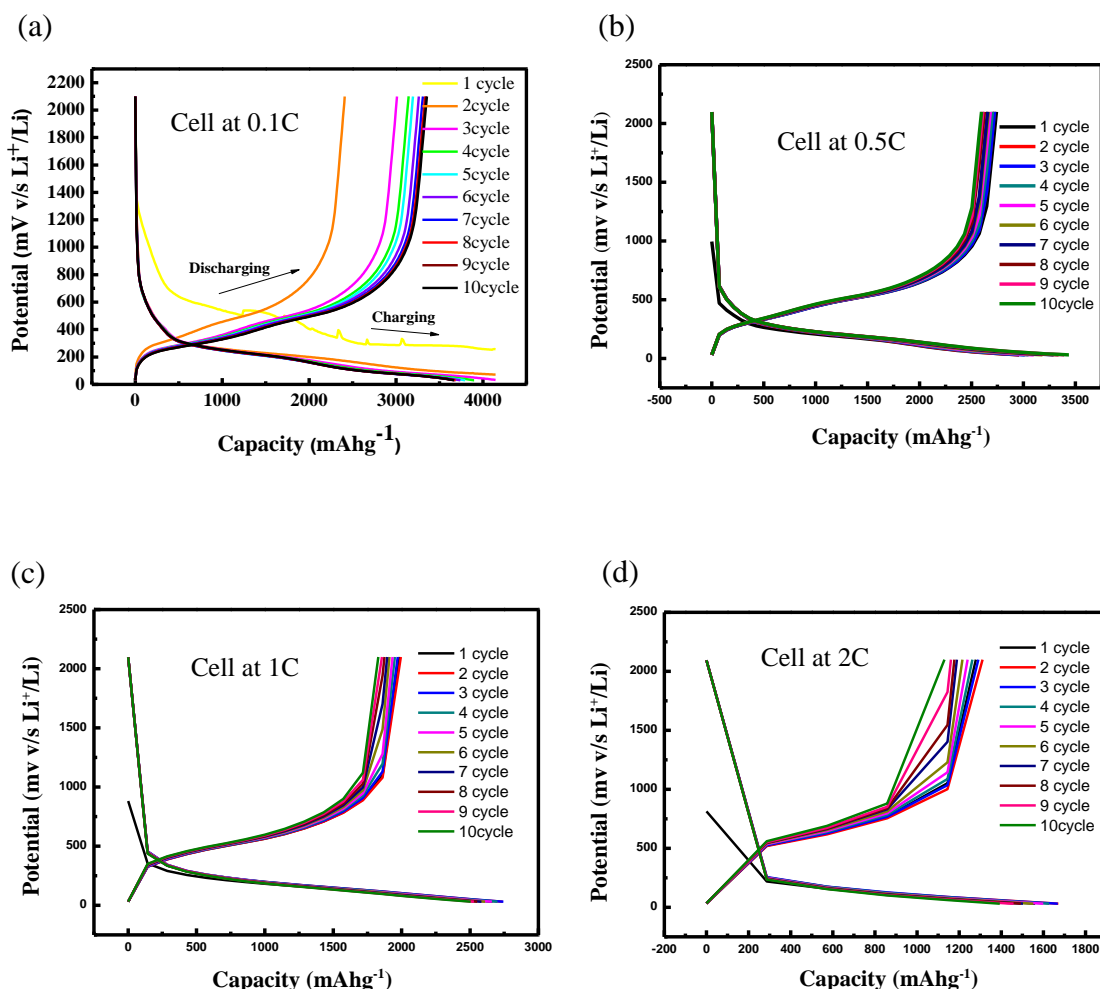**Fig. 12** Set-up of the assembled anodic-half cells.

Fig. 13 Charge-discharge profiles of Li/electrolyte/Si cell fabricated using **30 wt%** MOF (IL) in AMImTFSI with 30μL of EC :DEC=1:1 for 10 cycles at (a) 0.1C, (b) 0.5C, (c) 1C, (d) 2C current rates.

Fig. 14 shows the cycling performance of Li/electrolyte/Si cell fabricated using **30 wt%** of **2** in AMImTFSI at different rates in order to evaluate the practical use of the electrolytes in lithium ion batteries. The constructed cell with 30 wt% of **2** in AMImTFSI exhibited a stable cycling behavior and showed reversible discharge capacity of 3000 mAhg^{-1}. Coulombic efficiency of the cell was observed to be ~90% which indicated few electrochemical reaction was occurring resulting in the decomposition of the electrolyte material.
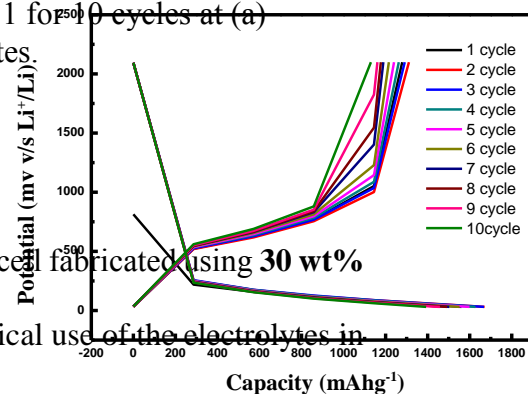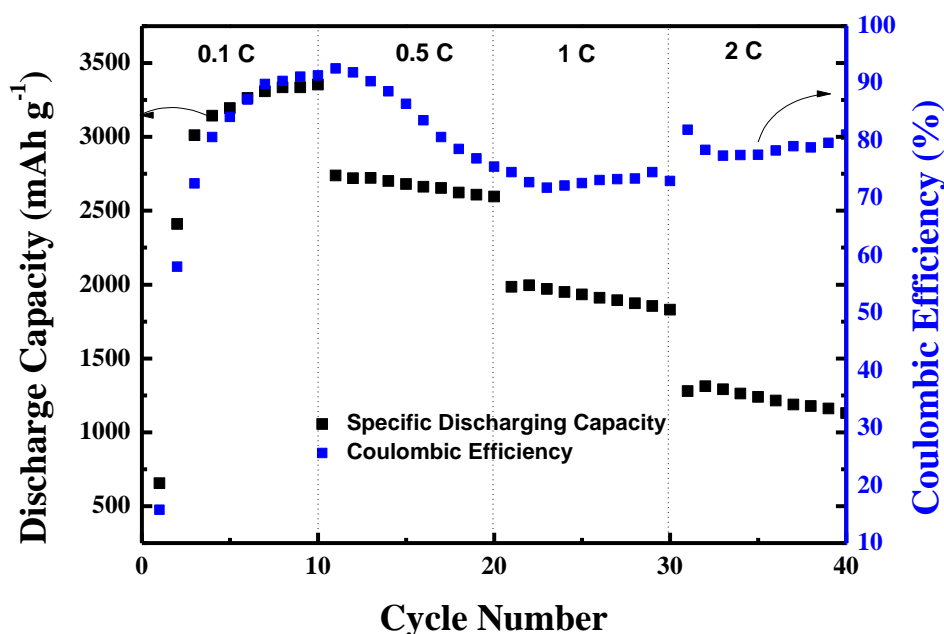
Fig. 14 Rate cycling performance of Li/electrolyte/Si cell
fabricated using **30 wt%** MOF (IL) in AMImTFSI with 30 μL of
EC : DEC = 1:1 for 40 cycles.

Fig. 15(a) and **(b)** shows the cycling performance of Li/electrolyte/Si cell fabricated using 1**0 wt%** and **20 wt%** of **2** in AMImTFSI. These two electrolyte show better electrochemical properties because of its state being liquid but the cycling performance is comparatively lower than **30 wt%** of **2** in AMImTFSI. This can be attributed to the lesser amount of MOF (IL) in the two samples which provides the long range ordered pathway for the free ions to move. The mobility of ions in the charge-discharge mechanism plays a huge role because of its intercalation and de-intercalation chemistry.
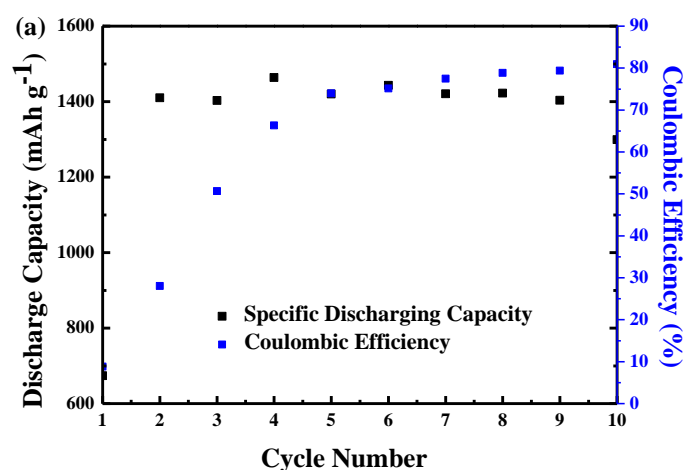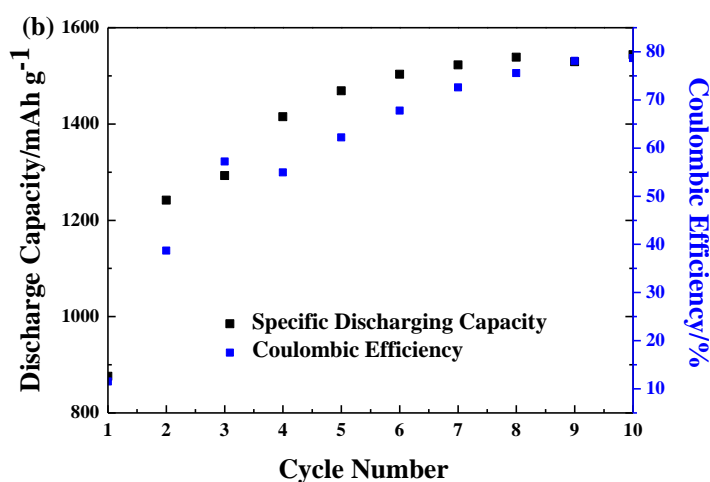
Fig. 15 (a) Discharge capacity of Li/electrolyte/Li cell fabricated using 10 wt% MOF (IL) in AMImTFSI with 30 µL of EC : DEC = 1:1 for 10 cycles at 0.1C. **(b)** Discharge capacity of Li/electrolyte/Li cell fabricated using 20 wt% MOF (IL) in AMImTFSI with 30 µL of EC : DEC = 1:1 for 10 cycles at 0.1C.

2.5 Conclusion

A modified MOF with ionic liquid framework was synthesized by the electrochemical reaction resulting in a modified MOF-5 with AMImTFSI. The obtained crystalline product was characterized by XRD, FT-IR, SEM and TEM analysis. XRD analysis showed the crystallinity of the MOF in ionic liquid matrix. The FT-IR spectrum of modified MOF (IL) **1** showed close resemblance with MOF structure. SEM and TEM showed the change in morphology from conventional cubic to more porous distinct flower shaped morphology because of the incorporation of highly conducting AMImTFSI ionic liquid.

The electrochemical analysis of the sample was done by doping the electrolyte with lithium salt by the modified procedure. After incorporation of Li-salt in MOF (IL) **1** samples with different wt%, resulting MOF (IL) matrices showed the highest ionic conductivity for **10 wt%** MOF (IL) in AMImTFSI. The DC polarization measurements showed the successful incorporation of lithium in MOF (IL) matrix. The compound showed an electrochemical

window of 5.22-5.55 V. After fabricating Si/electrolyte/Li type half cell, 90% coulombic efficiency was observed in the presence of 30 µL of EC: DC=1:1.

Thus, we conclude that the modified MOF with ionic liquid framework prepared in ionic liquid system by electrochemical method revealed high ionic conductivity as a solidified ion-gel electrolyte and wide electrochemical window. Further when Li/electrolyte/Si type anodic half cell was fabricated, the cell exhibited a reversible capacity of 3000 - 3300 mAhg^{-1}. These enhanced attributes attained from new MOFs (**Fig. 16**) affirm that the prepared modified MOF (IL) to be a prospective electrolyte in energy storage devices.
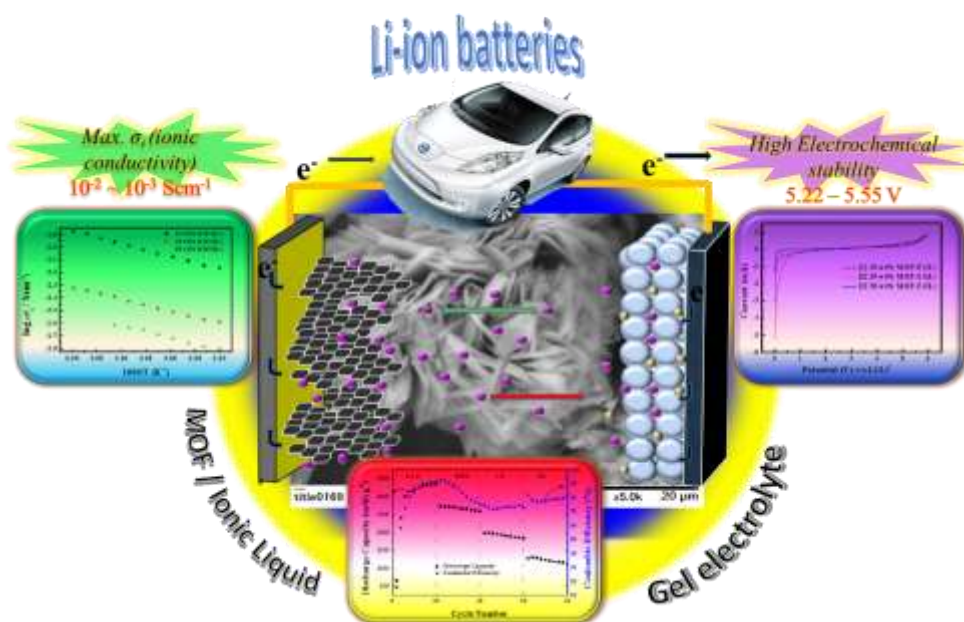
Fig. 16 Graphical illustration showing high electrochemical aspects of synthesized gel electrolyte.

References

[1]   H.-C. Zhou, J. R. Long, O. M. Yaghi, Chem. Rev. 112 (2012) 673.

[2]   D. J. Tranchemontagne, J. R. Hunt, O. M. Yaghi, Tetrahedron 64 (2008) 8553.

[3]   O. K. Farha, A. Ö. Yazaydın, I. Eryazici, C. D. Malliakas, B. G. Hauser, M. G. Kanatzidis, S. T. Nguyen, R. Q. Snurr, J. T. Hupp, Nat. Chem. 2 (2010) 944.

[4]   C. Zhang, Y. Xiao, D. Liu, Q. Yang, C. Zhong, Chem. Commun. 49 (2013) 600.

[5]   J. S. Seo, D. Whang, H. Lee, S. Im Jun, J. Oh, Y. J. Jeon, K. Kim, Nature 404 (2000) 982.

[6]   C.-D. Wu, A. Hu, L. Zhang, W. Lin, J. Am. Chem. Soc. 127 (2005) 8940.

[7]   L. E. Kreno, K. Leong, O. K. Farha, M. Allendorf, R. P. Van Duyne, J. T. Hupp, Chem. Rev. 112 (2011) 1105.

[8]   H. Kitagawa, Y. Nagao, M. Fujishima, R. Ikeda, S. Kanda, Inorg. Chem. Commun. 6 (2003) 346.

[9]   H. Kitagawa, Nat. Chem. 1 (2009) 689.

[10]   S. Bureekaew, S. Horike, M. Higuchi, M. Mizuno, T. Kawamura, D. Tanaka, N. Yanai, S. Kitagawa, Nat. Mater. 8 (2009) 831.

[11]   B. M. Wiers, M.-L. Foo, N. P. Balsara, J. R. Long, J. Am. Chem. Soc. 133 (2011) 14522.

[12]   R. Ameloot, M. Aubrey, B. M. Wiers, A. P. Gómora-Figueroa, S. N. Patel, N. P. Balsara, J. R. Long, Chem. Eur. J. 19 (2013) 5533.

[13]   C. Yuan, J. Li, P. Han, Y. Lai, Z. Zhang, J. Liu, J. Power Sources 240 (2013) 653.

[14]   C. Gerbaldi, J. R. Nair, M. A. Kulandainathan, R. S. Kumar, C. Ferrara, P. Mustarelli, A.M. Stephan, J. Mater. Chem. 2 (2014) 9948.

[15]   P. Wasserscheid, W. Keim, Angew. Chem. Int. Ed. 39 (2000) 3772.

[16]   R. Sheldon, Chem. Commun. (2001) 2399.

[17]   J. Huddleston, R. Rogers, Chem. Commun. (1998) 1765.

[18]   L. A. Blanchard, D. Hancu, E. J. Beckman, J. F. Brennecke, Nature 399 (1999) 28.

[19]   H. Ohno, Electrochemical Aspects of Ionic Liquids, John Wiley & Sons, 2011.

[20]   M. J. Earle, K. R. Seddon, Pure Appl. Chem. 72 (2000) 1391.

[21]   T. Welton, Chem. Rev. 99 (1999) 2071.

[22]   T. Ogoshi, N. Ueshima, T. Yamagishi, Y. Toyota, N. Matsumi, Chem. Commun. 48 (2012) 3536.

[23]   Q. Luo, M. Ji, M. Lu, C. Hao, J. Qiu, Y. Li, J. Mater. Chem. 1 (2013) 6530.

[24]   Q. Luo, B. An, M. Ji, S.-E. Park, C. Hao, Y. Li, J. Porous Mater. 22 (2015) 247.

[25]   K. M. Gupta, Y. Chen, Z. Hu, J. Jiang, Phys. Chem. Chem. Phys. 14 (2012) 5785.

[26]   K. Fujie, R. Ikeda, K. Otsubo, T. Yamada, H. Kitagawa, Chem. Mater. 27 (2015) 7355.

[27]   J. Dupont, C. S. Consorti, P. A. Suarez, R. F. de Souza, Org. Synth. 79 (2002) 236.

[28]   H. M. Yang, X. L. Song, T. L. Yang, Z. H. Liang, C. M. Fan, X. G. Hao, RSC Adv. 4 (2014) 15720.

[29]   A. Schneemann, V. Bon, I. Schwedler, I. Senkovska, S. Kaskel, R. A. Fischer, Chem. Soc. Rev. 43 (2014) 6062.

[30]   D. Saha, S. Deng, Z. Yang, J. Porous Mater. 16 (2009) 141.

[31]   H. Vogel, Phys. Z 22 (1921) 645.

[32]   G. S. Fulcher, J. Am. Ceram. Soc. 8 (1925) 339.

[33]   G. Tammann, W. Hesse, Z. Für Anorg. Und Allg. Chem. 156 (1926) 245.

[34]   N. Angulakshmi, R. S. Kumar, M. A. Kulandainathan, A. M. Stephan, J. Phys. Chem. C 118 (2014) 24240.

[35]   W. C. West, J. F. Whitacre, J. R. Lim, J. Power Sources 126 (2004) 134.

[36]   L. Puech, C. Cantau, P. Vinatier, G. Toussaint, P. Stevens, J. Power Sources 214 (2012) 330.

[37]   L. Y. Yang, D. X. Wei, M. Xu, Y. F Yao, Q. Chen, Angew. Chem. Int. Ed. 53 (2014) 3631.

[38]   J. H. Park, K. Suh, M. R. Rohman, W. Hwang, M. Yoon, K. Kim, Chem. Commun., 51 (2015) 9313.

Chapter 3

Surface modification of Zn Anode by MOFs Coating for Improved Zinc-Air Batteries

Abstract

Modified MOF-5 (IL) was successfully synthesized over the zinc electrode by a mild in-situ electrochemical method using imidazolium based ionic liquid as a templating agent. After the synthesis of MOF-5 (IL), controlled electro-polymerization of thiophene was also done over the Zn electrodes for polythiophene coated Zn anodes. The as-synthesized MOF-5 (IL) and PTh@ MOF-5 (IL) was characterized by using XRD and SEM. The corrosion behavior of Zn anode with different surface modifications was investigated by employing potentio-dynamic experiment in a conventional 3-electrode setup. Chronopotentiometry experiment was performed to see the discharge behavior of different Zn based anodes. The zinc air battery with pure zinc as anode showed current density of ~ 7 mA cm^{-2}. On the contrary, zinc air batteries with zinc anodes decorated with MOF-5 (IL) showed 4 times enhanced current density of ~ 27-30 mA cm^{-2}. Considering corrosion current and current density, MOF (IL) decorated Zn anodes and PTh@ MOF (IL) coated Zn anodes showed the most favorable characteristics to be used in zinc-air batteries.

3.1 Introduction

Zinc-air battery is known to be one of the most reliable battery technology amongst other metal-air batteries. Zinc-air batteries have theoretical density nearly five times higher than that of the Li-ion batteries and is considered to be the post Li battery technology [1–3]. The development of zinc-air batteries took early start but even then their large scale commercialization could not happen. The applications of zinc-air batteries were only limited to the hearing aids and other small medical and telecommunications field only [2]. The main cause for its limited applications is associated with one of its important component- "Anode". In commercial zinc-air batteries, zinc is employed as anode [4–8] due to its low cost, high abundance, low toxicity and stability but its advantages comes up with problems like self-corrosion and hydrogen evolution reaction [9–15]. The reason behind the hydrogen evolution reaction in zinc-air batteries is the parasitic reaction between zinc and water shown below:

Parasitic reaction: $Zn + 2H_2O \longrightarrow Zn(OH)_2 + H_2$
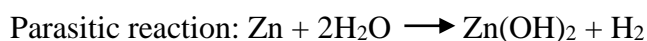
This undesired reaction leads to the self-corrosion of the zinc anode in batteries resulting in the low performance and limited energy density of the zinc-air batteries. To overcome the problems associated with zinc anode, many strategies were implied by the active researchers all over the world. In the early stage, mercury was used with zinc to avoid the problem of hydrogen evolution reaction by increasing the hydrogen overpotential of anode but its high toxicity raised the environmental concerns [1]. As an alternative different possible solutions were proposed like addition of metal oxides, alloying zinc metal and surface modification of zinc anode [7,16,17].

In this context, suppression of hydrogen evolution by adding lithium boron oxide (LBO) was observed by Y. Cho et al [18]. In another report by S. M. Lee et al., Al, Bi and In oxides were added to the Zn-based anodes to study the suppression in hydrogen evolution [19]. Al_2O_3

as an additive showed the most interesting results and was further coated over the zinc anode in the same study. And it was observed that surface coating zinc particles with Al_2O_3 led to the better discharge performance instead of adding Al_2O_3 as additive.

Metal Organic Frameworks (MOFs) have stimulated immense attention in the last few decades due to their simple synthetic procedure, high surface area, low cost, and high tunable porosity depending on the length of organic ligands [20–25]. These fascinating properties of MOFs are of vital importance and are exploited in various fields such as fuel cells, Li-ion batteries, supercapacitors etc. for clean energy [26–31]. Many studies have been conducted for the application of MOFs as anti-corrosion material [32–35], but scarcely any investigation was performed to understand the effect of MOF coatings on zinc anode for zinc-air battery applications.

Also, conducting polymers have been extensively used to inhibit the corrosion of various metal surfaces. Some of the widely used such polymers are polypyrrole (PPy), polyaniline (PAni) and polythiophene (PTh) [36]. These conducting polymers act as a passivation layer against the active corrosive species like (O_2, H^+, Cl^-) and thus provide stability to the metal surfaces. Among various conducting polymers studied so far, PTh is most impressive because of its certain advantages like structural versatility easy processability, high stability in strong electrolyte systems and well established electrochemistry [37,38]. These inherent properties of PTh have widen its applications in various fields including energy storage devices, anticorrosion paints and modified electrodes.

In this work, coating of zinc surface by thin passivation layer of MOFs will be investigated to improve the zinc air battery performance. The dimensionally and morphologically controlled MOFs deposition on zinc anode by electrochemical method in imidazolium based ionic liquids is studied. Furthermore, to give the stability to the MOFs layer over zinc anode, polymerization of thiophene will also be done as illustrated in **Fig. 1**.
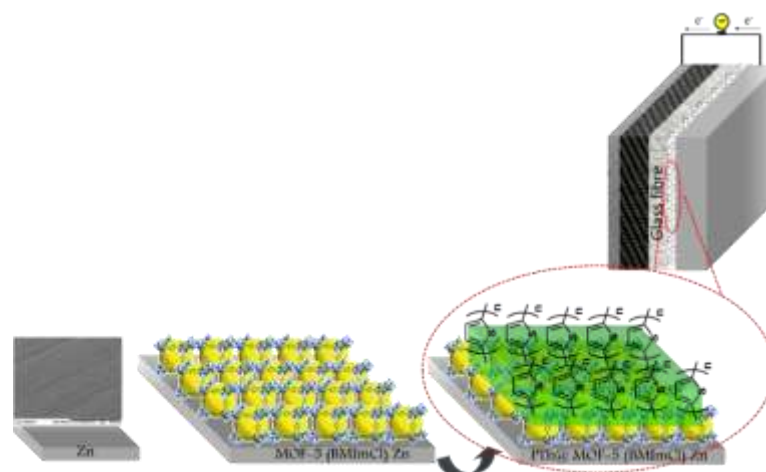

Fig. 1 Schematic illustration of decoration of MOF thin films over zinc surface followed by electropolymerization of thiophene.

Why MOF-5?

During the electrochemical preparation of MOF-5 in chapter 2 we observed the growth of MOF-5 on the surface of working electrode i.e. zinc plate, which inclined us to thought of its utilization in zinc-air battery applications. The added advantage of using MOF-5 for corrosion protection of zinc anode was that it involves zinc metal clusters as secondary building unit. So while modifying the electrode surface it was thought to contribute to the activity also.

3.2 Experimental

1-Butyl-3-methylimidazolium chloride (BMImCl) was synthesized according to the literature [39]. MOF (IL) was decorated electrochemically with a modification in an already reported method by our group with an introduction of ionic liquid. Dimethylformamide (DMF) and tetrahydrofuran (THF) was purchased from WAKO Co. Ltd. and used as received. Thiophene was purchased from TOKYO CHEMICAL INDUSTRY Co. Ltd. Scanning Electron Microscopy (SEM) analysis was done on a Hitachi TM3030 plus (Hitachi Ltd., Chiyoda-ku, Japan). X-ray diffraction data was collected using Rigaku SmartLab (Rigaku, Japan) operating at 40 kV, 30 mA at a rate of 1° min^{-1}, using Cu Kα radiation. Electrochemical deposition of MOFs, polymerization of thiophene, potentiodynamic polarization and chronoamperometric studies were carried out on Biologic VSP s/n 1190.

3.2.1 *Synthesis of MOF-5 (IL) decorated zinc anodes* – Modified MOF-5 (IL) was successfully synthesized over the zinc electrode by a mild in-situ electrochemical method using BMImCl ionic liquid as a templating agent in a two electrode system by employing a modified procedure of reported method [40] (**Fig. 2**). Synthesis of the MOF-5 (IL) was achieved by a constant dissolution of Zn^{2+} ion from Zn anode. The dissolution was carried out by applying a constant direct current (DC) of 0.20 A. A titanium electrode was employed as cathode. The electrolyte used in this procedure was a solution containing terephthalic acid (0.5 g, 0.003 moles), zinc nitrate hexahydrate (0.65 g, 0.002 moles) and BMImCl (1.99 g, 0.014 moles) in DMF. The electrochemical galvanostatic procedure was carried out for 1hr to get uniform coating of MOF (IL) over the zinc electrode. After that electrode was kept for drying at room temperature for 6 hours (**Fig. 3**).
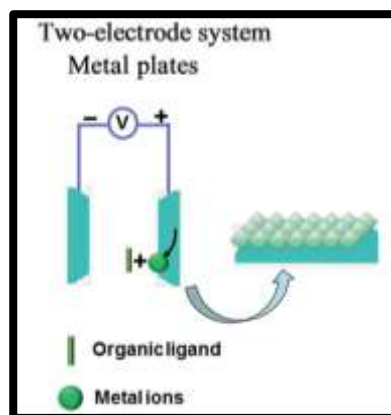
Fig. 2 A two electrode system used for electrochemical decoration of MOF-5 (IL) on zinc surface at room temperature (Anode- Zinc sheet, Cathode- Titanium sheet).
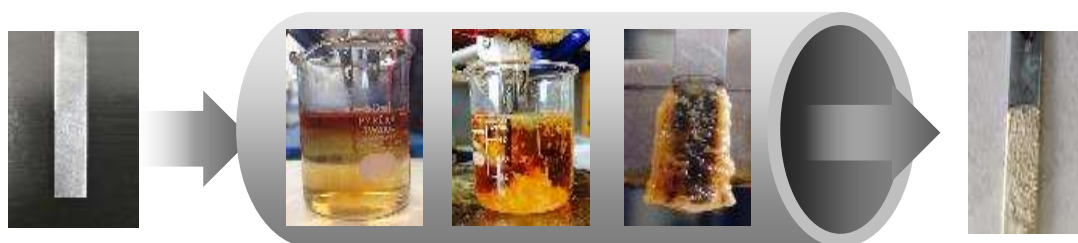

Fig. 3 Illustration of growth of MOF-5 (IL) films on zinc surface during electrochemical synthesis.

3.2.2 _Synthesis of MOF-5 (IL) / polythiophene decorated zinc anodes_ – After the synthesis of MOF-5 (IL), 0.5 M thiophene was added in the solution described for the synthesis of MOF-5 (IL) films on zinc. Further cyclic voltammetry experiment was performed using Ag/Ag$^+$ as reference electrode, titanium as counter electrode and MOF-5 (IL) decorated Zn as working electrode in three electrode system (**Fig. 4**) . The experiment was performed for 10 cycles and rise in the current with increasing cycle number confirms the electropolymerization of thiophene (**Fig. 5**). After electropolymerization, the electrode was kept for drying in closed container at room temperature.
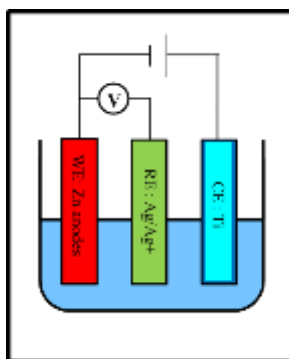
Fig. 4 A three electrode system used for electropolymerization of thiophene
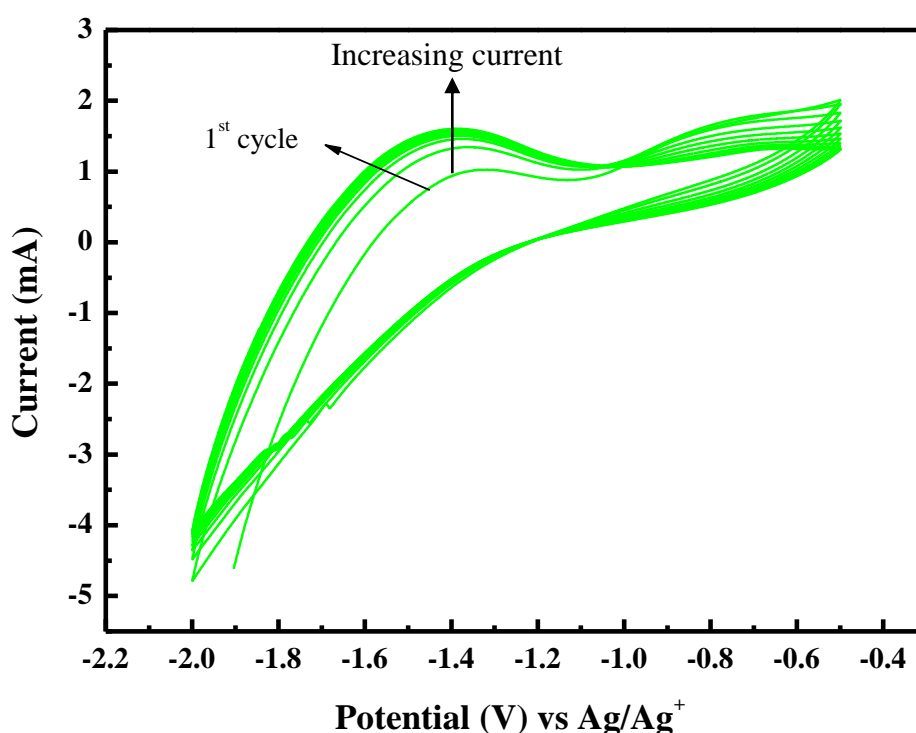at room temperature (W.E- Zn sheet, R.E- Ag/Ag+, C.E- Ti sheet).

Fig. 5 Cylic voltammogram for electropolymerization of thiophene on MOF-5 (IL)
decorated Zn electrode (W.E- Zn sheet, R.E- Ag/Ag+, C.E- Ti sheet).

3.2.3 *Synthesis of polythiophene decorated zinc anodes* - The zinc electrodes were
mechanically polished with abrasive paper and rinsed with acetone before electrochemical
experiment. The electropolymerization of thiophene on zinc was performed in
dichloromethane in the presence of 0.1M NBu_4BF_4 and 0.5M thiophene according to already

reported literature [41]. The electrodes were polarized in galvanostatic mode to deposit homogenous PTh films, and with optimized current density higher than 2.5 mA cm^{-2}.

3.3 Characterization

The synthesized BMImCl prepared according to the literature was characterized using 400 MHz nuclear magnetic resonance (NMR) spectrometer (Bruker) by ^{1}H NMR in DMSO as shown in **Fig. 6**.
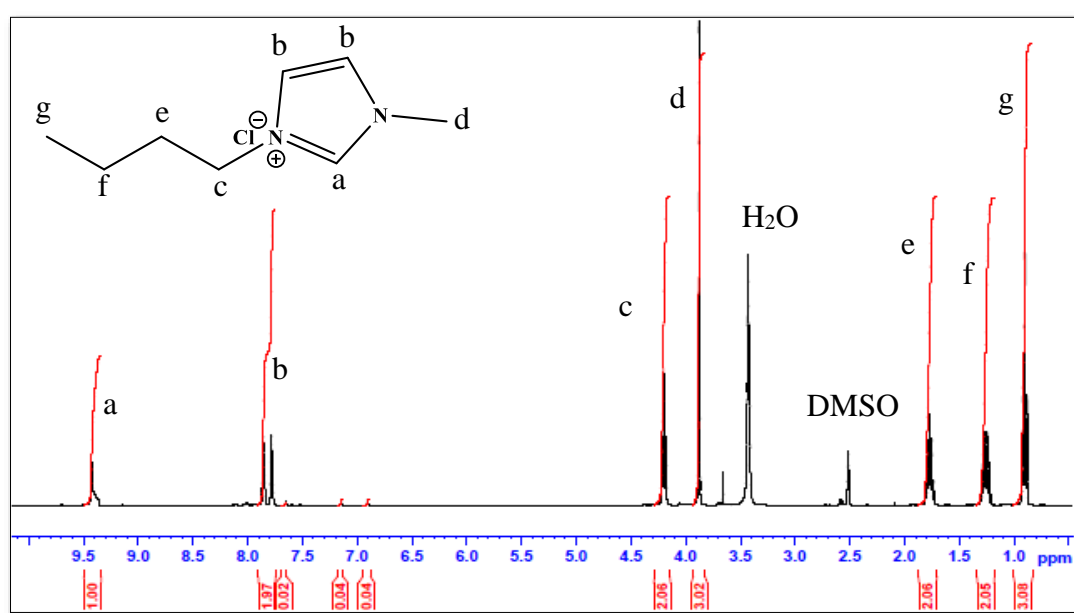

Fig. 6 ^{1}H NMR spectrum of BMImCl in DMSO.

The correspondence of the four main peaks (6.8°, 9.7°, 13.7° and 15.4°) illustrated that MOF-5 can be successfully prepared in ionic liquid system. Also, after electropolymerization of thiophene, structure of MOF-5 was intact with generation of some amorphous peaks as well which can be attributed to polythiophene (**Fig.7**).
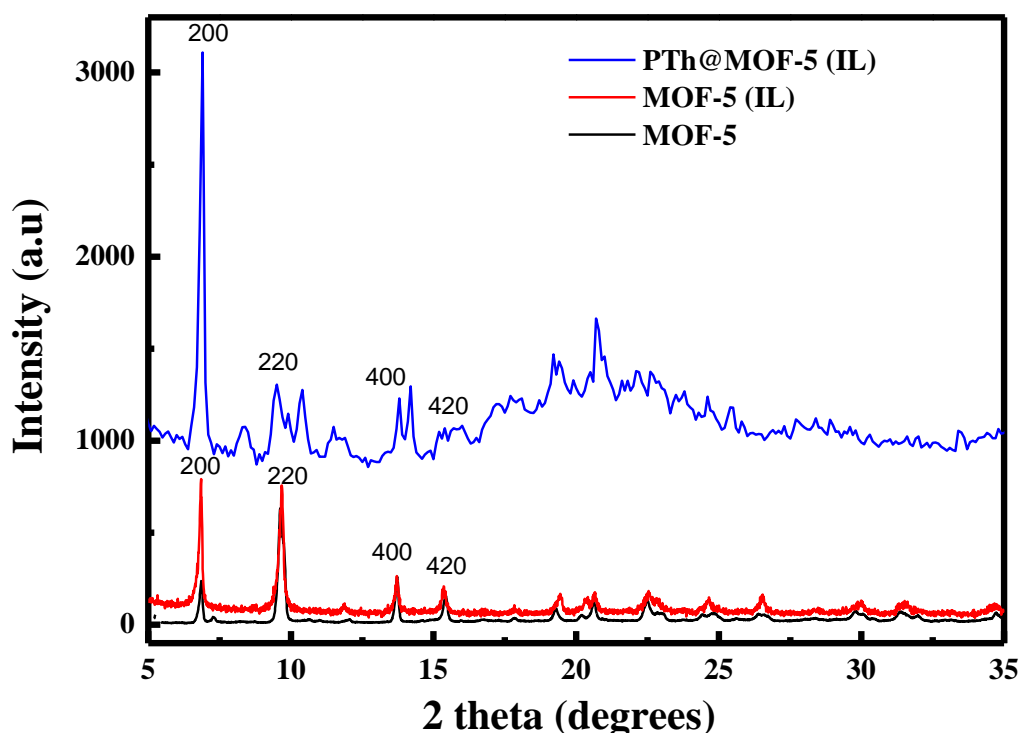

Fig. 7 X-ray diffractograms of conventional MOF-5, MOF-5 (IL) and PTh@ MOF-5 (IL).

SEM images in **Fig. 8** shows the **(a)** bare zinc surface, **(b,c)** show flower shaped morphology of MOF-5 (IL) crystals prepared by electrochemical method over zinc electrode using 3 electrode system. It forms the porous passivation layer over the zinc surface to avoid its direct contact with highly alkaline solution and thereby improving the battery performance ; **(d,e)** images show electropolymerized polythiophene films decorated over zinc surface; and **(f,g)** images demonstrate the polythiophene layer decorated over the MOF-5 (IL) crystals. The strategy behind electropolymerizing thiophene over MOF-5 (IL) layer was to improve

adherence of MOF layer on zinc surface. Furthermore, as polythiophene has high electronic conductivity and porous structure it will not affect the performance of MOF decorated zinc electrode rather will provide stability to the electrode.
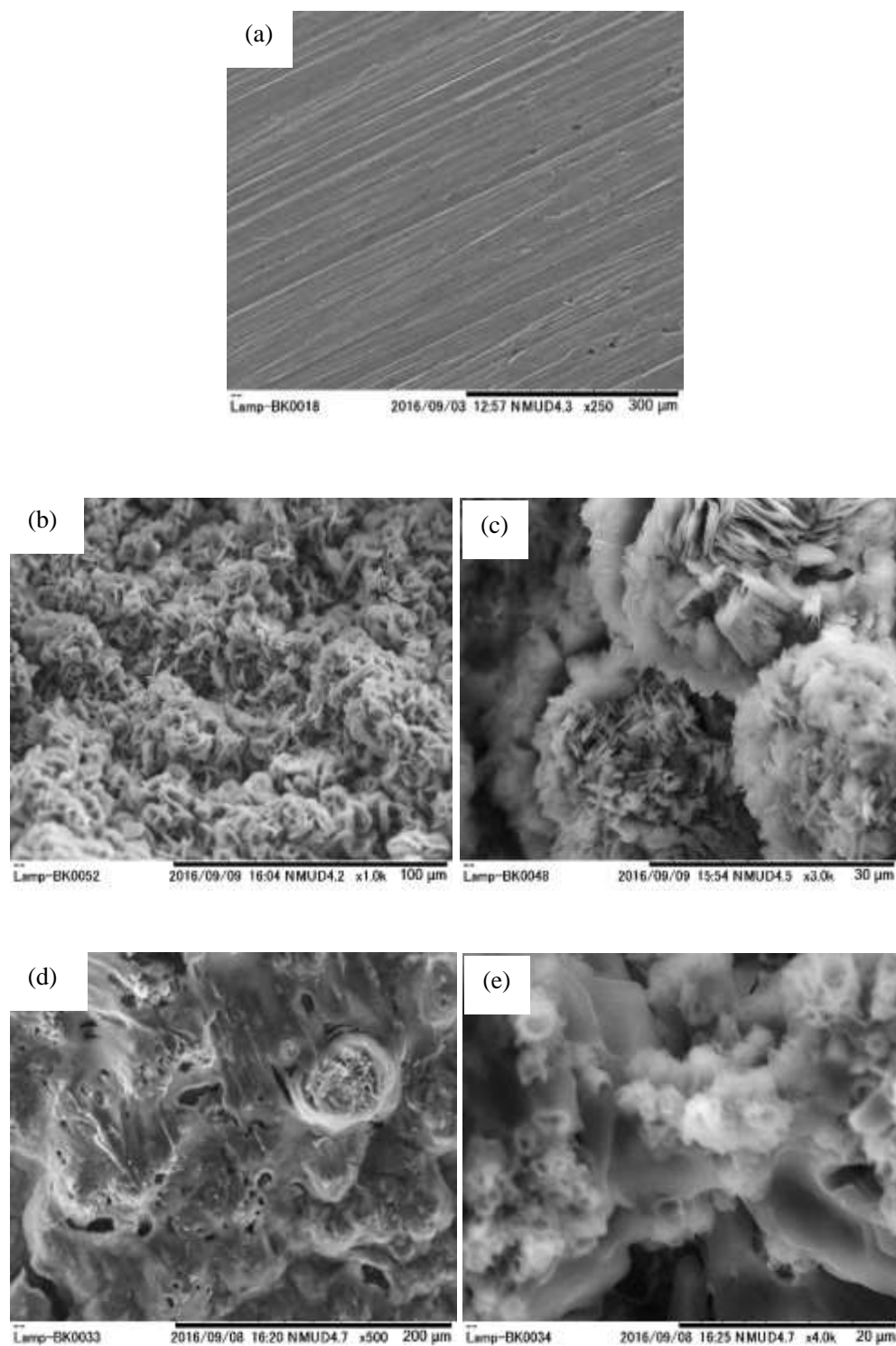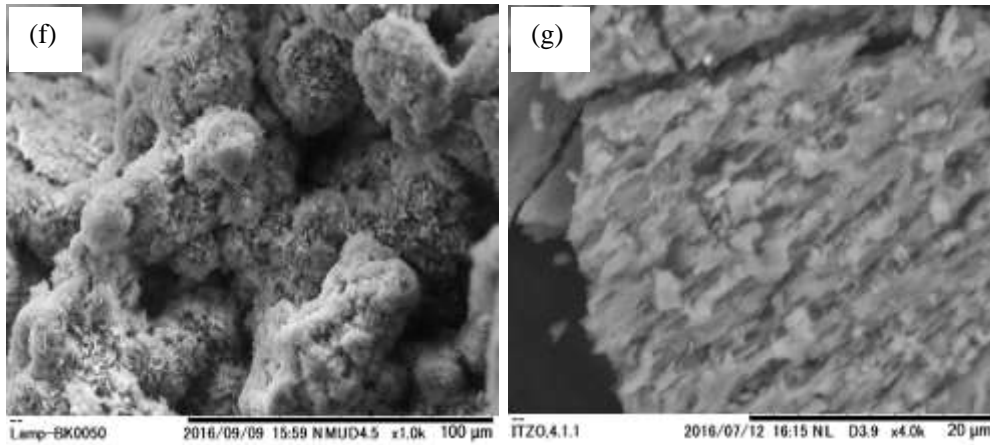
Fig. 8 SEM images of bare Zn **(a)**; MOF-5 (IL) Zn **(b,c)**;
PTh@Zn **(d,e)**; and PTh@ MOF-5 (IL) Zn **(f,g)**.

3.4 Results and Discussion

To evaluate the polarization behaviour of surface modified zinc anodes, potentio-dynamic polarization experiment was carried out in three electrode system using 0.1M KOH as electrolyte. Pure zinc and modified zinc based anodes served as working electrode, platinum as counter electrode and Ag/AgCl as reference electrode. For measuring the electrochemical parameters (E_{corr}, I_{corr}) for metal corrosion in aqueous solutions it is important to study the electrode kinetics using Tafel's plot (potentio-dynamic polarization). The Butler-Volmer equation is generally employed to evaluate the cathodic and anodic reaction in the corrosive system [19]:

$$I = Icorr\{\exp\left[\frac{2.303\ (E - Ecorr)}{ba}\right] - \exp[-\ \frac{2.303(E - Ecorr)}{bc}]\}$$

Where, I is the external current density, I_{corr} is the measure of the corrosion current, E is the electrode potential, E_{corr} is referred as corrosion potential and b_a and b_c are the Tafel's slope for anodic and cathodic region.

The polarization curves for zinc based anodes are shown in **Fig. 9**. And the values of corrosion current density (I_{corr}) and corrosion potential (E_{corr}) obtained by Tafel's fit on the linear polarization data are listed in **Table 1**. The corrosion potential of MOF modified zinc electrode shifted towards positive potential (-0.87 V) compared to pure zinc (-1.34 V) with significant drop in corrosion density indicating the effectiveness of surface coating. The lower performance of PTh@Zn is attributed to its amorphous structure which covers all the active Zn metal responsible for the activity. The lower I_{corr} observed in MOF decorated zinc electrode shows the controlled dissolution of zinc anode after the formation of porous passivation layer of MOF. The corrosion current is directly related to hydrogen evolution in zinc-air batteries as hydrogen evolution takes place with formation of oxides. Therefore, the lower values of I_{corr} suggested that surface coating on zinc electrode was highly effective strategy to supress hydrogen evolution and thereby increasing the battery discharge performance.

The I_{corr} value calculated for PTh@ MOF-5 (IL) Zn was even lower than the MOF-5 (IL) Zn, indicating the effect of polymerization of thiophene in improving the battery characteristics with MOF-5 (IL). The electropolymerization of a conducting polymer like polythiophene proves to be an efficient approach for modification of the anodes as it provides high thermal and chemical stability.
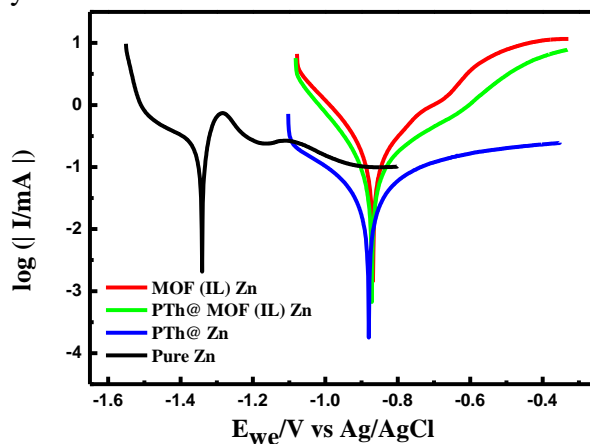

Fig. 9 Comparison of potentiodynamic polarization curves of pure zinc, MOF-5 (IL) Zn, PTh@MOF-5 (IL) Zn and PTh@ Zn in 0.1 M KOH electrolyte at room temperature. (W.E- Zn sheet, R.E- Ag/AgCl, C.E- Pt).

Table. 1 Electrochemical parameters of modified Zn anodes derived from potentio-
dynamic polarization curves in 0.1 M KOH electrolyte

Zn anodes	Corrosion potential (E_{corr}: V)	Corrosion current density (I_{corr}:μA cm^{-2})
Pure Zn	-1.340	503.2
MOF (IL) Zn	-0.868	186.7
PTh@MOF (IL) Zn	-0.872	128.1
PTh@ Zn	-0.880	493.1

Chronopotentiometry experiment was performed to see the discharging behavior of different Zn based anodes. The potential went down abruptly in case of pure zinc anode while the potential with zinc anodes decorated with MOF-5 (IL) sustained for a longer cycle (**Fig. 10**). The zinc air battery with pure zinc as anode showed current density of ~ 7 mA cm^{-2}. On the contrary, zinc air batteries with zinc anodes decorated with MOF-5 (IL) and PTh@ MOF-5 (IL) showed 4 times enhanced current density of ~ 30 mA cm^{-2} as shown in **Fig.11**. The enhanced performance can be explained by the formation of conducting passive layer of MOF (IL) and MOF (IL) / polythiophene on the surface of pure zinc electrode which prevented the active Zn metal from direct exposure to the KOH electrolyte and thus minimizing the spontaneous side reactions that occur in conventional zinc-air batteries like hydrogen evolution.
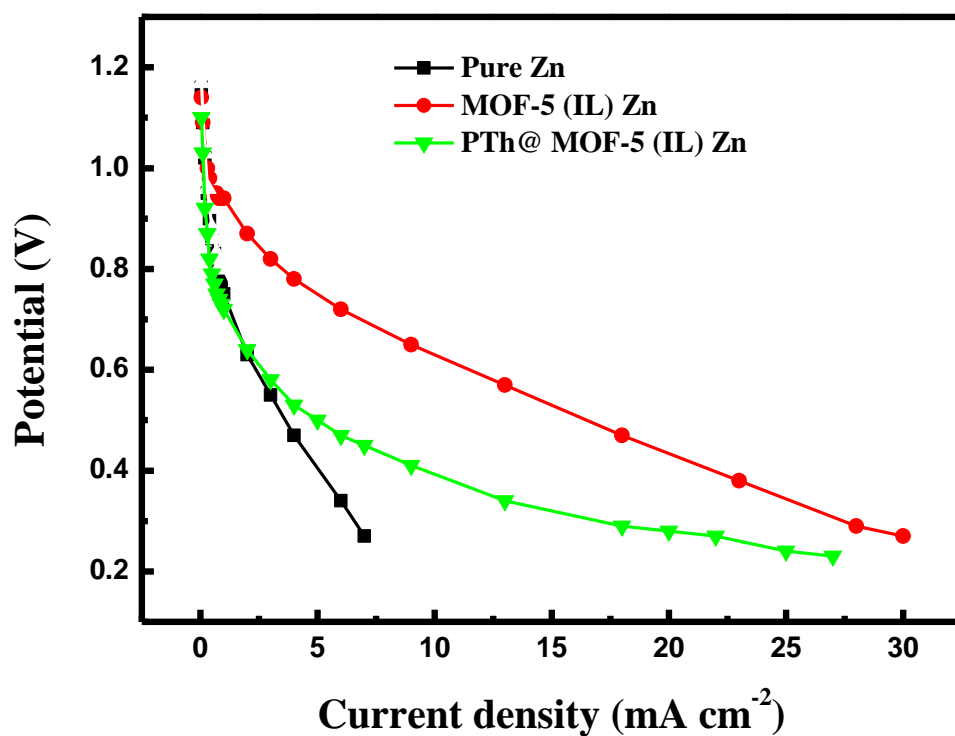
Fig. 10 Comparison of polarization curves (V~ I) of pure zinc, MOF-5 (IL) Zn, and PTh@MOF-5 (IL) Zn in 0.1 M KOH electrolyte.
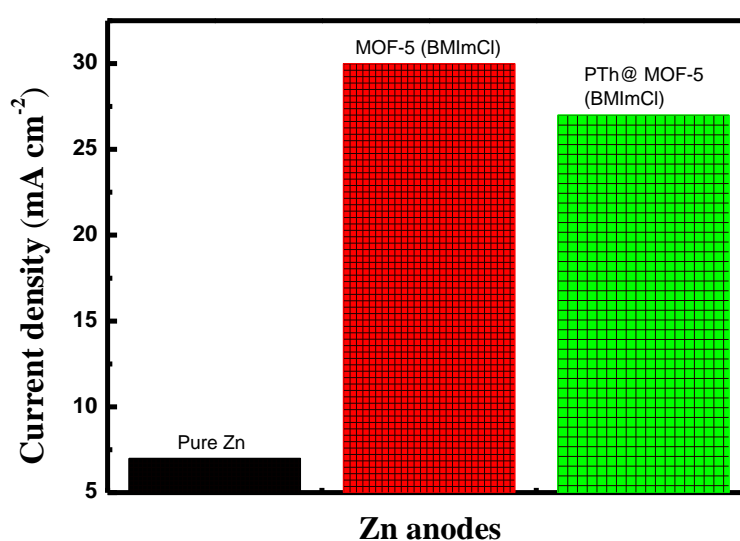

Fig. 11 Comparison of current densities of cell fabricated using pure Zn, MOF-5 (IL) Zn and PTh@ MOF-5 (IL) Zn based anodes.

To examine the practical effect on cell performance, unit cell was fabricated in this work. PTFE case in rectangular shape (5 cm length and 3.5 cm width) were used to assemble the components of the zinc-air batteries. The order of the cell components was: pure Zn and Zn based anodes (2 cm x 2 cm x 0.2 cm), glass microfiber filters soaked in 5M KOH solution, carbon cloth as porous air cathode (2 cm x 2 cm x 0.1 cm) for the permeation of air, and nickel mesh (2 cm x 2 cm x 0.1 cm) as a current collector covered with PTFE type case with holes for the diffusion of air. The top view and components of zinc air battery cell setup is shown in **Fig.12.**
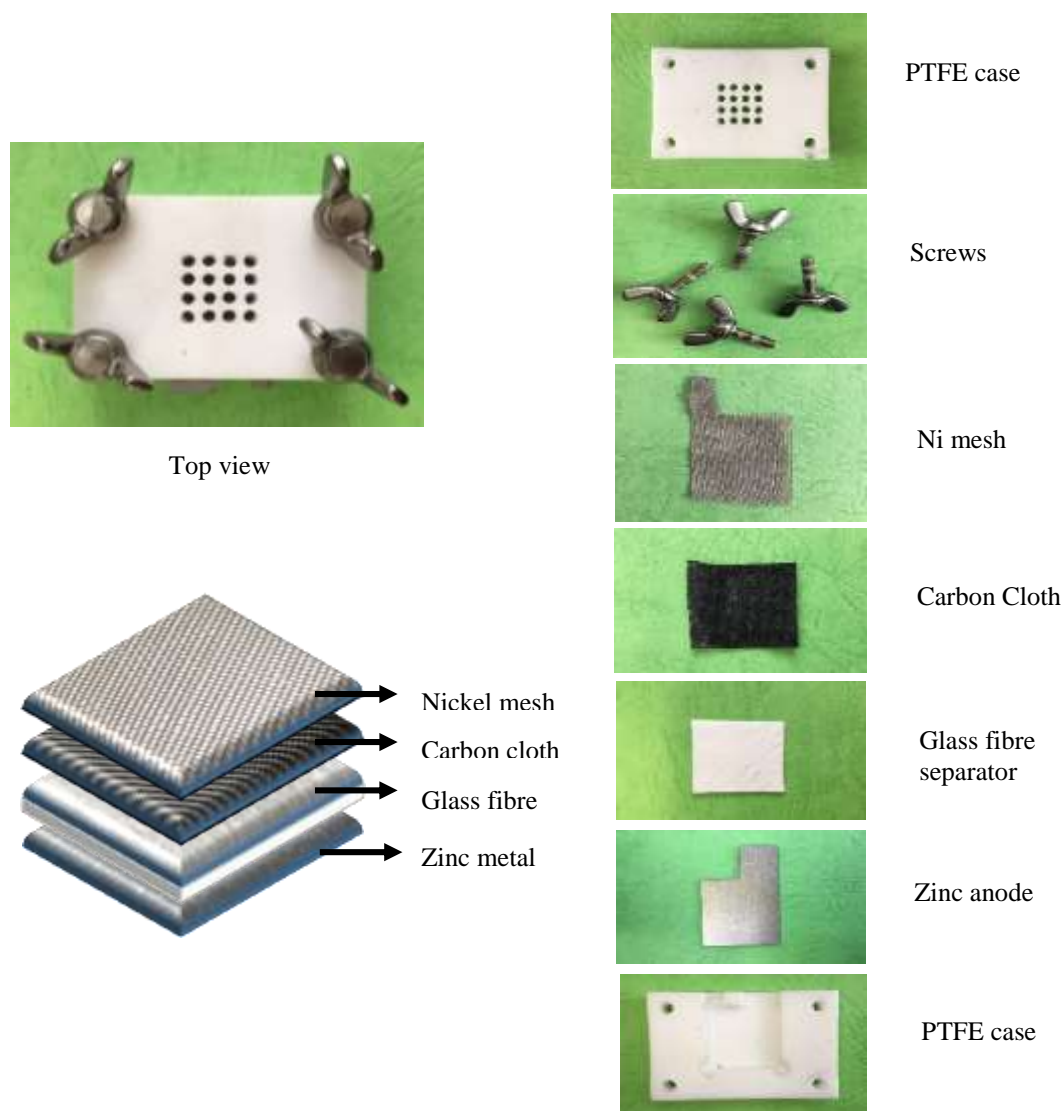

Fig. 12 Zinc-air battery cell setup.

The open circuit voltage (OCV) measurements for fabricated zinc-air batteries were done before the discharge experiment. **Fig. 13** shows the OCV values of different Zn-based anodes at 1.38 ± 0.02 V. In order to study the practical application of surface modified Zn anodes and effectiveness of MOF and polythiophene coating, discharging studies were done. The cell was allowed to discharge at constant current of 3 to 7 mA cm^{-2} over the period of time. **Fig.14** shows the discharging profile for zinc-air batteries fabricated using pure Zn, MOF-5 (IL) Zn and PTh@MOF-5 (IL) Zn based anodes. The surface modified Zn anodes with MOF-5 (IL) and PTh@MOF-5 (IL) showed the longer discharging time than pure zinc even at higher current density of 7 mA cm^{-2}. This enhanced performance or longer discharging time seen after modification of anode can be attributed to the porous passivation layer over zinc electrode which prevents the zinc surface from oxidation. The zinc anode gets easily consumed when it comes in contact with highly alkaline solution but after the modification, MOF layer provides controlled dissolution of highly consumable zinc electrode. Also the effect of polythiophene coating over MOF decorated zinc electrodes can also be observed from the discharging characteristics. The electropolymerized thiophene provides high thermal and chemical stability to the electrode adding to the performance of the battery. It is well explained from the results that the modified Zn electrodes with MOF can be prospective anodes in Zn-air batteries.
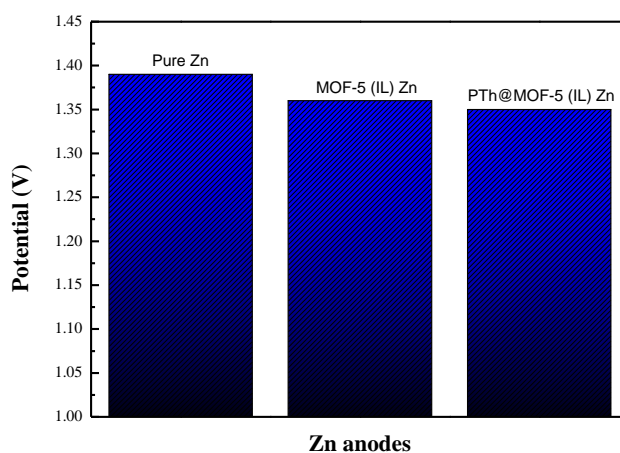

Fig. 13 OCV values of Zn-air batteries fabricated using pure Zn, MOF-5 (IL) Zn and PTh@ MOF-5 (IL) Zn as anodes.
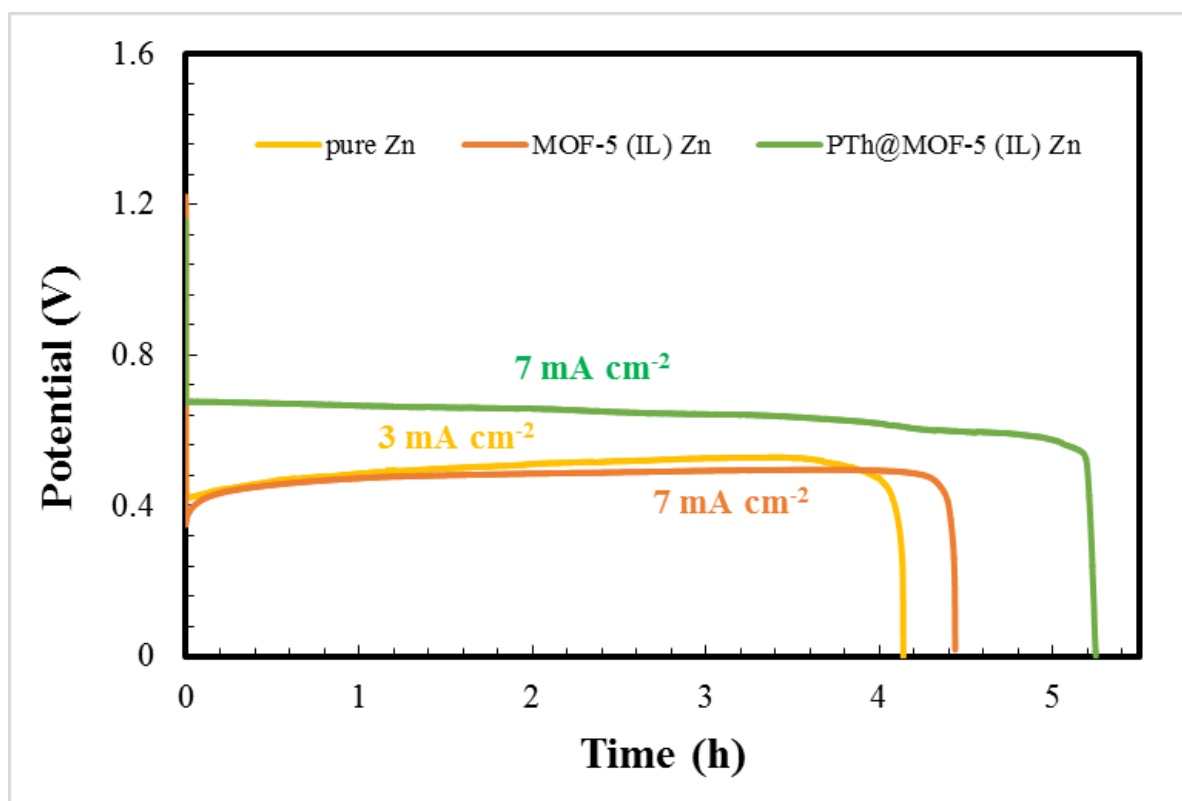
Fig. 14 Discharge curves of the primary Zn-air batteries using pure Zn, MOF-5
(IL) Zn and PTh@ MOF-5 (IL) Zn based anodes at various current densities in
open atmosphere.

Fig. 15 shows the cyclic voltammograms measured in 5.0 M KOH solution. These CVs

showed two oxidation peaks in both pure zinc and MOF-5 (IL) Zn. This indicates that the zinc

was first oxidized to $Zn(OH)_4^{2-}$ and then readily converted to ZnO or $Zn(OH)_2$ passivation film.

The current density of peak B is higher than B` which tells that the oxidation is more in case

of pure zinc compared to MOF coated Zn. This can be because of the corrosion resistant layer

of MOF over Zn that makes the oxidation of zinc difficult.

Fig. 15 Cyclic voltammograms of pure Zn and MOF-5 (IL) Zn in 5.0 M KOH at 50 mV s^{-1} (W.E- Zn sheet, R.E- Hg/HgO, C.E- Ti).
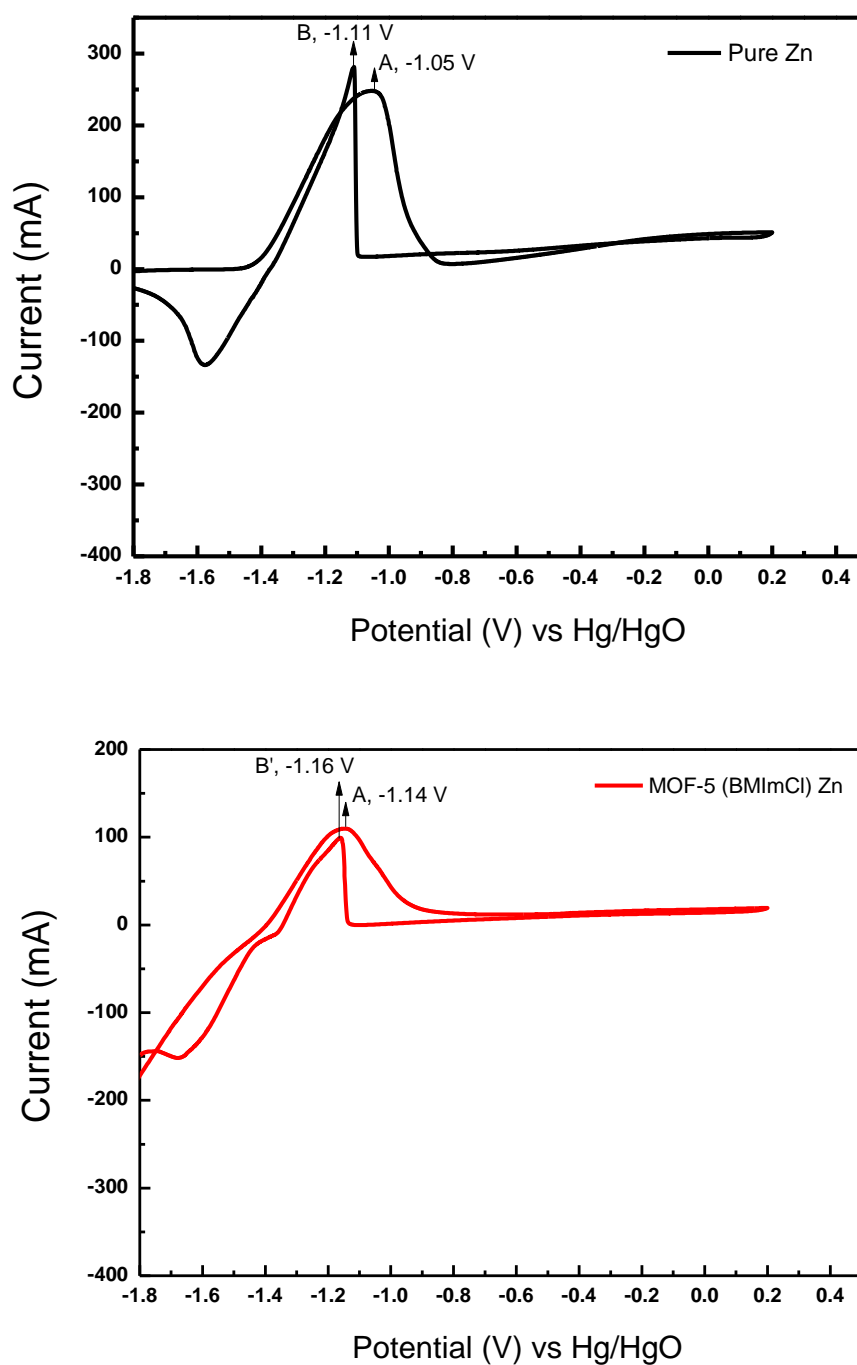
3.5 Conclusion

MOF-5 (IL) decorated Zn anodes and MOF-5 (IL) / polythiophene coated Zn anodes were successfully synthesized by electrochemical method. Modified Zn anodes were characterized using XRD, FTIR and SEM. Considering corrosion current and corrosion potential, MOF-5 (IL) decorated Zn anodes and MOF-5 (IL) / polythiophene coated Zn anodes showed the most favorable characteristics to be used in zinc-air batteries. Zn-air battery with pure zinc showed current density of $\sim$ 7 mA cm^{-2}. On the contrary, Zn-air batteries with modified Zn anodes showed 4 times enhanced current density of $\sim$ 30 mA cm^{-2}. The MOF-5 (IL) Zn and PTh@ MOF-5 (IL) Zn based anodes showed the longer discharging time than pure zinc even at higher current density of 7 mA cm^{-2}. It is well explained from the results that the modified Zn electrodes with MOF and polythiophene can be prospective anodes in Zn-air batteries (**Fig. 16**).
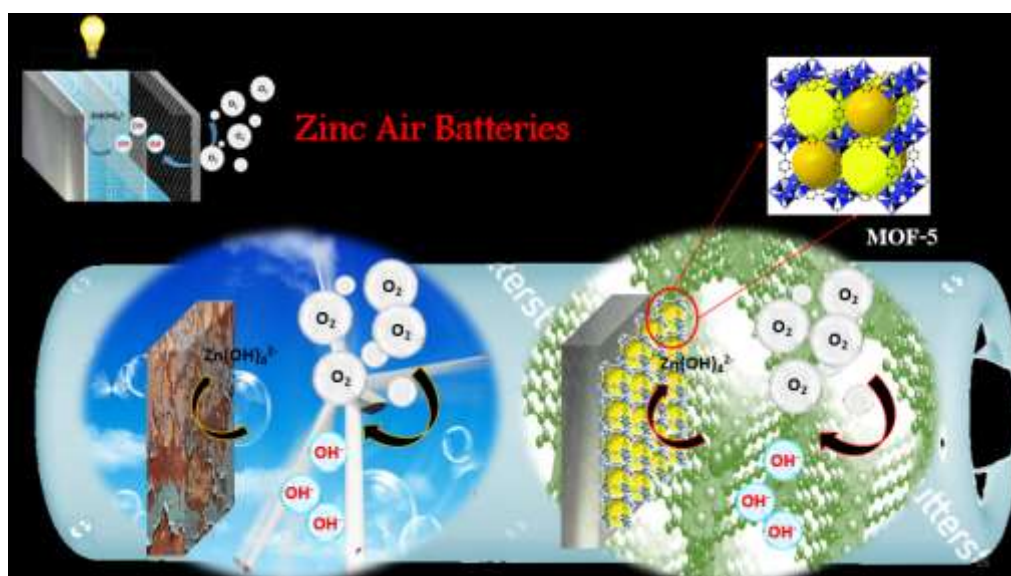

Fig. 16 Graphical illustration of corrosion protection of zinc by MOFs surface coating.

References

[1]   Y. Li, H. Dai, Chem. Soc. Rev. 43 (2014) 5257.

[2]   Y. Li, M. Gong, Y. Liang, J. Feng, J.-E. Kim, H. Wang, G. Hong, B. Zhang, H. Dai, Nat. Commun. 4 (2013) 1805.

[3]   M. A. Rahman, X. Wang, C. Wen, J. Electrochem. Soc. 160 (2013) A1759.

[4]   C. W. Lee, K. Sathiyanarayanan, S. W. Eom, M. S. Yun, J. Power Sources 160 (2006) 1436.

[5]   C. Chakkaravarthy, A. K. A. Waheed, H. V. K. Udupa, J. Power Sources 6 (1981) 203.

[6]   G. X. Zhang, ECS Trans. 3 (2008) 1.

[7]   M. A. Rahman, X. Wang, C. Wen, J. Electrochem. Soc. 160 (2013) A1759.

[8]   X. G. Zhang, J. Power Sources 163 (2006) 591.

[9]   V. Caramia, B. Bozzini, Mater. Renew. Sustain. Energy 3 (2014) 1.

[10]   D. D. Macdonald, C. English, J. Appl. Electrochem. 20 (1990) 405.

[11]   Y. Tang, L. Lu, H. W. Roesky, L. Wang, B. Huang, J. Power Sources 138 (2004) 313.

[12]   P. Pei, K. Wang, Z. Ma, Appl. Energy 128 (2014) 315.

[13]   D. P. Gregory, P. C. Jones, D. P. Redfearn, J. Electrochem. Soc. 119 (1972) 1288.

[14]   X. G. Zhang, Corrosion and Electrochemistry of Zinc, Springer Science & Business Media, 2013.

[15]   S. Thomas, N. Birbilis, M. S. Venkatraman, I. S. Cole, Corrosion 68 (2012) 015009.

[16]   C. J. Lan, T. S. Chin, P. H. Lin, T. P. Perng, J. New Mater. Electrochem. Syst. 9 (2006) 27.

[17]   J. McBreen, E. Gannon, Electrochim. Acta 26 (1981) 1439.

[18]   Y. -D. Cho, G. T. -K. Fey, J. Power Sources 184 (2008) 610.

[19]   S. -M. Lee, Y. -J. Kim, S. -W. Eom, N. -S. Choi, K. -W. Kim, S. -B. Cho, J. Power

Sources 227 (2013) 177.

[20]   N. Stock, S. Biswas, Chem. Rev. 112 (2011) 933.

[21]   C. -M. Wu, M. Rathi, S. P. Ahrenkiel, R. T. Koodali, Z. Wang, Chem. Commun. 49 (2013) 1223.

[22]   A. Dhakshinamoorthy, M. Alvaro, H. Garcia, ChemCatChem 2 (2010) 1438.

[23]   A. R. Millward, O. M. Yaghi, J. Am. Chem. Soc. 127 (2005) 17998.

[24]   H. K. Chae, D. Y. Siberio-Pérez, J. Kim, Y. Go, M. Eddaoudi, A. J. Matzger, M. O'Keeffe, O. M. Yaghi, Nature 427 (2004) 523.

[25]   H. Furukawa, N. Ko, Y. B. Go, N. Aratani, S. B. Choi, E. Choi, A. O. Yazaydin, R. Q. Snurr, M. O'Keeffe, J. Kim, O. M. Yaghi, Science 329 (2010) 424.

[26]   Y. Ren, G. H. Chia, Z. Gao, Nano Today 8 (2013) 577.

[27]   F. Zheng, Y. Yang, Q. Chen, Nat. Commun. 5 (2014) 5261.

[28]   B. Liu, H. Shioyama, H. Jiang, X. Zhang, Q. Xu, Carbon 48 (2010) 456.

[29]   S. -L. Li, Q. Xu, Energy & Environ. Sci. 6 (2013) 1656.

[30]   J. Hu, H. Wang, Q. Gao, H. Guo, Carbon 48 (2010) 3599.

[31]   H. Kitagawa, Nat. Chem. 1 (2009) 689.

[32]   A. Mesbah, S. Jacques, E. Rocca, M. François, J. Steinmetz, Eur. J. Inorg. Chem. 2011 (2011) 1315.

[33]   A. Mesbah, C. Juers, F. Lacouture, S. Mathieu, E. Rocca, M. François, J. Steinmetz, Solid State Sci. 9 (2007) 322.

[34]   S.E.H. Etaiw, A.E.-A.S. Fouda, S.A. Amer, M.M. El-bendary, J. Inorg. Organomet. Polym. Mater. 21 (2011) 327.

[35]   S. Kumaraguru, R. Pavulraj, S. Mohan, Trans. IMF 95 (2017) 131.

[36]   P. P. Deshpande, N. G. Jadhav, V. J. Gelling, D. Sazou, J. Coatings Technol. Res. 11 (2014) 473.

[37]   Y. Dai, Int. J. Electrochem. Sci. 11 (2016) 4084.

[38]   E. M. Fayyad, S. H. Sanad, A. A. Ismail, Silicon 9 (2017) 901.

[39]   J. Dupont, C. S. Consorti, P. A. Suarez, R. F. de Souza, Org. Synth. (2003) 236.

[40]   A. Singh, R. Vedarajan, N. Matsumi, J. Electrochem. Soc. 164 (2017) H5169.

[41]   S. Aeiyach, E. A. Bazzaoui, P. -C. Lacaze, J. Electroanal. Chem. 434 (1997) 153.

Chapter 4

ZIF-8/Functionalised Acetylene Black (FAB) hybrid nanocomposites as efficient non precious metal catalyst for ORR

Abstract

The ZIF-8/FAB hybrid nanocomposites were successfully synthesized by simple procedure for oxygen reduction reaction. The synthesized hybrid nanocomposites with varying amount of FAB were characterized using various techniques and evaluated for their activity towards ORR. Amount variation of FAB with ZIF-8 allowed tunability in morphology as well as porosity. Cyclic Voltammograms showed high peak current of ~0.569 mA exhibiting high catalytic activity of ZIF-8/FAB hybrid composites in reducing oxygen. Futher, these hybrid nanocomposites show excellent tolerance against methanol crossover and presented long term stability without significant activity loss.

4.1 Introduction

Electrocatalytic Oxygen Reduction Reaction (ORR) is the key factor responsible for the performance of metal-air batteries and fuel cells. But the sluggish kinetics and expensive catalysts of ORR have restricted the growth of commercialized ORR based devices [1,2]. Since the evolution of this field started, Pt-based catalysts have been so far the best serving catalysts for the reduction of oxygen but its high cost and poisoning towards methanol has hindered the mass production [3–5]. Therefore, widespread research is going on to explore an electrocatalyst with high catalytic activity, low cost, high durability and low methanol crossover. In this context, Metal Organic Frameworks (MOFs) have attracted huge attention in the recent past because of its simple synthetic procedure. The diverse nature of MOFs formed by selecting suitable metal clusters and functional organic linkers gives range of its applications in the fields of gas storage [6–8], separation [9–12], catalysis [13–16] and sensors [17–20]. Because of its organic-inorganic hybrid nature and porosity, it has already gained the interest in the field of energy storage ranging from batteries, supercapacitors and electrocatalyst. The widespread researches on MOFs and MOF derived materials by the materials science communities have already proven it as a promising energy conversion material for the future. In last few years, there have been so much studies on MOFs as electrocatalysts for ORR in fuel cells and metal air batteries [21–25]. The carbon materials synthesized using MOF as non-precious metal catalysts have proven to be a boon for the field of electrocatalyts. These materials show high catalytic activity, long term stability and resistance towards the methanol poisoning owing to its unique structural properties.

Recently, many studies conducted on the use of MOFs or MOF derived materials show the decoration of MOFs nanoparticles over different carbon support. In this context, Bing Ni et al. reported the use of ZIF-67 to modify the commercial carbon Vulcan XC-72 [26]. The

study showed improved ORR activity and durability compared with the commercial carbon. Another report by Jing Wei et al. showed the synthesis of ZIF nanocrystals over graphene oxide to prepare N-doped nanoporous carbon nano sandwiches after calcination [27]. Furthermore the synthesized material was evaluated for the electrochemical behaviour and showed high durability and methanol tolerance compared to the existing commercial electrocatalyst. However, most of the reports show the catalytic activity of the MOF derived materials after calcination once the structure is lost.

ZIFs as active precursor for N-doped carbon electrocatalysts

In recent past it has been discovered that the heteroatom doping in the carbon matrix enhances the ORR performance to great extent. In particular the N-doping is recognized more viable option because it enhances the electronic properties of the carbon matrix because of its comparable size to that of the carbon. Also its high electronegativity creates more positive charge density in the matrix which induces large number of active sites for the oxygen reduction [28]. Therefore, in the search of various precursors for doping nitrogen in the carbon matrix one of the most widely explored MOFs is Zeolitic Imidazolate Frameworks (ZIFs). These ZIFs apart from having high surface area and porosity also possess relatively high chemical and thermal stability compared to other MOFs. Also the organic ligand used for the synthesis of ZIFs i.e. imidazole based ligands contain high nitrogen content that makes ZIFs attractive materials for the preparation of electrocatalysts for fuel cells and metal-air batteries [27]. The electrocatalysts prepared from the decoration of ZIFs nanocrystals on wide varieties of carbon substrate like CNT, graphene, etc. have been evaluated for ORR performances widely by the electrochemical community.

In recent past our group Matsumi et al. showed novel single step functionalization and exfoliation of acetylene black (AB) to prepare functionalized acetylene black (FAB) which showed high performance with Pt nanoparticles for ORR [29]. Deriving inspiration from such literatures, novel hybrid nano composites of ZIF-8 and FAB were synthesized which introduces the unique properties of MOF in the efficient carbon materials to integrate its activity as an electrocatalyst. To achieve this, ZIF-8 was chosen because of its already proven ORR efficiency in the past and functionalised acetylene black as carbon material.

4.2 Experimental

The functionalization and exfoliation of acetylene black were done by already reported single pot method by Matsumi et al. AB was treated with H_2SO_4: HNO_3 (3:1) mixture followed by ultrasonication for 3h. Sulfuric acid and Nitric acid were purchased form WAKO Co. Ltd. and used as received. Scanning Electron Microscopy (SEM) and Energy-dispersive X-ray spectroscopy (EDS) mapping analysis was done on a Hitachi S-4500 (Hitachi Ltd., Chiyoda-ku, Japan). Transmission Electron Microscopy (TEM) analysis was done on a Hitachi 7100 (Hitachi Ltd., Chiyoda-ku, Japan). A Perkin Elmer 100 FT-IR spectrometer was used to record IR spectra. X-ray diffraction data was collected using Rigaku SmartLab (Rigaku, Japan) operating at 40 kV, 30 mA at a rate of 1° min^{-1}, using Cu Kα radiation. Cyclic voltammetry measurements were carried out on Biologic VSP s/n 1190.

4.2.1 Synthesis of ZIF-8 particles:

ZIF-8 nanocrystals were prepared using typical synthetic method reported in the literature [30]. $Zn(NO_3)_2 \cdot 6H_2O$ and 2-methylimidazole were dissolved in 25 mL of methanol separately and mixed slowly under vigorous stirring. The stirring continued till the resultant solution turned milky in colour and the product was further collected by centrifugation. The resultant solid was washed with methanol solution and dried under vacuum for 4 hours at 80 ^{o}C.

4.2.2 Synthesis of ZIF-8@FAB hybrid nanocomposite:

In a typical synthesis, 183 mg of Zinc nitrate hexahydrate (0.615mmol) was dissolved in 25 mL methanol and 405.5 mg of 2-methyl imidazole (4.94mmol) was also dissolved in 25 mL methanol. For the synthesis of ZIF-8/FAB composites with different wt% of FAB, desired

amount of FAB was dissolved in 25 mL methanol and sonicated for 1 hour. The hybrid nanocomposites were synthesized by simultaneous addition of methanolic Zinc nitrate hexahydrate solution and FAB solution to the 2-methyl imidazole solution with vigorous stiring. The resulting mixture was stirred for 2 hours at room temperature (**Fig. 1**). Then the mixture was recollected by centrifugation (4000 rpm, 10 min) and washed repeatedly 3 times with water-methanol mixture. The obtained solid was then dried under vacuum at 80 ^{o}C. The samples with different amount of FAB (X= 2, 5, 10 wt%) were named as ZIF-8@FAB-2, ZIF-8@FAB-5 and ZIF-8@FAB-10, respectively.
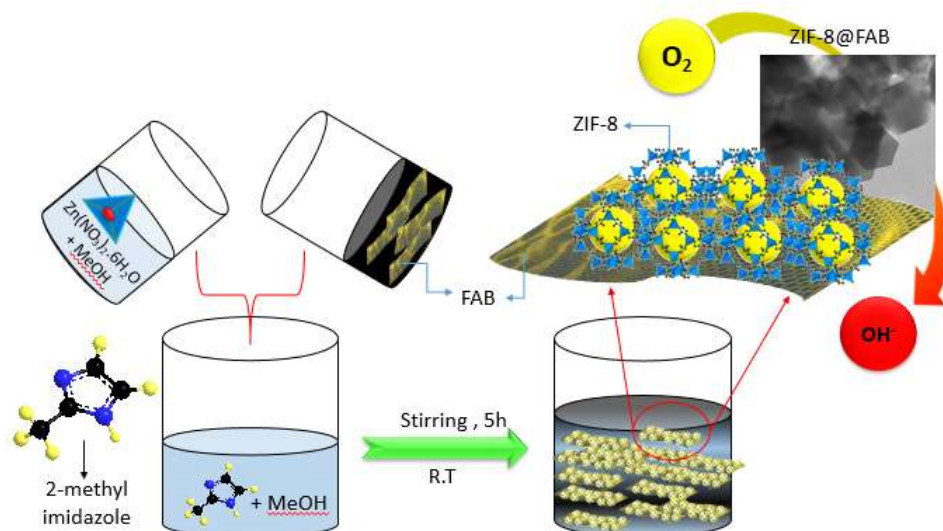

Fig. 1 Schematic illustration of ZIF-8/FAB nanocomposite preparation at room temperature.

4.3 Characterization

The synthesized hybrid nanocomposites were characterized by XRD, FTIR, TEM and SEM- EDS, Raman, XPS and BET measurements. The XRD pattern shown in **Fig. 2** showed complete resemblance with the pristine ZIF-8 pattern indicating the successful formation of crystalline hybrids. The presence of peaks corresponding to ZIF-8 and FAB in the XRD diffractograms of nanocomposites were found out to be in good agreement with the pure samples.
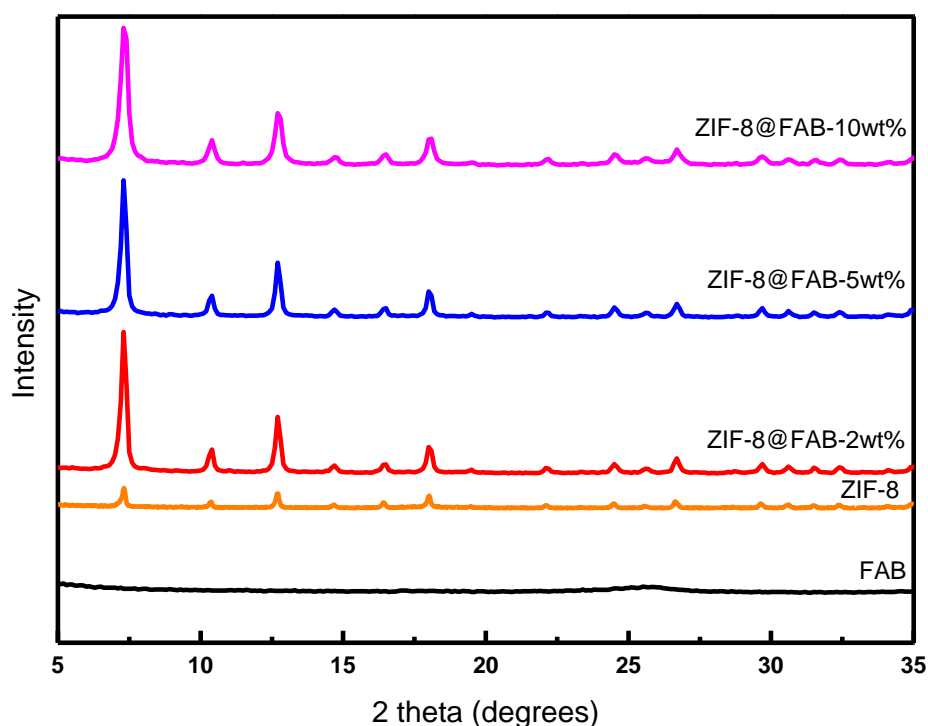

Fig. 2 Comparison of XRD patterns of FAB, ZIF-8, ZIF-8@FAB-2wt%, ZIF-8@FAB-5wt% and ZIF-8@FAB-10wt% materials.

Fig. 3 shows the FTIR spectra of ZIF-8 and ZIF-8@FAB composite materials were almost identical proving the presence of similar functional groups on the surface. The peak at $1582\ cm^{-1}$ indicates the $C=N$ stretching vibration. The peak at $750\ cm^{-1}$ corresponds to the

double bonds vibration of imidazole ring and the stretching of Zn-N was at 420 cm^{-1}. And the peak at 1147 cm^{-1} corresponds to the C-N stretching.
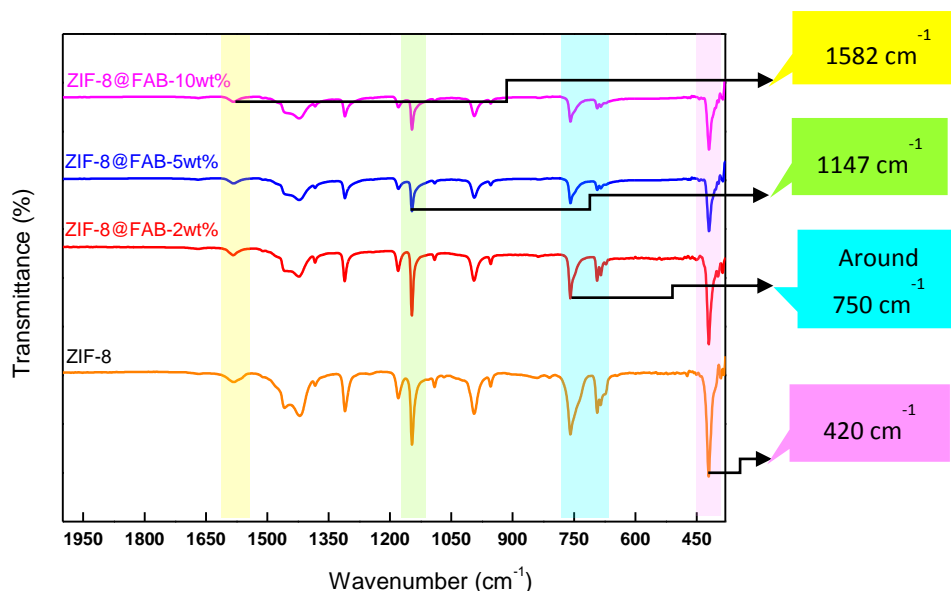

Fig: 3 IR spectra of ZIF-8, ZIF-8@FAB-2wt%, ZIF-8@FAB-5wt% and ZIF-8@FAB-10wt% materials.

The Raman spectra in **Fig. 4** shows the D and G bands corresponding to the FAB. The bands for ZIF-8 cannot be seen in the spectra because of the wide D and G band intensities. As the concentration of FAB is increased from 2 wt% to 10 wt%, the intensities of D and G bands tends to increase. Increase in the I_D/I_G value from FAB to ZIF-8@FAB nanocomposites confirms the successful incorporation of ZIF-8 nanoparticles in the carbon matrix of FAB.

Elemental surveys by X-ray photoelectron spectroscopy (XPS) in **Fig. 5**, showed the presence of the ZIF-8 framework elements (Zn, C, N) and O in ZIF-8@FAB samples and clearly confirmed the presence of ZIF-8 particles in the Functionalized Acetylene Black (FAB) matrix.
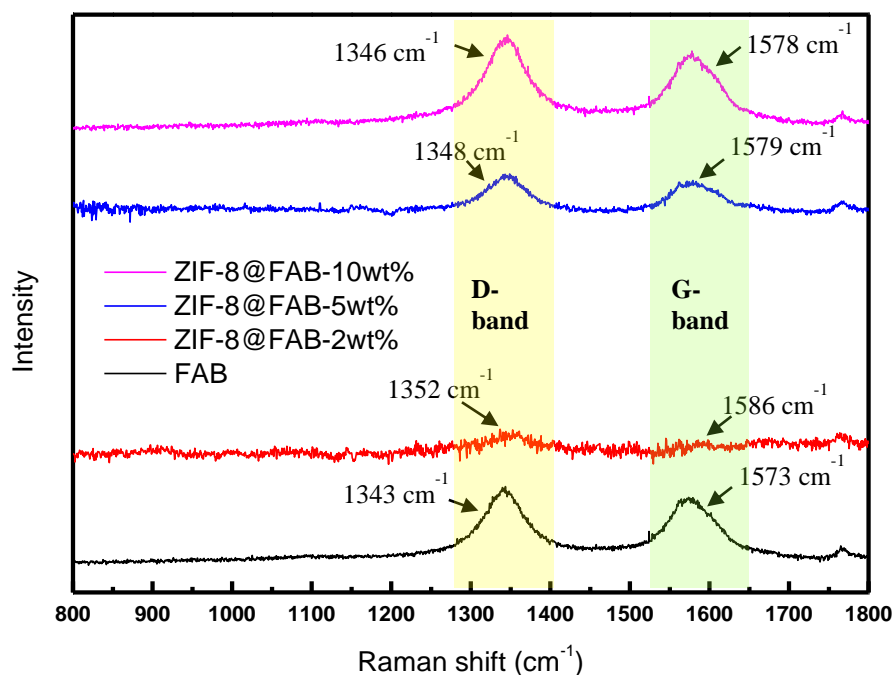
Fig: 4 Raman spectra of FAB, ZIF-8@FAB-2wt%, ZIF-8@FAB-5wt%, ZIF-8@FAB-10wt% materials showing D-band and G-band of different intensities depending on FAB concentration.
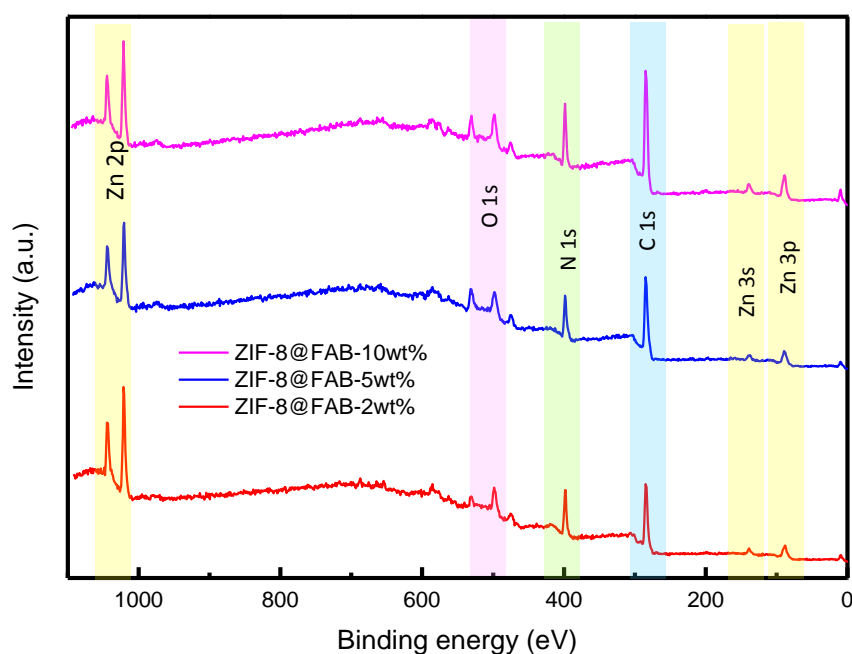

Fig: 5 XPS survey spectra of ZIF-8@FAB-2wt%, ZIF-8@FAB-5wt% and ZIF-8@FAB-10wt% nanocomposites.

N$_2$ adsorption and desorption measurements were done to see the surface area and pore size of the hybrid nanocomposites. The BET surface areas of AB, FAB, ZIF-8@FAB-2wt%, ZIF-8@FAB-5wt%, ZIF-8@FAB-10wt% were 60.0, 66.5, 1020, 912, 645 m^{2}g^{-1}, respectively. The BET surface area of the composites decreases with increasing FAB content. The continuous decrease in surface area of nanocomposites with increasing percentage of FAB can be attributed to its nonporous nature (**Fig. 6**).
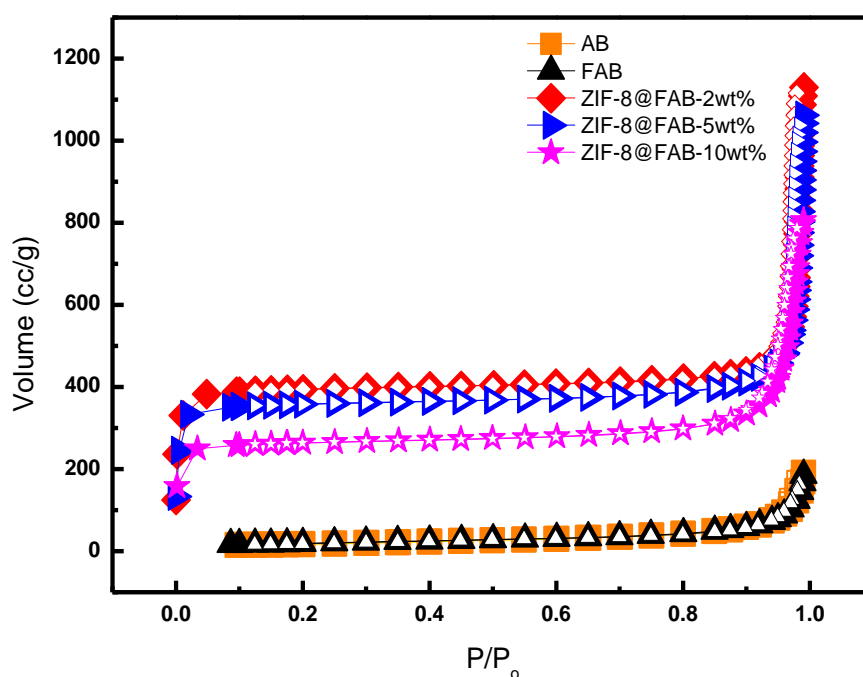

Fig: 6 N$_2$ adsorption-desorption isotherms of AB, FAB, ZIF-8@FAB-2wt%, ZIF-8@FAB-5wt%, ZIF-8@FAB-10wt% materials.

Fig. 7 shows the TEM images of AB, FAB and ZIF-8@FAB hybrid nanocomposites to observe the morphology of each. The multi-layered AB can be seen in the image **Fig. 7a**. After the functionalization and exfoliation of AB to synthesize FAB, the image **Fig. 7b** exhibits graphene like transparent features. The ZIF-8@FAB hybrid nanocomposites showed hexagonal particles (similar to pristine ZIF-8 particles) with FAB layer on it (**Fig. 7c-e**). The hexagonal morphology of ZIF-8 particles remains unaffected on increasing the percentage of FAB in the composites. But the size of the particles varied slightly on increasing the proportion of FAB in the hybrid nanocomposites. The size of ZIF-8 hexagonal particles remained almost same (60-70 nm) in ZIF-8@FAB-2wt% and ZIF-8@FAB-5wt% composition. On increasing the FAB concentration further the size reduced slightly to 40-50 nm for the ZIF-8@FAB-10wt%. The size of the hexagonal ZIF-8 nanoparticles seems to be modulated by the functional groups on FAB surface. The TEM results showing decreased size for ZIF-8@FAB-10wt% are also in accordance with the BET results, where it was observed that the pore size became less on increasing the FAB concentration.
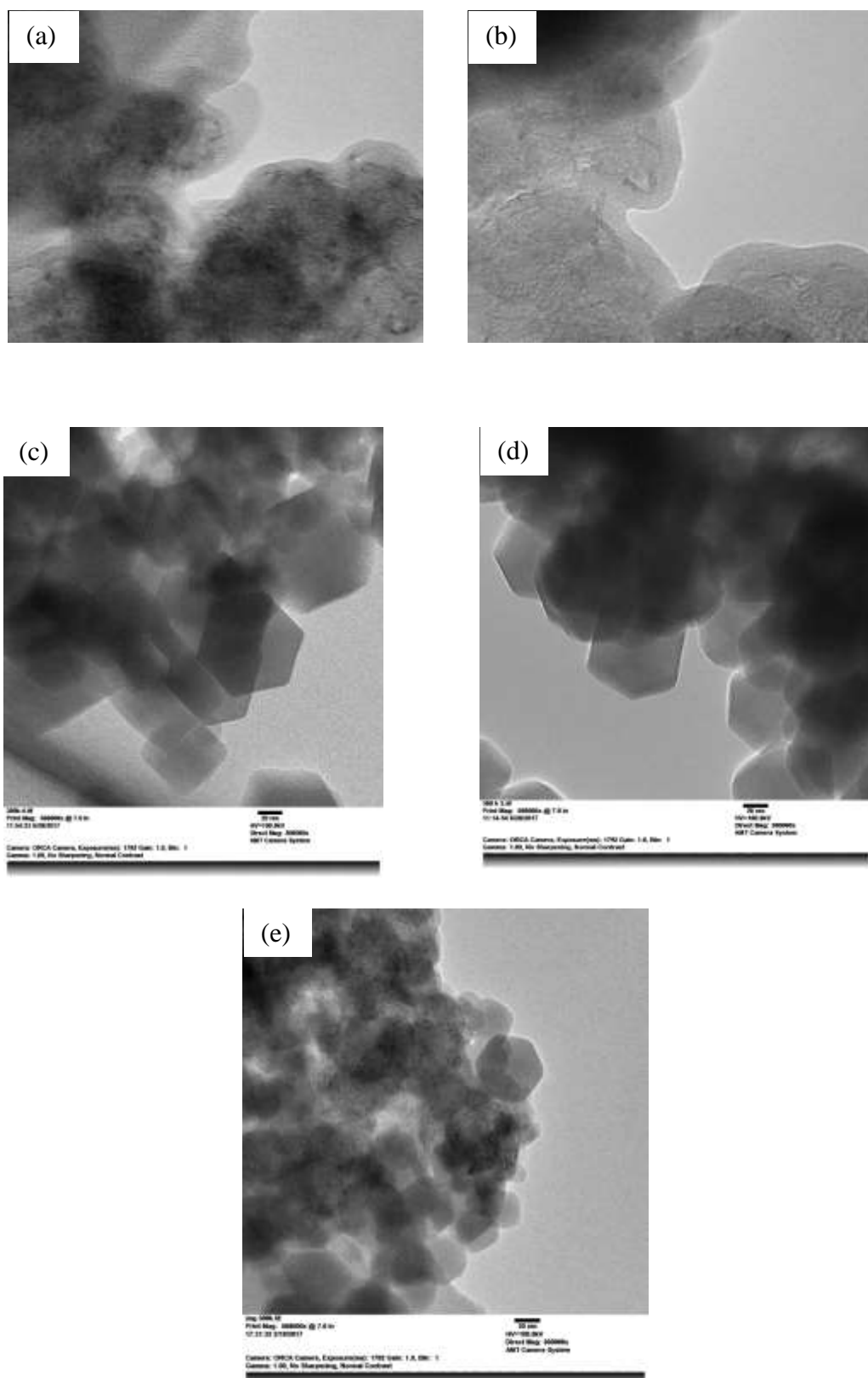
Fig. 7 showing the TEM micrographs of (a) Acetylene Black (AB), (b) Functionalized Acetylene Black (FAB), (c) ZIF-8@FAB-2wt%, (d) ZIF-8@FAB-5wt%, (e) ZIF-8@FAB-10wt% materials.

The presence of ZIF-8 nanoparticles in the carbon matrix of FAB was further confirmed by Energy dispersive spectroscopy (EDS) and elemental mapping as shown in **Fig. 8**.

Fig: 8 (a) SEM image of ZIF-8@FAB-10wt%, (b) EDS of ZIF-8@FAB-10wt%, (c-f) the corresponding C-,N-,O- and Zn elemental mappings, respectively.

4.4 Results and Discussion

To evaluate the electrocatalyst activity, first the electrocatalyst was dispersed in a mixture of isopropyl alcohol and Nafion. The cata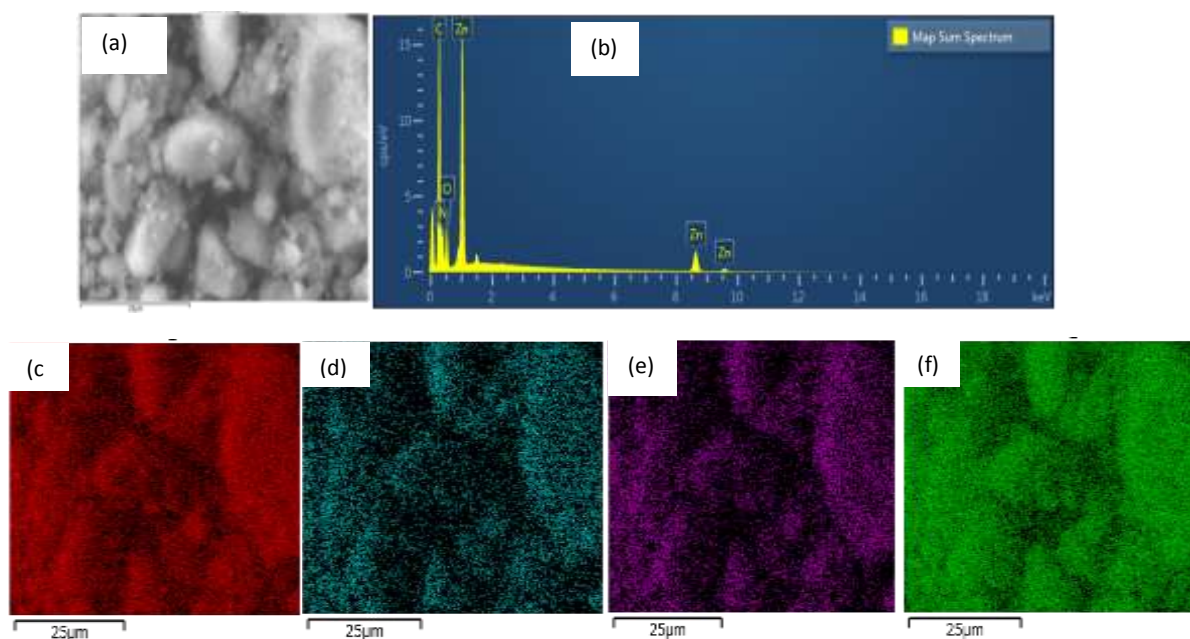lyst (1.3 mg) was first mixed with isopropyl alcohol (100 µL) and then Nafion (15 µL) was added to the mixture. The resulting mixture was sonicated to get thick uniform catalyst ink. This ink was then drop casted on the glassy carbon (GC) electrode to conduct electrochemical measurements. The preparation of the GC electrode from catalyst is shown in **Fig. 9.**
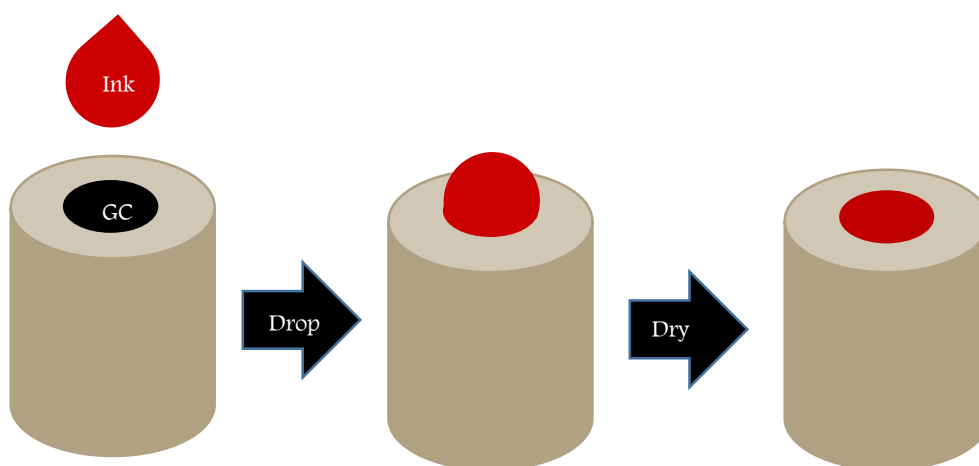
Fig: 9 Illustration of glassy carbon electrode preparation.

To evaluate the electrocatalytic performance of the synthesized hybrid nanocomposites, cyclic voltammograms (CVs) were performed. In CV, the potential of working electrode is ramped linearly versus time. Once the votammogram reaches the desired potential, the potential of working electrode is ramped in reverse direction. This reverse ramping or cycling can take place multiple times during an experiment. Basically, this technique is employed to see at what potential the reaction is under equilibrium. The cyclic voltammetry measurements were done in N_2 and O_2 saturated 0.1 M KOH using mercury/ mercury oxide (Hg/HgO) as reference electrode, platinum wire as the counter electrode, and the glassy carbon electrode

loaded with electrocatalyst as the working electrode. The alkaline electrolyte (0.1 M KOH) was completely saturated by bubbling O_2 at room temperature at least 20 min prior to the measurement. A continuous flow of oxygen was maintained during the cyclic voltammetry measurements.

The cyclic voltammetry measurements were conducted in both N_2 and O_2 saturated 0.1 M KOH at a scan rate of 50 mV s^{-1} in the potential range -1.5 to 0 V as shown in **Fig. 10**. Clearly, all the hybrid nanocomposites showed obvious peaks in O_2 saturated 0.1 M KOH including FAB. There was no noticeable change in the current when the measurement was done in oxygen free electrolyte (N_2 saturated 0.1 M KOH). The cyclic voltammogram for FAB showed large over potential when tested for electrocatalytic activity owing to its poor conductivity. But the syntheisized hybrid nanocomposites of ZIF-8@FAB showed high cathodic current density compared to pristine FAB. The highest peak current was obtained for ZIF-8@FAB-2 wt% i.e. 0.569 mA compared to higher concentration FAB composites (**Table 1**). The results are in good agreement with Raman and BET results showing higher degree of disorderness and high BET surface area for ZIF-8@FAB-2 wt%. Hence, these results demonstrate the excellent electrocatalytic activity of ZIF-8@FAB hybrid composites as non-precious metal catalyst.

ZIF-8 is widely explored in the field of ORR by many researchers because it possess high nitrogen content present in the imidazole-based ligands. Therefore it is considered as one of the most effective precursor for the synthesis of nitrogen doped carbon materials. The high ORR activity can be because of the fact that FAB itself is an ORR active material and after the loading of ZIF-8 nanocrystals on the FAB the surface area increases significantly which in turns improves the activity. And therefore we can say that the defects of FAB and positively charged carbon adjacent to nitrogen has been considered to be active.
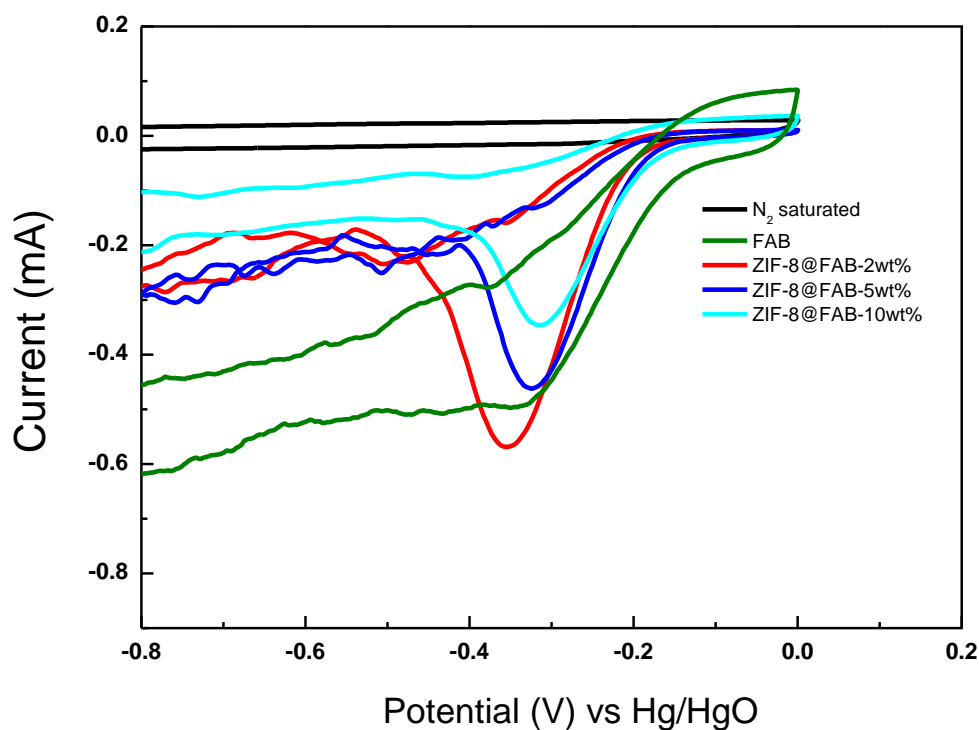
Fig: 10 CVs of FAB, ZIF-8@FAB-2wt%, ZIF-8@FAB-5wt% and ZIF-8@FAB-10wt% nanocomposites in N_2-or O_2 saturated 0.1M KOH solution

Table 1: Peak current (mA) values from cyclic voltammograms for different nanocomposites.

Samples	Peak current
ZIF-8@FAB-2wt%	**0.569 mA**
ZIF-8@FAB-5wt%	0.478 mA
ZIF-8@FAB-10wt%	0.346 mA

To better understand the ORR with the ZIF-8@FAB hybrid composites as electrocatlyst, linear sweep voltammograms were carried out on a rotating disk electrode (RDE) in the potential range -0.8 V to 0 V at a scan rate of 50 mV s^{-1}. The experiment was performed at different rotation speeds from 100 rpm to 4000 rpm in O_2 saturated 0.1 M KOH solution.

To examine the ORR performance, the Koutecky-Levich (K-L) plots were plotted to calculate the number of electrons. The inverse of current is plotted versus inverse of electrode rotation at different rotation speed at different potential. The intercept on Y-axis and slope were used to determine the number of electron transfer and the kinetic current density, respectively.

The equation (1) shown below was used to calculate the number of electron transfer:

$$B = 0.6 \ nFv^{-1/2}C_{O2}D_{O2}^{\ 2/3} \ \ldots\ldots\ldots\ldots.. (1)$$

Where 'B' is Levich slope, 'n' is the number of transferred electrons for ORR, 'F' is the Faraday constant (96485 C mol^{-1}), 'v' is the kinetic viscosity, 'C_{O2}' is the concentration of oxygen in 0.1 M KOH (1.2 X 10^{-3} mol L^{-1}), and 'D_{O2}' is the diffusion coefficient of O_2 in 0.1 M KOH (1.9 X 10^{-5} cm s^{-1}) [1,2].

The current density enhanced with increase in the rotation speed in RDE from 100 rpm to 4000 rpm indicating the diffusion limited process. The higher kinetic current density in case of ZIF-8@FAB-2 wt% implied that the surface area and concentration of FAB were crucial factors for the ORR activity in the synthesized hybrid composites. The Koutecky-Levich (K-L) plots in the range of -0.6 V to -1 V showed good linear trend, indicating the first order kinetics occurring in the oxygen reduction (**Fig. 11**). The electron transfer during ORR 'n' was calculated from Koutecky-Levich (K-L) plots using equation (1). The n values for ZIF-8@FAB-2wt%, ZIF-8@FAB-5wt%, ZIF-8@FAB-10wt% hybrid composites are 4.01 to 4.03

over the potential range -0.6 V to -1 V, indicating the 4e⁻ transfer type reaction mechanism pathway for all the samples. These results clearly reveal that incorporation of nitrogen atoms (in ZIF-8) into the carbon matrix (FAB) can significantly enhance the surface polarity, conductivity and electron donor tendency of the porous materials leading to enhanced ORR activity.
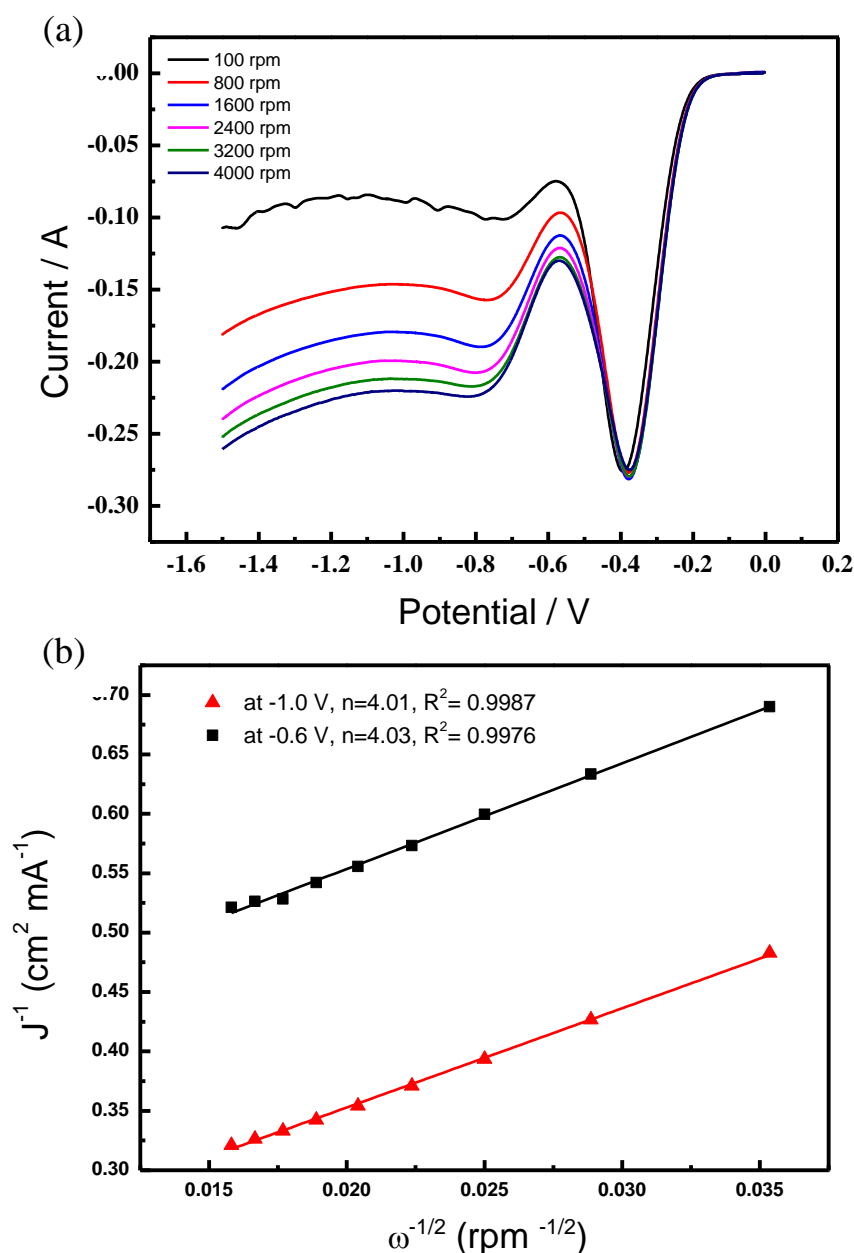

Fig: 11 (a) RDE curves for ZIF-8@FAB-10wt% at 30 ℃ in oxygen saturated 0.1 M KOH aq. at scan rate of 20 mV/s at different rotation speeds (100, 800, 1600, 2400, 3200, 4000 rpm) and (b) respective Koutecky-Levich plots at -0.6 and -1.0 V.

To employ any electrocatalyst in practical application it is important to know its stability towards methanol. To evaluate the performance of synthesized electrocatalyst regarding resistance and durability towards methanol, cyclic voltammetry experiments were carried out. CVs were recorded in oxygen saturated 0.1 M KOH solution with and without methanol (1.0 M) (**Fig. 12**). The voltammograms showed no significant changes on addition of methanol in the electrolyte solution. The peak current density remained almost same at scan rate of 50 mV s^{-1}. This indicates the excellent ability of the electrocatalyst for avoiding methanol crossover.
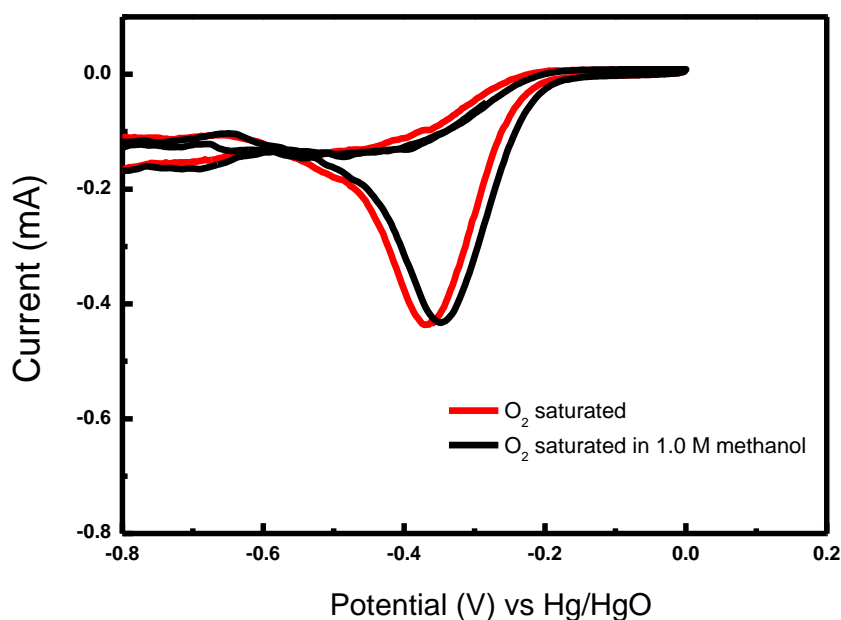

Fig: 12 CVs of ZIF-8@FAB-2wt% in O_2 saturated 0.1M KOH solution and upon addition of 1.0 M methanol at 50 mV s^{-1} (W.E- GC, R.E- Hg/HgO, C.E- Pt wire).

4.5 Conclusion

In summary, we have synthesized novel hybrid ZIF-8@FAB nanocomposites by simple procedure. The unique properties of two interesting materials helped in designing an efficient non precious metal catalyst for ORR. The growth of ZIF-8 nanoparticles on FAB surface was initiated by the linkage of Zn to the functional groups of FAB. XRD, IR, XPS, Raman, BET, EDS and TEM were employed to characterize the material successfully. The ORR performance of the hybrid nano composite was evaluated using cyclic voltammetry and RDE. Cyclic Voltammetry curves revealed clear oxygen reduction peak for the synthesized ZIF-8/FAB nanocomposites in O_2 saturated 0.1 M KOH solution comparing with that in N_2 saturated solution, implying an oxygen reduction activity. ZIF-8@FAB-2wt% showed a better electrocatalytic activity because of high surface area, pore size and degree of disorderness (I_D/I_G). The reduction of oxygen by synthesized catalysts was 4 electron transfer type predominantly in all the samples. The easy preparation and cheap raw products provide promising future of this electrocatalyst in future applications.

References

[1]   C. Song, J. Zhang, PEM Fuel Cell Electrocatalysts and Catalyst Layers (2008) 89.

[2]   H. Meng, P. K. Shen, Electrochem. Commun. 8 (2006) 588.

[3]   C. Zhang, X. Shen, Y. Pan, Z. Peng, Front. Energy 11 (2017) 268.

[4]   C. Sealy, Mater. Today 11 (2008) 65.

[5]   Y. Nie, L. Li, Z. Wei, Chem. Soc. Rev. 44 (2015) 2168.

[6]   B. Li, H.-M. Wen, W. Zhou, B. Chen, J. Phys. Chem. Lett. 5 (2014) 3468.

[7]   M. Eddaoudi, Science 295 (2002) 469.

[8]   S. Ma, H.-C. Zhou, Chem. Commun. 46 (2010) 44.

[9]   Z. Zhao, X. Ma, A. Kasik, Z. Li, Y. S. Lin, Ind. & Eng. Chem. Res. 52 (2012) 1102.

[10]   P. K. Thallapally, J. Tian, M. Radha Kishan, C. A. Fernandez, S. J. Dalgarno, P. B. McGrail, J. E. Warren, J. L. Atwood, J. Am. Chem. Soc. 130 (2008) 16842.

[11]   R. Krishna, J. M. van Baten, Phys. Chem. Chem. Phys. 13 (2011) 10593.

[12]   S. Qiu, M. Xue, G. Zhu, Chem. Soc. Rev. 43 (2014) 6116.

[13]   L. Zhu, X.-Q. Liu, H.-L. Jiang, L.-B. Sun, Chem. Rev. 117 (2017) 8129.

[14]   L. Ma, C. Abney, W. Lin, Chem. Soc. Rev. 38 (2009) 1248.

[15]   J. Lee, O. K. Farha, J. Roberts, K. A. Scheidt, S. T. Nguyen, J. T. Hupp, Chem. Soc. Rev. 38 (2009).

[16]   F. Llabresixamena, A. Abad, A. Corma, H. Garcia, J. Catal. 250 (2007) 294.

[17]   Y. Cui, B. Chen, G. Qian, Coord. Chem. Rev. 273-274 (2014) 76.

[18]   B. Chen, L. Wang, F. Zapata, G. Qian, E. B. Lobkovsky, J. Am. Chem. Soc. 130 (2008) 6718.

[19]   S. Achmann, G. Hagen, J. Kita, I. M. Malkowsky, C. Kiener, R. Moos, Sensors 9 (2009) 1574.

[20]   L. E. Kreno, K. Leong, O. K. Farha, M. Allendorf, R. P. Van Duyne, J. T. Hupp, Chem. Rev. 112 (2011) 1105.

[21]   J. Mao, L. Yang, P. Yu, X. Wei, L. Mao, Electrochem. Commun. 19 (2012) 29.

[22]   B. Y. Xia, Y. Yan, N. Li, H. B. Wu, X. W. Lou, X. Wang, Nat. Energy 1 (2016) 15006.

[23]   P. Zhang, F. Sun, Z. Xiang, Z. Shen, J. Yun, D. Cao, Energy Environ. Sci. 7 (2014) 442.

[24]   S. Zhao, H. Yin, L. Du, L. He, K. Zhao, L. Chang, G. Yin, H. Zhao, S. Liu, Z. Tang, ACS Nano 8 (2014) 12660.

[25]   B. Chen, G. Ma, Y. Zhu, Y. Xia, Sci. Reports 7 (2017) 5266.

[26]   B. Ni, C. Ouyang, X. Xu, J. Zhuang, X. Wang, Adv. Mater. 29 (2017) 1701354.

[27]   J. Wei, Y. Hu, Y. Liang, B. Kong, J. Zhang, J. Song, Q. Bao, G. P. Simon, S. P. Jiang, H. Wang, Adv. Funct. Mater. 25 (2015) 5768.

[28]   M. Thomas, R. Illathvalappil, S. Kurungot, B. N. Nair, A. A. P. Mohamed, G. M. Anilkumar, T. Yamaguchi, U. S. Hareesh, ACS Appl. Mater. & Interfaces 8 (2016) 29373.

[29]   R. Badam, R. Vedarajan, N. Matsumi, Chem. Commun. 51 (2015) 9841.

[30]   R. Kumar, K. Jayaramulu, T. K. Maji, C. N. R. Rao, Chem. Commun. 49 (2013) 4947.

[31]   S. M. Unni, S. Ramadas, R. Illathvalappil, S. N. Bhange, S. Kurungot, J. Mater. Chem. 3 (2015) 4361.

Chapter 5
Conclusions

5.1 General Conclusions

Development in renewable energy and electrified transportation will render electrochemical energy storage high importance in the future than it has ever been in the past. Both primary and secondary batteries are gathering momentum. Both primary batteries such as metal air batteries and secondary batteries such as Lithium-ion batteries are widely accepted as the next generation power source in portable electrical and electronic products. Considering the vitality of these energy devices, the present research will be addressing various hurdles in each of this technologies and a possible solution to overcome these problems by the utilization of Metal Organic Frameworks (MOFs).

In **Chapter 1**, the introduction of Metal Organic Frameworks (MOFs) and its synthetic procedures are discussed in detail. With a brief introduction about working principle of Li-on battery, its major components including cathode, anode and electrolyte have been discussed. Some of the important literatures which proves the use of MOF as safer electrolytes in Li-ion batteries were also reported. The chapter also focuses on, introduction about zinc-air batteries with problems and challenges in the development of battery technology. And how MOFs can be successful in overcoming those challenges is provided in brief. Finally in the later half, the Oxygen Reduction Reaction (ORR) is focused upon and evolution of ORR catalysts have been discussed thoroughly. The detailed description of active research in the field of electrocatalysts ranging from Pt-based, metal free to non-preious metal catalysts has also been included in this chapter.

In **Chapter 2**, the research is directed towards improving safety and performance standards for lithium-ion batteries. In this context, modified MOF was synthesized by electrochemical

method in an ionic liquid system using two electrode system. Further, doping of lithium bis(triflouromethylsulfonyl) imide (LiTFSI) in MOF (IL) was done before evaluating its performance in Li-ion batteries. Samples with amount variation of MOF (IL) were prepared in ionic liquid and electrochemical behaviour was analysed. The synthesized gel electrolyte system showed high ionic conductivity in order of 10^{-2}–10^{-3} Scm^{-1} at 51°C and exceptionally low activation energy of ion transport ever reported. The possible reasons for such enhanced performance is explained in detail in this chapter. Also high reversible capacity of over 3000 mAh g^{-1} was observed in coin anodic half-cell (**Fig. 1**).
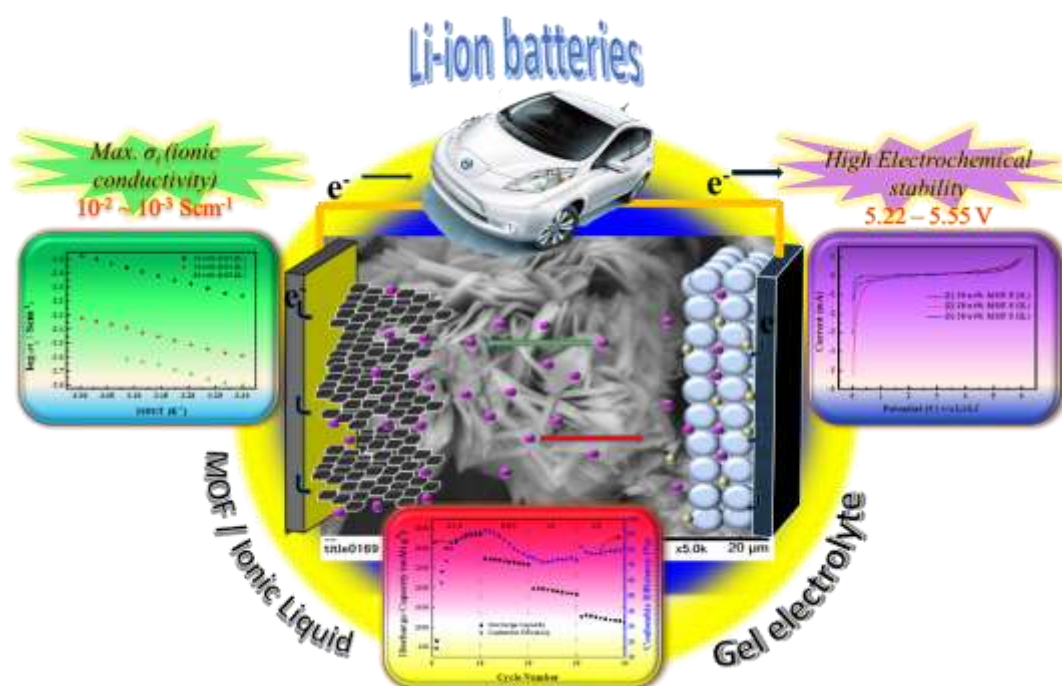

Fig. 1 Graphical illustration showing high electrochemical aspects of synthesized gel electrolyte.

Chapter 3 includes the surface modification of zinc metal used as anode in high performance zinc-air batteries. To carry out this work we got inspiration while we were working on electrochemical synthesis of MOF in ionic liquid medium (Chapter 2). During the electrochemical synthesis of MOF using zinc plate as working electrode, we observed the growth of MOF initiating on the surface of zinc and this led us to the objective of chapter 3. In this chapter, growth of MOF-5 (IL) on zinc surface using electrochemical method for corrosion protection is described in detail. Also to provide the stability to the MOF layer over zinc surface, electropolymerization of thiophene was done and modified zinc anodes were evaluated for battery performance. The zinc air battery with pure zinc as anode showed current density of ~ 7 mA cm^{-2}. On the contrary, zinc air batteries with zinc anodes decorated with MOF-5 (IL) showed 4 times enhanced current density of ~ 27-30 mA cm^{-2} (**Fig. 2**). These MOF/Polythiophene modified zinc anodes showed suppression in hydrogen evolution and enhanced discharging performance was also observed.
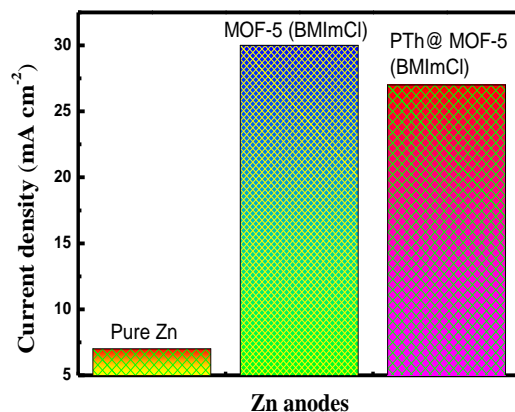

Fig. 2 Comparison of current densities of cells fabricated using
pure Zn and modified Zn anodes.

Metal-air batteries like zinc-air batteries and Li-air batteries requires electrocatalyst for the reduction of oxygen. And while working on surface treatment of zinc anodes for zinc air batteries, we thought of synthesizing MOF-based electrocatalyst for high performance metal-

air batteries. Therefore, **Chapter 4** deals with the synthesis of ZIF-8/FAB based non-precious metal catalyst for ORR. In the recent past, it was observed that non-precious metal catalysts based on transition metal and nitrogen doped carbon materials are potential candidate to replace high cost Pt-based catalysts. MOFs' entire framework which is built by weak co-operative forces or coordination bond are highly interesting materials for ORR because of high surface area and tunable pore size. Therefore in this work ZIF-8 nanocrystals were dispersed on functionalized acetylene black and its utilization for oxygen reduction reaction was evaluated using techniques like CV and RDE. The materials showed high activity towards ORR and excellent methanol tolerance in alkaline solution (**Fig.3**).
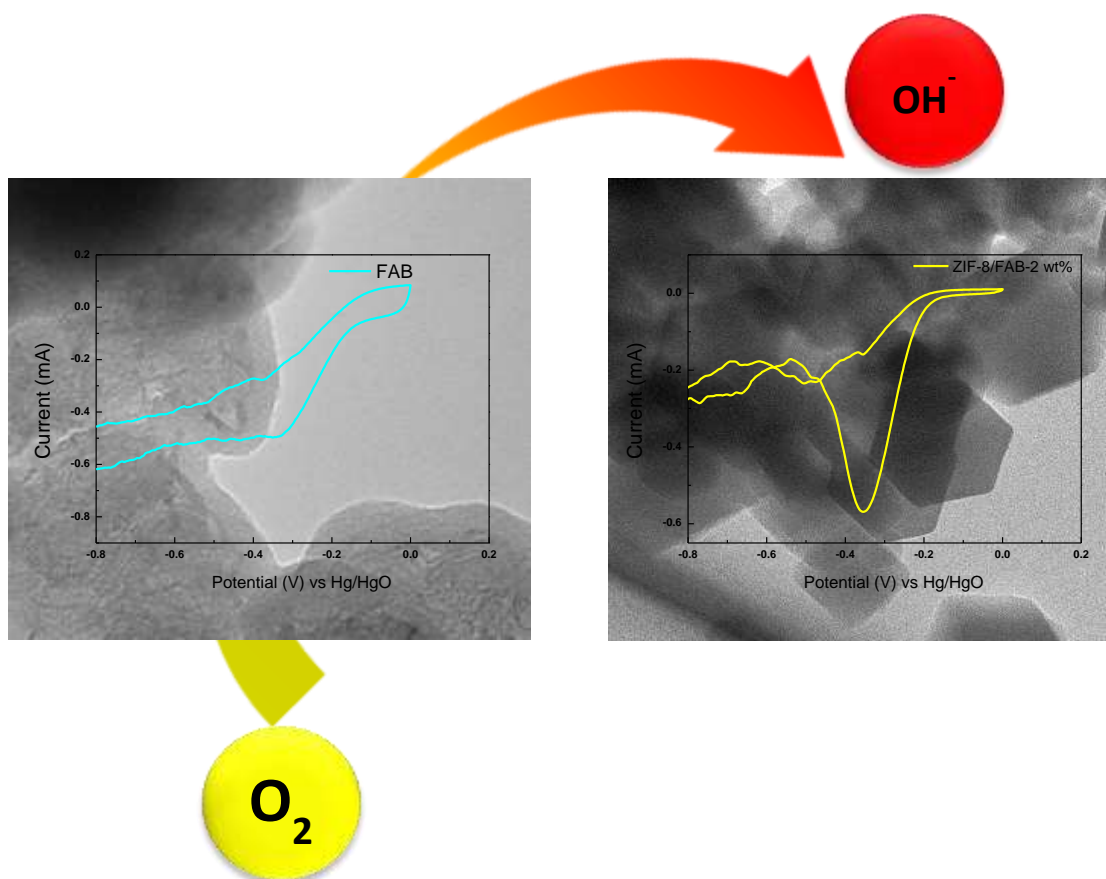

Fig. 3 Graphical illustration showing high ORR activity of ZIF-8/FAB hybrid composites.

5.2 Possible future of research

The results shown in the thesis opens up wide range of possibilities for future application of MOFs. Apart from the results reported in this work, there is still a room for improvement and extension. Some of the possible future research interests can be as follows:

1. The growth of MOF by electrochemical method in ionic liquid leads to the formation of new MOFs as observed in chapter 2. Therefore, optimization of electrochemical parameters can led to the generation of MOFs with different structure from same precursors.

2. Further, dimensionally and morphologically controlled MOFs can be carefully used in forming stable SEI at carbon electrodes for Li-ion batteries.

3. The electrochemical modification of metal surface shown in chapter 3 can open up the possibility of protecting various metal surfaces through MOFs. The in-situ formation of MOFs on metal surface during charge discharge can also improve the performance of energy storage devices.

4. Generation of ORR electrocatalyst without high temperature pyrolysis can be of great importance. As the pyrolysis spoils the synthetic control, which is one of the fascinating property of MOFs and thereby restricts the scope for future improvement in the electrocatalytic activity.

5. Formation of MOFs nanocrystals on various highly conducting carbon materials can be interesting approach to substitute the high cost platinum based catalysts.

List of publications and presentations at international/domestic conferences

Publication

1. **Ankit Singh**, Raman Vedarajan and Noriyoshi Matsumi, Modified Metal Organic Frameworks (MOFs)/Ionic Liquid Matrices for Efficient Charge Storage, **J. Electrochem. Soc., 2017, 164 (8), H5169-H5174.**

International Conferences

1. **Poster:** <u>Ankit SINGH</u>, Raman VEDARAJAN and Noriyoshi MATSUMI, "Application of Metal Organic Frameworks/Ionic Liquid Composites in Li-ion Batteries", **IISc-JAIST Joint Workshop** in JAIST, Ishikawa, Japan. (March 2016).
2. **Oral:** <u>Ankit SINGH</u>, Raman VEDARAJAN and Noriyoshi MATSUMI, "Metal Organic Frameworks/Ionic Liquid Composites As Electrolytes for Li-Ion". **230th meeting of ECS (The Electrochemical Society) PRiME**, Hawaii Convention Center, Hawaii, Honolulu, USA. (Oct 2016).
3. **Poster:** <u>Ankit SINGH</u>, Raman VEDARAJAN and Noriyoshi MATSUMI, "Corrosion Protection By MOF-5 Coatings for Sustained Zinc-Air Battery". **230th meeting of ECS (The Electrochemical Society) PRiME**, Hawaii Convention Center, Hawaii, Honolulu, USA. (Oct 2016).
4. **Oral:** <u>Ankit SINGH</u>, Raman VEDARAJAN, Noriyoshi MATSUMI, "Enhanced Electrochemical Performance of Zn-Air Batteries Using MOF-5 (ILs) / Polythiophene Nanocomposites by Anode Modification", **The 57th Battery Symposium** in Makuhari Messe, Chiba, Japan. (December 2016).
5. **Poster:** <u>Ankit SINGH</u>, Raman VEDARAJAN and Noriyoshi MATSUMI, "Enhanced Electrochemical Behavior of Modified Zn Anodes in Zn-Air Batteries Using MOF-5 (ILs) / Polythiophene Composites" **JAIST Japan-India Symposium on Materials Science 2017,** Japan Advanced Institute of Science and Technology, Ishikawa, Japan. (Mar 2017).
6. **Oral:** <u>Ankit SINGH</u>, Raman VEDARAJAN and Noriyoshi MATSUMI, "Synthesis of ZIF-8 / Functionalised Acetylene Black Hybrid Nanocomposites as Non Precious Metal Catalysts for ORR in Fuel Cells", **ACS National Meetings,** New Orleans, LA, USA. (March 2018).

Domestic Conferences

7. **Oral:** <u>Ankit SINGH</u>, Raman VEDARAJAN, Noriyoshi MATSUMI, "Ion Conductive Behavior of Metal Organic Frameworks (MOF-5)/Ionic Liquid Matrices", **Inorganic Polymer Conference (IPC),** Tokyo University of Science, Tokyo, Japan. (November, 2014).

8. **Poster:** Ankit SINGH, Raman VEDARAJAN, Noriyoshi MATSUMI, "Ion Conductive Properties of MOF/Ionic Liquid Composite", **Chemical Society of Japan (CSJ),** University of Toyama, Toyama, Japan. (November, 2014).

9. **Poster:** Ankit SINGH, Raman VEDARAJAN, Noriyoshi MATSUMI, "Application of Metal Organic Frameworks/Ionic Liquid Composites in Li-ion Batteries", **CSJ (Chemical Society of Japan) Meeting** in Kanazawa University, Ishikawa, Japan. (November 2015).

10. **Poster:** Ankit SINGH, Raman VEDARAJAN, Noriyoshi MATSUMI, "Ion Conductive Properties of MOF/Ionic Liquid Matrices", **SPSJ (Society of Polymer Science, Japan) Spring Meeting** in Hi-Tech Centre, Ishikawa, Japan. (November 2015).

11. **Poster:** Ankit SINGH, Raman VEDARAJAN, Noriyoshi MATSUMI, "Polythiophene/MOF Coating on Zn as Zn-air Battery Anode", **SPSJ (Society of Polymer Science, Japan) Annual Meeting** in Kobe Convention Center, Kobe, Japan. (May 2016).

12. **Poster:** Ankit SINGH, Raman VEDARAJAN, Noriyoshi MATSUMI, "MOF / Polythiophene Nanocomposite Coatings for Sustained Zn-Air Battery Anodes", **SPSJ (Society of Polymer Science, Japan)** in Yokohama, Japan. (September 2016).

13. **Oral:** Ankit SINGH, Raman VEDARAJAN, Noriyoshi MATSUMI, "Design of Zn-Air Batteries by MOF / Polythiophene Coating on Zn Electrode", **Inorganic Polymer Conference** in Tokyo University of Science, Tokyo, Japan. (November 2016).

14. **Poster:** Ankit SINGH, Raman VEDARAJAN, Noriyoshi MATSUMI, "Effect of Ionic Liquids on Zinc-air Battery Based on MOF-5(IL)/Polythiophene Decorated Zn Anode", **SPSJ (Society of Polymer Science, Japan) Annual Meeting** in Makuhari Messe, Chiba, Japan. (May 2017).

15. **Poster:** Ankit SINGH, Raman VEDARAJAN, Noriyoshi MATSUMI, "ZIF-8 Embedded Functionalised Acetylene Black Hybrid Nanocomposites as Efficient Non Precious Metal Catalysts for ORR", **SPSJ (Society of Polymer Science, Japan)** in Matsuyama, Japan. (September 2017).